Parametric Optimization in Electric Discharge Machining of Cladded Materials

Ph.D. Dissertation

SUBMITTED BY
KASHIF ISHFAQ
2013-PhD-MNF-03

SUPERVISED BY
PROF. DR. NADEEM AHMAD MUFTI

Department of Industrial and Manufacturing Engineering
University of Engineering and Technology
Lahore-Pakistan

August-2018

Parametric Optimization in Electric Discharge Machining of Cladded Materials

By

Kashif Ishfaq
2013-PhD-MNF-03

A dissertation submitted for the degree of
Doctor of Philosophy
in Manufacturing Engineering

Internal Examiner	**External Examiner**	**External Examiner**

Chairman	**Dean**
Department of Industrial & Manufacturing Engineering	Faculty of Mechanical Engineering

Department of Industrial and Manufacturing Engineering
University of Engineering and Technology
Lahore-Pakistan
August-2018

DEDICATION

I dedicate this thesis to my parents whose love, prayers and endless support provided me the strength to carry out this research work.

DECLARATION

I, Kashif Ishfaq, hereby state that this Ph.D. thesis titled "Parametric Optimization in Electric Discharge Machining of Cladded Materials" is my own work and has not been submitted previously by me for taking any other degree from this university or anywhere else in the country/world.

COPYRIGHT STATEMENT

ACKNOWLEDGEMENTS

The author would like to acknowledge the support provided by the faculty and staff of The Department of Industrial and Manufacturing Engineering, University of Engineering, Lahore, Pakistan, during this research work.

ABSTRACT

The use of cladded materials has increased in manufacturing industry as it provides a blend of properties in end use applications. For instance, copper is cladded with steel to combine the thermal and electrical properties of cooper with the strength of steel and stainless steel is cladded to mild steel to improve the corrosion, oxidation and abrasion resistance. Cladded materials offer desired level qualities at relatively low cost in comparison to using a single solid alloy. However, the cutting of a cladded material is really considered as a challenging task owing to its heterogeneous nature, therefore, it is often subjected to thermal cutting processes like gas cutting or plasma arc cutting. But thermal cutting processes offer poor surface finish and require subsequent finishing operations. Wire electric discharge machining (WEDM) is a competent alternate in terms of surface finish but this process offers relatively low cutting rates. Additionally, the surface roughness imparted to both layers of material is different because both layers possess different properties. Moreover, the formation of spark gap tends to reduce the dimensional accuracy of the machined part.

Therefore, a research work has been carried out to address the issues pertaining to the WEDM of cladded material. Stainless-clad steel which is commonly used material in manufacturing industry has been selected as a workpiece material. This material is used in variety of applications like in boilers, pressure vessels, tubing, fractionators, heat exchangers, reactors and chemical plants etc. Taguchi's L18 experimental design technique has been used to conduct the experimentation by considering workpiece orientation, layer thickness of each individual layer, wire diameter, servo voltage, wire feed, pressure ratio and pulse on-time as input factors. Brass wire electrode has been employed for WEDM of cladded material. Cutting speed, surface roughness and spark gap have been selected as response characteristics. ANOVA is used to assess and quantify the effects of input parameters on the selected response attributes. In case of cutting speed pulse on-time, stainless steel layer thickness, mild steel layer thickness and wire diameter are the significant control factors whereas for surface roughness the role of workpiece orientation, wire diameter and pressure ratio is proved significant. Wire diameter and pressure ratio also found most contributing parameters for spark gap as per the ANOVA results. Finally, Optimal combinations of machining parameters are also extracted through various statistical analyses and it has been found that the proposed optimal set of parameters improves performance of WEDM during cutting of stainless-clad steel.

PUBLICATIONS

1. Kashif Ishfaq, Nadeem Ahmad Mufti, Mohammad Pervez Mughal, Muhammad Qaiser Saleem & Naveed Ahmed, "Investigation of wire electric discharge machining of stainless-clad steel for optimization of cutting speed", Int. J. Adv. Manuf. Technol., 96:1429-1443, (2018), DOI. 10.1007/s00170-018-1630-9.
2. Kashif Ishfaq, Nadeem Ahmad Mufti, Naveed Ahmed, Mohammad Pervez Mughal, Muhammad Qaiser Saleem, "An investigation of surface roughness and parametric optimization during wire electric discharge machining of cladded material", Int. J. Adv. Manuf. Technol., 97: 4065–4079, (2018), DOI. 10.1007/s00170-018-2240-2.

Table of Contents

LIST OF FIGURES

LIST OF TABLES

LIST OF ABBREVIATIONS

EDM	Electric Discharge Machining
WEDM	Wire Electric Discharge Machining
USM	Ultrasonic Machining
WJM	Water Jet Machining
AWJM	Abrasive Water Jet Machining
IJM	Ice Jet Machining
EBM	Electron Beam Machining
LBM	Laser Beam Machining
IBM	Ion Beam Machining
PBM	Plasma Beam Machining
CHM	Chemical Machining
PCM	Photochemical Machining
ECM	Electrochemical Machining
LT_{SS}	Stainless Steel Layer Thickness
LT_{MS}	Mild Steel Layer Thickness
D_w	Wire Diameter
Or	Workpiece Orientation
Pr	Pressure Ratio
SV	Servo Voltages
P_{ON}	Pulse On-time
F_W	Wire Feed
ANOVA	Analysis of Variance

Chapter 1
Introduction

This chapter covers the background, gap identification and the justification for current research work. The objectives and layout of the thesis are also described in this part of the study.

1.1 Background

The choice of material has become a critical consideration for manufacturing industry for their sustainability in the present competitive environment. One of the growing concepts to meet industrial requirements is cladding process in which, two or more metals or alloys are metallurgic ally bonded together to combine the characteristic properties of each in composite form. The use of cladded material enables to attain the desired level of product quality at comparatively low cost instead of using single solid alloy [1-3].

The use of the cladded material is growing in manufacturing industry owing to its advantage of offering a blend of properties. Copper-clad steel, for example, is used to combine the electrical and thermal characteristics of copper with the strength of steel. Another example is stainless steel clad aluminium that is used in aerospace components, in which aluminium is bonded with the stainless steel to have higher strength and lighter weight. A great variety of metals and alloys can be combined in two or more layers, and they are available in many forms, including sheets, strips, plates, tubing and wire [2].

Stainless-clad steel is another important cladded material used in variety of applications such as, in boilers, pressure vessels, tubings, fractionators, heat exchangers, reactors and chemical plants etc. [4]. Stainless steel cladding improves the resistance against corrosion, abrasion and oxidation whereas the backing material not only maintains the structural strength but improves the thermal conductivity of the composite as well [2]. The stainless steel layer is joined to the mild steel layer by the process of weld overlay or by hot rolling.

Keeping in view the industrial applications of stainless-clad steel, it has been selected as a workpiece material in the present research work. Although, this material offers a combination of properties but the real challenge regarding its application is its machining as this material possess a heterogeneous nature.

Cutting tool encountered an abrupt change in the magnitude of the cutting force as it enters from one layer to the other [5]. Consequently, the life of the cutting tool is compromised.

Generally, gas cutting or plasma arc cutting process is used in industry for machining of cladded materials. These cutting processes not only yield a poor surface quality but also the cut specimen is subjected to deeper heat affected zones. Moreover, subsequent finishing operations are carried out to attain the desired surface quality. Wire electric discharge machining (WEDM) is a competent alternate in terms of cut quality.

WEDM is a thermoelectric process in which erosion of workpiece material takes place by a series of discrete electric sparks occur between the workpiece material and the wire electrode. The temperature of these spark can rise upto 12,000°C that results into melting and vaporization of the target material. The flushing dielectric fluid is continuously circulated to remove the melted debris from the cutting zone [6-7].

This machining process has a tendency to machine higher strength, wear resistant and harder, materials with reasonably high degree of accuracy. The creation of intricate shapes that are challenging to form by conventional processes can be easily produced by this nonconventional cutting methodology [8]. The inherent problems of conventional machining processes such as, mechanical stresses, chatter and vibrations are completely abolished in WEDM as there is no physical contact between wire electrode and the target material workpiece [9]. WEDM process has been used in various industrial applications like in, automotive, dies and molds, aerospace and medical industry [10].

The potential of WEDM has been explored for a variety of difficult–to-cut materials such as titanium, stainless steels, ceramics, tool steels, metal matrix composites but cutting performance of this process is yet to be examined for machining of cladded material [11-15]. No literature was found in this regard.

Therefore, the potential of WEDM has comprehensively evaluated for cutting of stainless-clad steel in the present study. The effect of workpiece related parameters like workpiece orientation (Or) and layer thickness of the individual layer on machining performance of WEDM has not been investigated specifically which is primarily done in the current research work.

Additionally, despite using common parameters for investigation, focus is shifted to analyze the effect of wire diameter (D_W) and pressure ratio (Pr) of the dielectric fluid on the cutting performance of WEDM of stainless-clad steel.

Taguchi's (L18) experimental design technique has been used for experimentation considering, workpiece orientation (Or), layer thickness of individual layer (LT_{SS} and LT_{MS}), wire diameter (D_W), servo voltage (SV), wire feed (F_W), pressure ratio (Pr) and pulse on time (P_{ON}) as input factors whereas cutting speed, surface roughness and spark gap are the selected response attributes. The results of the experimentation are then subjected to a comprehensive statistical analyses (Analysis of variance, Main effects plot and Signal-to-Noise ratio etc.) Finally, regression model for the selected response variables have been developed and validated through confirmatory experiments during WEDM of stainless-clad steel.

1.2 Research objectives

The aim of the present research is to evaluate the cutting performance of WEDM for machining of stainless-clad steel material in terms of cutting speed, surface roughness and spark gap with an emphasis on developing the optimal settings of parameters to optimize the cutting performance of WEDM process for cutting of cladded materials. The salient objectives of the present study are listed below:

- To evaluate the potential of WEDM for cutting of cladded material.
- To investigate the effect of workpiece related parameters like orientation of workpiece (Or) and layer thickness of individual layer on cutting speed, surface roughness and spark gap in WEDM of stainless-clad steel.
- To develop the optimal parametric combination to maximize the process yield.
- To formulate a mathematical model for each selected response that can accurately predict the response.

1.3 Layout of thesis

Rest of the chapter presents the layout of the thesis. The hierarchy of the present study is presented in Figure 1.1.

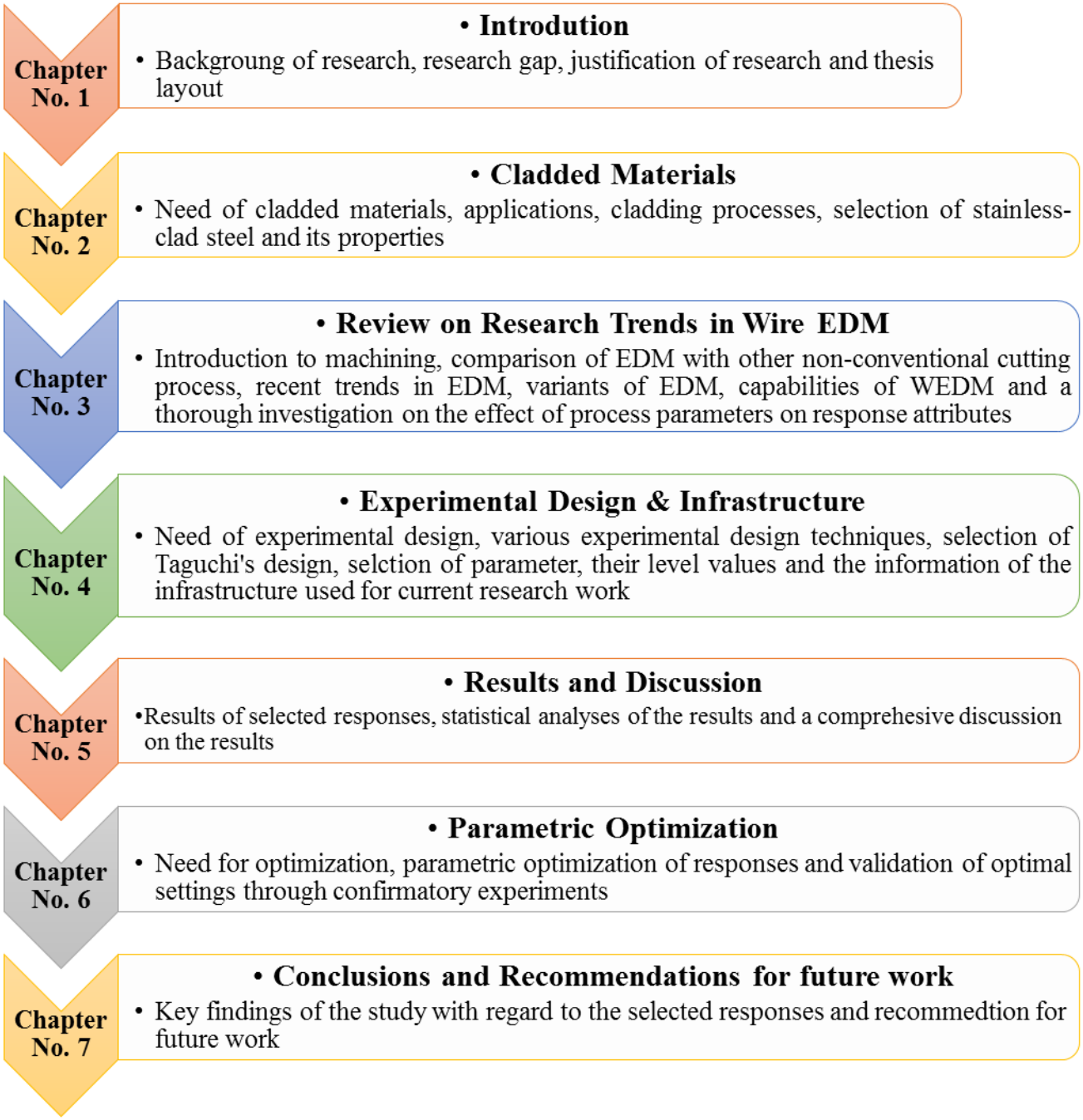

Figure 1.1 Thesis layout

Chapter 2
Cladded Materials

This chapter provides a brief review of various cladded materials, their applications and commonly used cladding processes for the manufacturing of cladded materials. The salient properties and applications of the selected cladded material (stainless-clad steel) are also elaborated.

2.1 Need of cladded materials

In the industry, certain materials are subjected to severe conditions and these materials have to survive for longer period of time. The choice of appropriate material for such kind of environment is a challenging task. There is a possibility that a material can endure the industrial harsh environment and can withstand for appreciable longer period of time but to use such kind of materials as a bulk structural materials is always costly [16]. Therefore, instead of using single solid alloy cladded materials are used. About 80% of cost can be saved by using cladded material instead of using single solid alloy [17]. In certain scenarios the use of cladded material is complementary as the desired properties might not be achieved using a single alloy.

Cladding is defined as the process of depositing a thick layer of erosion and corrosion resistant material on a base material to hamper the corrosion or erosion rate [18-21]. This process can provide two fold functions; one is the improvement in surface dependent characteristics such as resistance to corrosion, erosion and wear under abrasion, and the other is to improve the bulk dependent characteristics like hardness and strength [22]. Cladded components can survive for longer period of time without compromising their intended function in a hostile environment [23]. Therefore, the use of cladded materials is growing in every passing day. The details of applications of some cladded materials are presented in the forthcoming section.

2.2 Applications of cladded materials

Cladded materials are used in variety of industrial applications owing to the reason that a blend of desired properties is achieved. Below are some of the examples of industrial applications of cladded materials [24]:

- **Oil & Gas**:
  Separators, absorbers, slug catchers, flow lines, pipelines, catenary risers (SCR), fittings
- **Chemical Industry**:
  Pressure vessels, washers, heat exchangers, evapoators, columns, pipes, reactors
- **Food industry**:
  Premium induction cookware, fermenters, equipment for industrial kitchens
- **Power generation**:
  Nuclear plant componenets, coal gasifiaction, geothermal plants, tube sheets of condenser
- **Environmental technology**:
  Flue gas channels, chimney, scrubbers, ducts, garbadge incineration plant
- **Ship buliding**:
  Propeller system, ice breakers, chemical tankers
- **Fertilizer industry**:
  Heat excahngers, strippers, reactors
- **Reineries/ petochemicl industry**:
  Reactors, fractionators, distillation tower, hydocrackers, hydrosulfurises
- **Pulp and paper**:
  Evaporator pipe plates, evaporator, digesters, steaming vessels, pulp boiler
- **Seawater Desallination**:
  Evaporator shells, flash chambers, pump vessels, water boxes, heat exchangers

2.3 Advantages

Followings are some of prominent advantages associated with the use of cladded materials [25]:

- ❖ Better strength at a lighter weight
- ❖ Offers low cost solution
- ❖ Excellent thermal and electrical conductivity
- ❖ Corrosion resistant
- ❖ Withstand in harsh environment
- ❖ Incredible and durable

2.4 Cladding processes

There exists various cladding methodologies for the manufacturing of cladded materials like weld cladding, roll bonding, explosive welding plasma arc welding (PAW) and laser cladding etc. [1, 26-33]. The brief summary of all the narrated cladding processes is discussed in the coming sections.

2.4.1 Roll bonding

Roll bonding is a solid state welding process in which two or more layers of different materials are joined together by applying sufficient amount of pressure with the aid of a pair of flat rollers as demonstrated in Figure 2.1. The advantages of roll bonding include the following [34]:

- Homogeneous bonding
- Economical alternative
- Optimal combination of cladding material and base material properties
- Workability is better than solid plates

This process is classified into two categories i.e. hot roll bonding and cold roll bonding.

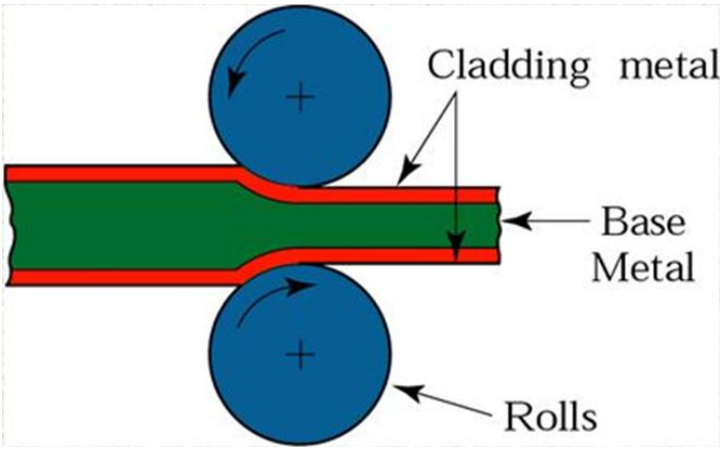

Figure 2.1 Schematic illustration of roll bonding process [35]

2.4.1.1 **Hot roll bonding**

Hot roll bonding (HRB) is also termed as heat and pressure process as in this process properly cleaned cladded components in the form of sandwich, are heated upto plastic range and then reasonable amount of pressure is applied. The complete process is schematically described in the below Figure 2.2.

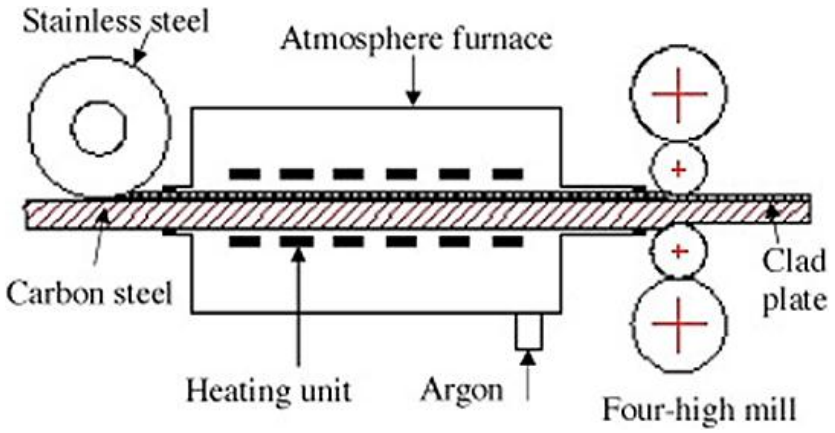

Figure 2.2 Schematic illustration of hot roll bonding process [36]

In hot roll bonding cladding thickness is usually specified as a percentage of total thickness which ranges from 5-50%.

2.4.1.2 Cold roll bonding

The cold roll bonding process comprises of three steps:

- Appropriate cleaning of the mating surfaces
- Development of bonding between the two mating surfaces passing them through bonding mill where about 50 to 80% thickness is reduced
- Finally the clad specimen is subjected to the sintering process

The only difference between hot rolling and cold rolling process is that in the former process the two mating surfaces are sufficiently heated (plastic range) before undergoing the rolling process whereas in the second one the mating surfaces are first subjected to rolling followed by annealing as presented in Figure 2.3 . It is important to note that microsturtures of clad components produced by the said processes are substanially the same. However, cold rolling process can not yield clad plates of appreciable size. It can only be used for producing thin claddings. Some of the typical properties of roll bonded stainless steel are shown in Table 2.1 [2].

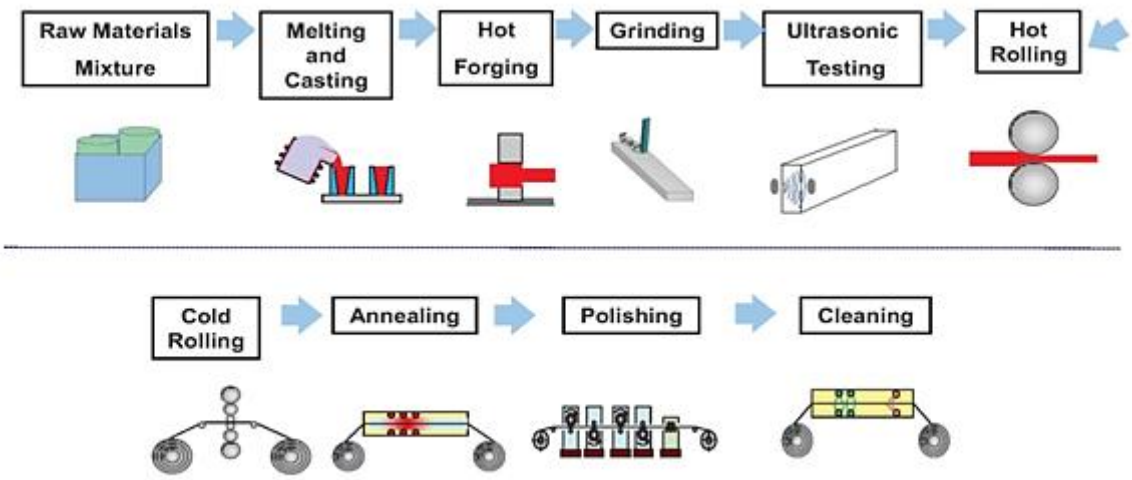

Figure 2.3 Schematic of hot and cold rolling process [37]

Table 2.1 Salient features and applications of roll bonded stainless steel [2]

Materials system	Composite ratio, %	Thickness		Width		Tensile strength		Yield strength		Elongation, %	Applications
		mm	in.	mm	in.	MPa	ksi	MPa	ksi		
Type 434 stainless/5052 aluminum	40:60	0.56-0.76	0.022-0.030	≤610	≤24	395	57	360	52	12	Widely used for automotive body moldings, drip rails, rocker panels, and other trim components, often replacing solid stainless steel or aluminum. Stainless steel provides bright appearance; the hidden aluminum base provides cathodic protection, corroding sacrificially to the body steel.
C1008 steel/type 347 stainless steel/C1008 steel	45:10:45	0.36	0.014	305	12	393	57	195	28	35	Used in hydraulic tubing in vehicles, replacing terne-coated carbon steel tubing. The outer layer of carbon steel cathodically protects the stainless core of the tube, extending its life significantly.
Nickel 201/type 304 stainless steel/nickel 201	7.5:85:7.5	0.20-2.41	0.008-0.095	25-64	1-2.5	...	...	310	45	40	Used in formed cans for transistor and button cell batteries, replacing solid nickel at a lower cost
Copper 10300/type 430 stainless steel/copper 10300	17:66:17, 20:60:20, 33:34:33	0.10-0.15	0.004-0.006	12.7-150	0.5-6	415(a)	60(a)	275	40	20(a)	Replaces heavier gapes of copper and bronze in buried communications cable. The stainless steel provides resistance to gnawing by rodents, which is a serious problem in underground installations.

(a) 20/60/20 three-layer laminate. Source: Ref 2

2.4.2 Explosive bonding

This cladding methodology is also known as explosion welding. In this process the bonding of two or more dissimilar metals is achieved by high velocity impact between the mating surfaces of metals. This impact provides sufficient amount of energy that ensures the solid state bonding. The impact is usually created with the aid of certain explosive material. The complete description of the process is presented in Figure 2.4 [38].

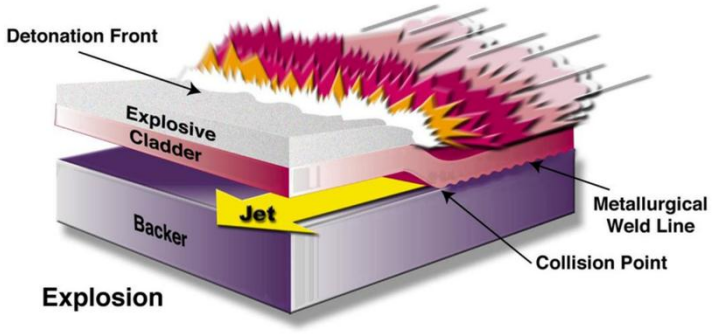

Figure 2.4 Schematic of explosive cladding process [38]

It is worthy to note that there is no appreciable increase in the temperature of both the mating surfaces during cladding process although detonation of explosive liberate noticeable amount of heat. Actually the detonation and subsequently the cladding process occur in a short period of time and therefore, heat transfer might not be possible in such a short span. As the two mating surfaces are not subjected to heating in this cladding process thus the mechanical properties, microstructures and corrosion properties of parent metal remain intact. The formation of heat affected zones is quite minimal. Moreover, brittle intermetallic layers are not formed in this cladding methodology [38].

Some of the commercially availed explosively clad combinations of different materials are shown in Figure 2.5.

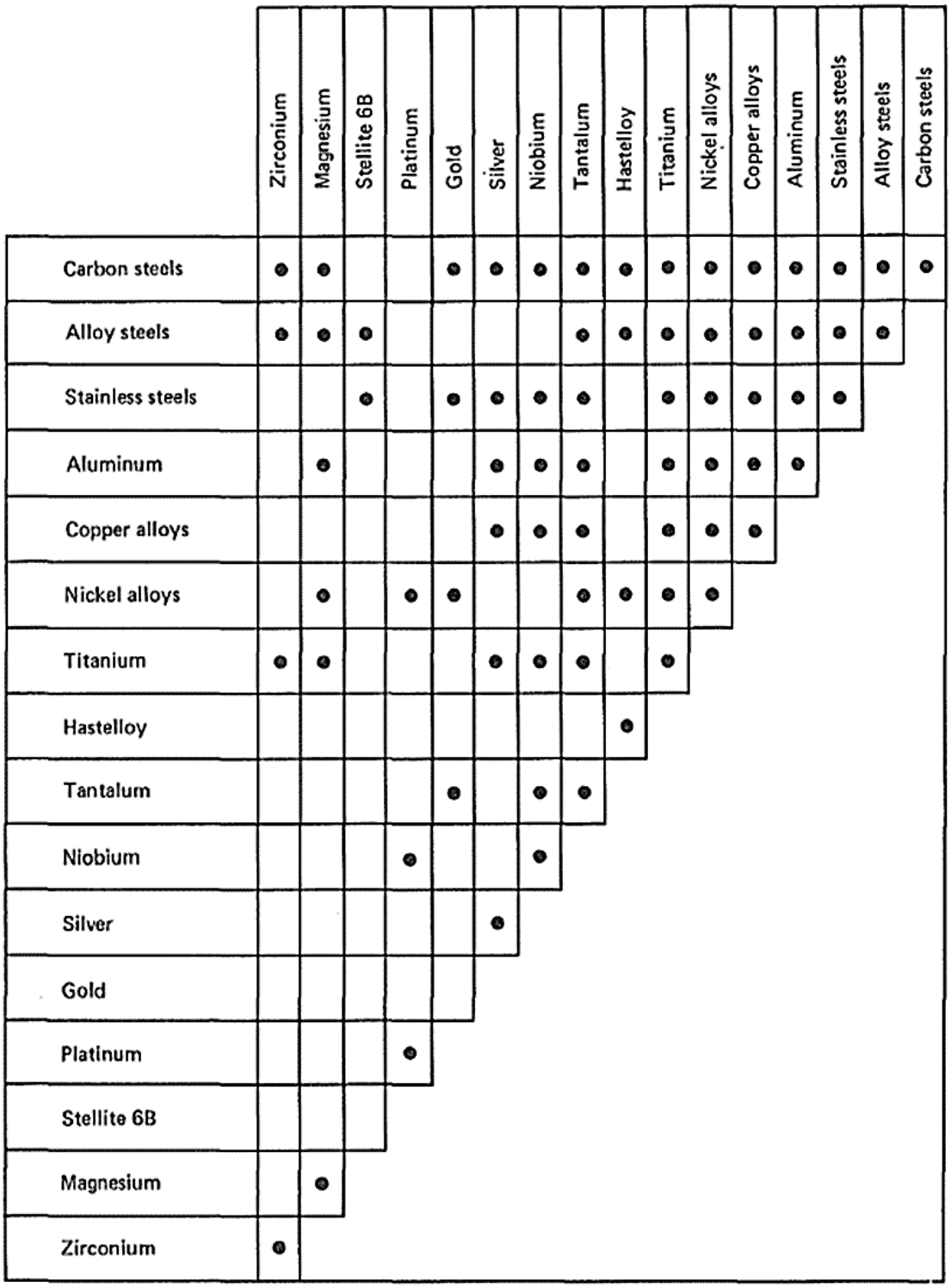

Figure 2.5 Commercially available explosively clad combinations [2]

- **Advantages of explosive cladding process**

  Following are the some advantages pertaining to the explosive cladding technique [34]:

  - Higher resistance to corrosion
  - Inherent material's properties are not degraded
  - Considerable bond strength
  - Multilayer composites can also be developed
  - Can be used to clad titanium to aluminium which is impossible by overlay techniques

- **Explosive cladding process limitations**

  Limitations of the explosive cladding process are described below [2] :

  - Both the mating surface should possess sufficient ductility and fracture toughness. So, that the rapid deformation is possible without fracture.
  - Setup cost is high
  - Required high level safety protocols

2.4.3 Weld cladding process

This process refers to deposit a layer of a filler metal to the substrate (base metal) to impart certain properties that are not intrinsic in the substrate [39-40]. Weld cladding process is typically used for making internal surfaces of low-alloy and carbon steel pressure vessel, boiler tubings, paper digesters, reactors, tube sheets, hydrocrackers and nuclear reactor containment vessels. In most of the applications the cladding material is austenitic stainless steel or Ni-based alloy. The process of weld cladding can be performed in variety of different ways such as submerged arc welding (SAW), flux cored arc welding (FCAW), plasma arc welding, electroslag welding and gas metal arc welding (GMAW) [30, 41-43]. However, submerged arc and electroslag welding techniques are found to be the most economical for making stainless steel claddings [2]. The schematics of both the processes are presented in Figure 2.6 and Figure 2.7.

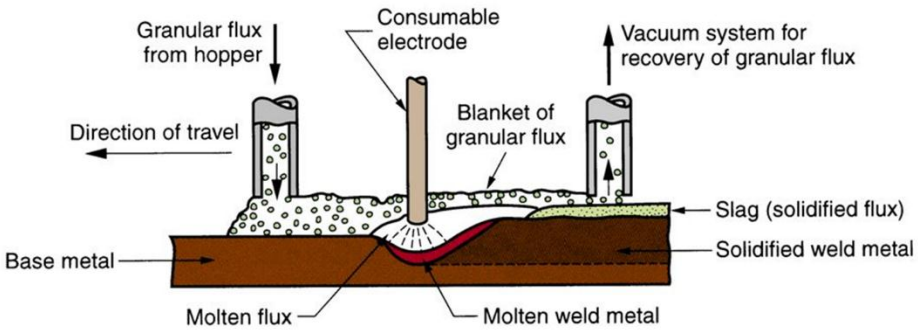

Figure 2.6 Schematic of SAW process [44]

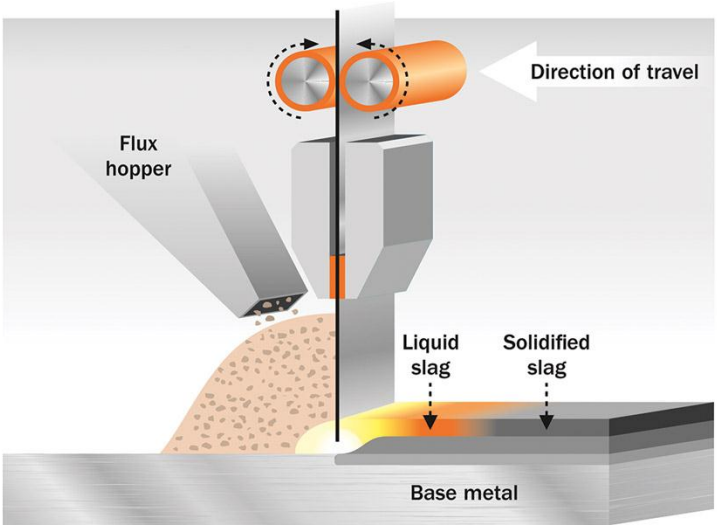

Figure 2.7 Schematic of electro slag welding [45]

2.4.4 Plasma arc cladding

Plasma arc cladding (PAC) also termed as plasma arc welding (PAW), is a novel modification of gas tungsten arc welding. This cladding technique is similar to that of gas tungsten arc welding with the only difference of the design of torch as shown in Figure 2.8.

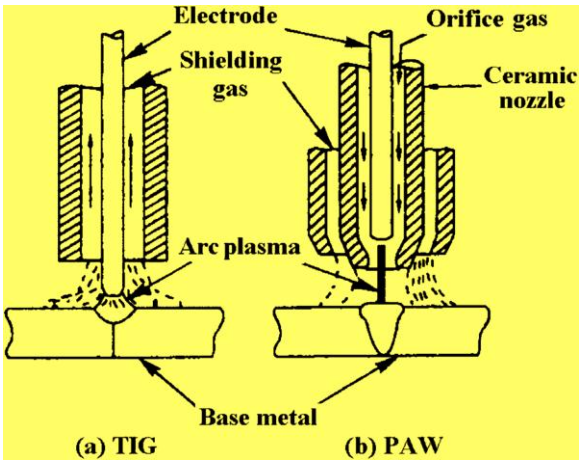

Figure 2.8 Schematic illustration; (a) TIG welding torch (b) PAW torch [42]

In this welding process, cladding is done by melting and joining the two metals by heating them through a focused plasma arc developed between the non-consumable electrode of tungsten and the metal surface as shown in Figure 2.9. The heat contained per unit volume of plasma arc increases owing to the constriction provided by the nozzle. The arc temperature reaches upto 11,000℃ in the aforementioned cladding process that results into the melting and joining of the metals. Usually, the process of PAC can be performed in two modes either in melt-in mode or in keyhole mode.

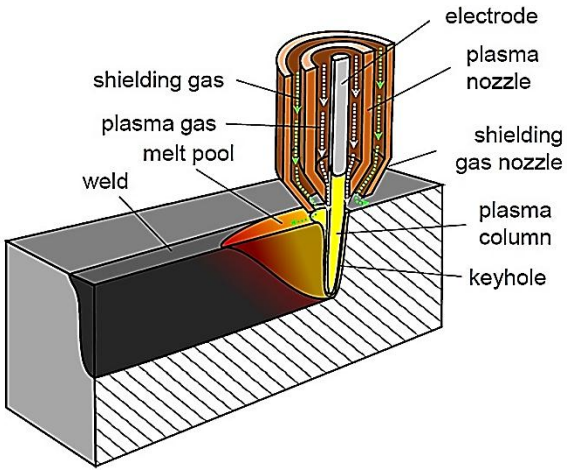

Figure 2.9 Schematic demonstration of plasma arc cladding process [46]

In the former mode, energy is directly transferred from the arc to the workpiece that causes heating of the surface through conduction and conversion into kinetic energy. If the conduction rate of the energy by the metal surface is lower than the deposition rate of energy, an immediate rise in temperature takes place that tends to melt the metal and subsequently a fusion weld is formed. This mode is also known as conduction mode. In the later mode of operation, the density of the energy provided by arc is sufficiently higher than the amount of energy being lost through conduction by metal surface. In this case, plasma arc can penetrate into the weld pool and form a through hole in the molten pool, termed as keyhole as presented in Figure 2.10. The keyhole process produces more penetration depth in comparison to the melt-in mode.

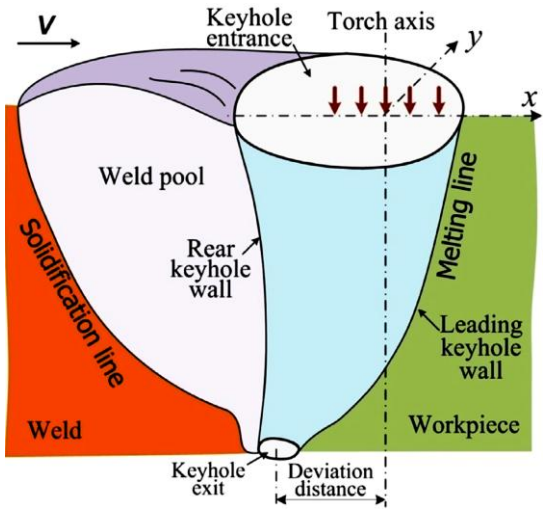

Figure 2.10 Schematic description of keyhole mode cladding process [47]

2.4.4.1 Plasma arc cladding process characteristics

PAC is found to have many advantages over conventional tungsten gas arc welding (GTAW) in terms of joint preparation, thermal distortion and penetration depth etc. As, it has high velocity of arc (300-2000m/s) and greater heat intensity (10^9–10^{10} W/m^2) in comparison to the other alternative. Some specific characteristics of PAC process are mentioned below[42].

- Provides better welding speed
- Higher efficiency
- Higher penetration depth
- Can weld a thick material in a single pass
- Electrode contamination is minimized
- Provide a large tolerance to misalignment and joint gaps
- The diameter of the plasma column is larger in comparison to laser or electron beam
- Minimum angular distortion and residual stress in comparison to GTAW

2.4.4.2 Disadvantages

The said process offers variety of advantages but certain disadvantages are also associated with this cladding technique. The detail of these disadvantages is mentioned below [48]:

- This technique produces harmful radiations like infrared and ultraviolet
- It is a source of noise pollution
- PAC yields wider and deeper heat affected zones in comparison to laser beam welding
- Equipment cost is high
- Trained and specialized operator is required

2.4.4.3 Applications of PAC

Some of the applications of PAC process are described in Figure 2.11.

Figure 2.11 Applications of PAC process [49]

2.4.5 Laser cladding process

Laser cladding is a process of coating a substrate part by melting and consolidating the powder or wire feedstock material with the aid of coherent energy source called a laser. The high energy beam of laser creates a molten pool in a base material for its bonding with the filler material through a diffusion type of weld. Laser cladding technique is mainly used for repair purposes or for additive manufacturing. This cladding method is not recommended for bulk cladding to improve the structural properties like corrosion resistance, wear resistance and abrasion resistance etc. The schematic illustration of laser cladding process is described in Figure 2.12.

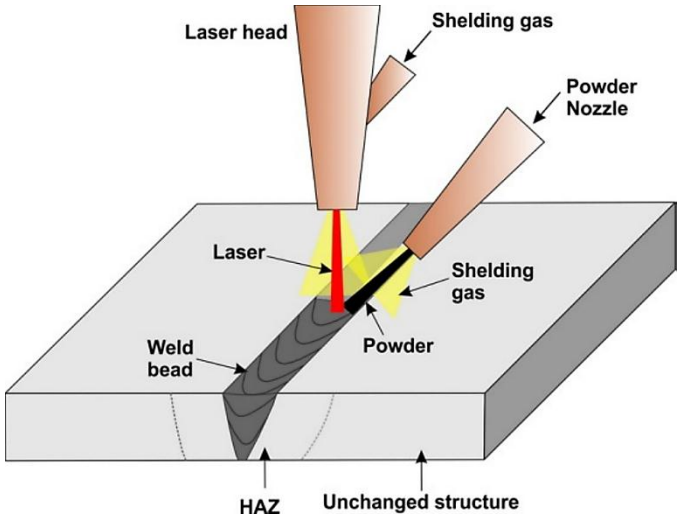

Figure 2.12 Schematic of laser cladding process [50]

2.4.5.1 Advantages of laser cladding process

The use of laser cladding results into following some advantages [50]:

- High processing speed owing to the inertia less nature of light
- High energy density can be produced
- This technique can be used at room temperature
- No electrode/filler material is required
- Precise welds in terms of penetration and relative position can be achieved
- Contamination level is quite low
- Very small heat affected zones
- Can be used for repair applications

2.4.5.2 Effect of process parameters

The process of laser cladding is controlled by number of parameters such as spot size and type of laser, laser power, welding speed, shielding gas etc.[50]. Dhahri et al. evaluated the effects of laser power on penetration depth and bead depth. The results revealed that penetration depth and bead depth both increases with the increase in the power of laser. However, the trend of penetration depth is somewhat different from that of bead width i.e. in case of penetration depth a kind of linear relationship was found but for the case of bead depth an exponential trends was reported as described in Figure 2.13 [51].

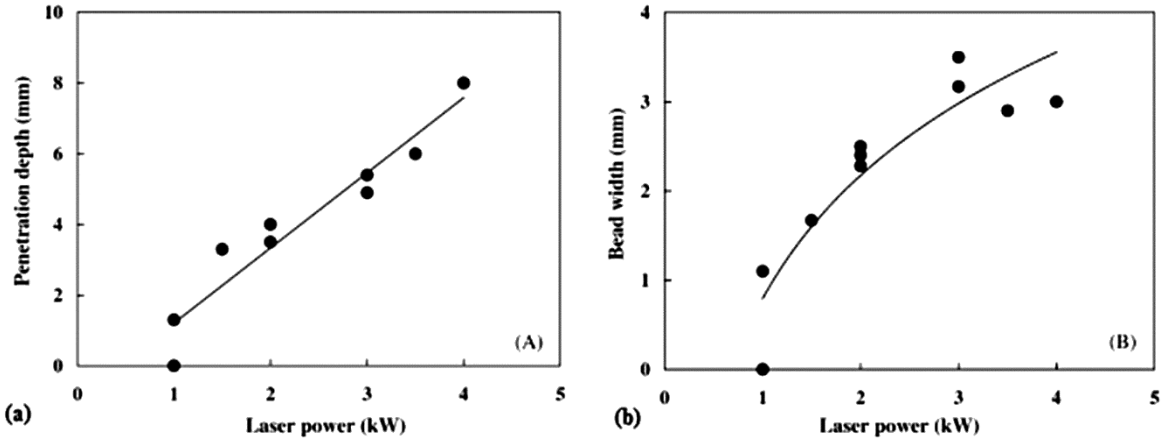

Figure 2.13 Effect of CO_2 laser power on penetration depth and bead width [51]

The use of high beam powers is associated with the formation of beads of higher depth and width and also tends to reduce ripples. It is important to mention that lower power level and lower welding speed results into better weld quality [52].

The penetration depth and bead width are also found to have a dependency on the welding speed. The relationships between welding speed and the said attributes for both CO2 and Nd:YAG laser are presented in Figure 2.14 [53].

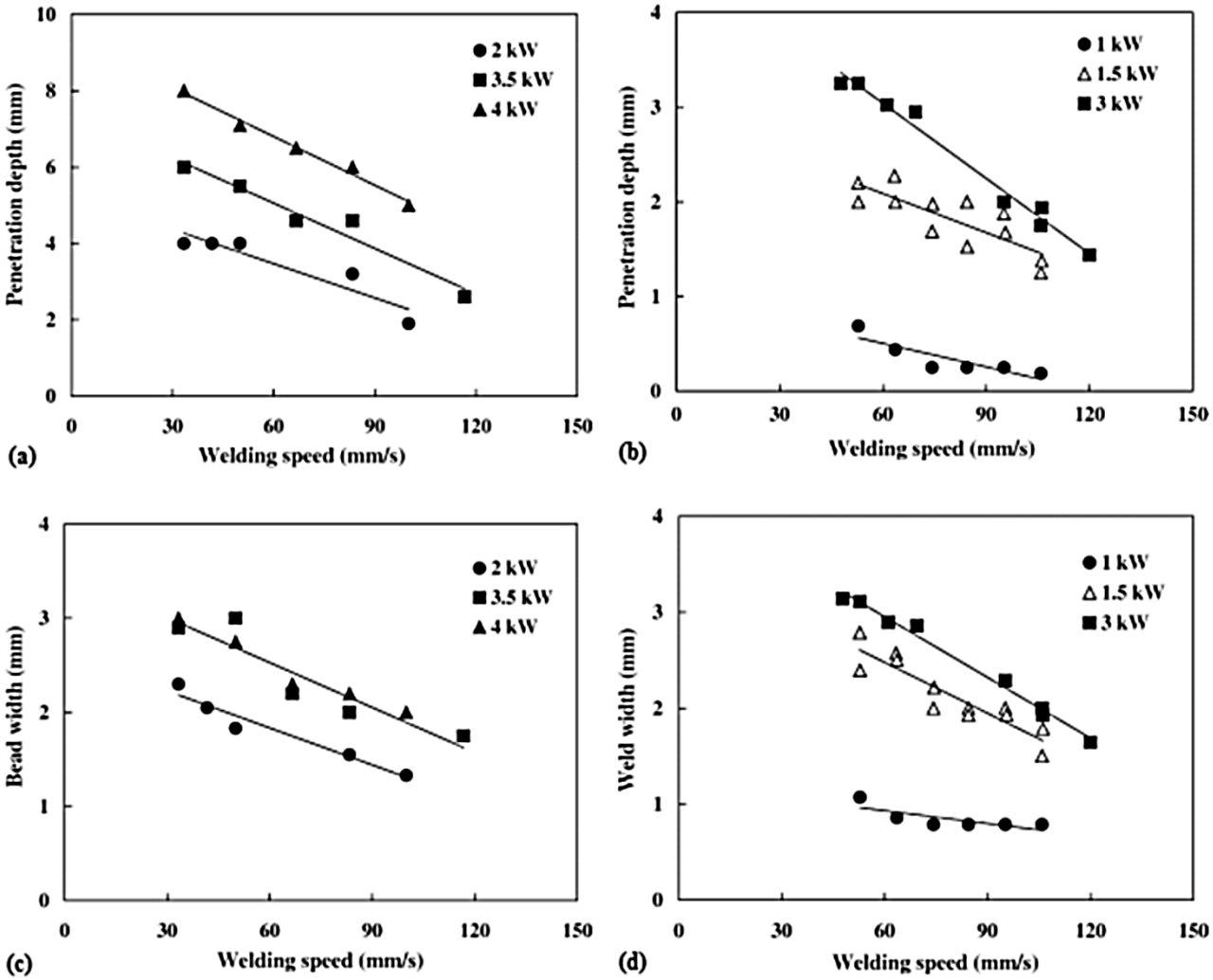

Figure 2.14 Effect of welding speed; (a,c) On penetration depth and bead width produced in WE43 alloy joints welded by CO2 laser, (b,d) On penetration depth and bead width produced in die-cast AM60B alloy joints welded by Nd:YAG laser [53]

2.4.5.3 Applications of laser cladding process

Some of the applications of laser cladding process are shown in Figure 2.15.

Figure 2.15 Applications of laser cladding process [54-59]

2.5 Stainless-clad steel

Stainless-clad steel is selected as a workpiece material in the current research work. This material is used in variety of industrial applications such as, boilers, pressure vessels, tubings, fractionators, heat exchangers, reactors and chemical plants etc. [24]. This material comprises of two layers, stainless steel layer (SS316) and mild steel layer (SA516 grade 70). The Schematic front view and 3D view of the workpiece material are shown in Figure 2.16. The two layers of material are joined together by weld overlay process. Electroslag welding methodology is adopted for performing weld overlay operation owing to the reason that this welding technique offers high deposition rates which in turns highlights its economic advantage. The chemical composition of the workpiece material is described in Table 2.2. The chemical composition of the selected material also got verified against the standard ASTM composition through optical emission spectrometry using standard method ASTM E 1676-4. It has been found that the nominal composition of the stainless-clad steel material is in agreement with the standard ASTM composition of the material.

Table 2.2 Chemical composition of stainless-clad steel

Stainless steel layer		**Mild steel layer**	
Element	**Actual (%)**	**Element**	**Actual (%)**
C	0.08	C	0.17
Si	0.83	Si	0.468
Mn	0.92	Mn	1.13
P	0.05	P	0.0420
S	0.013	S	0.0111
Cr	17.6	-	-
Mo	2.36	-	-
Ni	10.0	-	-
Fe	balance	Fe	balance

Salient workpiece material properties of the workpiece material are tabulated in Table 2.3.

Table 2.3 Workpiece material properties

Physical /Thermal Properties	**Stainless Steel**	**Carbon Steel**	**Mechanical Properties**		**Electrical Properties**	
Density	8.07 g/cc	7.8 g/cc	Hardness of stainless steel layer	50 (HRA)	Resistivity of Stainless steel layer	$81x10^{-6}$ ohm.cm
Specific Heat	0.5 J/g-°C	0.47 J/g-°C			Resistivity of mild steel layer	$17x10^{-6}$ ohm.cm
Thermal Conductivity	17 W/m-K	52.0 W/m-K	Hardness of mild steel layer	39 (HRA)	Conductivity of stainless steel layer	$12.35x10^{3}$ ohm^{-1} cm^{-1}
Coefficient of thermal expansion	16 µm/m-°C	12.0 µm/m-°C			Conductivity of mild steel layer	$58.52x10^{3}$ ohm^{-1} cm^{-1}

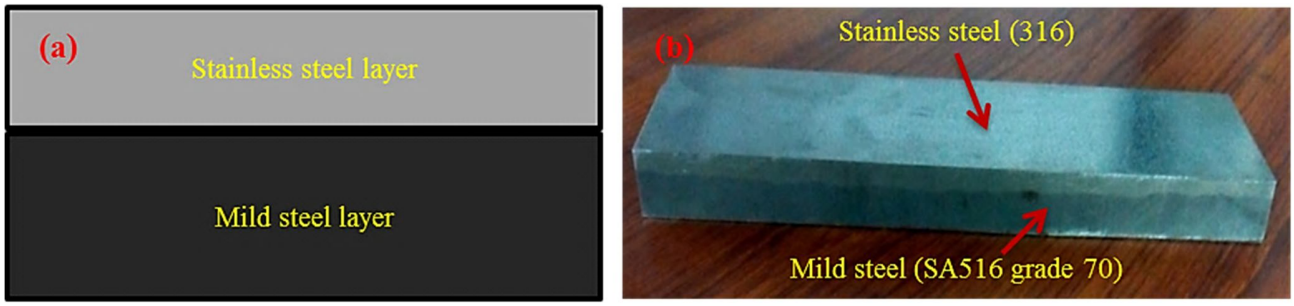

Figure 2.16 workpiece material; (a) 2D schematic front view, (b) 3D view

2.6 Chapter Summary

This chapter presented an overview of cladded materials, their need, applications and different cladding processes used in industry to develop these materials with a special emphasis on stainless-clad steel. This cladded material has variety of industrial applications such as boilers, pressure vessels, tubings, fractionators, heat exchangers, reactors and chemical plants etc. Keeping in view the industrial importance of stainless-clad steel, it is selected as workpiece material for current study. Moreover, literature described in the context of various cladding methods, it has been revealed that weld overlay cladding is the most promising choice for developing stainless-steel clad steel material and is therefore, used in present work for manufacturing the aforesaid cladded specimen.

Chapter 3

Recent Trends in Nontraditional Machining Processes

This chapter provides an overview about machining, its categories and the comparison of various non-conventional machining processes followed by a detailed discussion on the electric discharge machining process. Variants of the EDM process and effects of control factors on commonly used response attributes are also elaborated in this part of study.

3.1 Introduction to machining

Machining is defined as a manufacturing process used to attain the required shape of a part/ component by removal of material in the form of chips. The area of machining is categorized into two broader fields i.e. conventional and non-conventional machining process. Few of the differences between traditional and non-traditional machining processes are listed in Table 3.1.

Table 3.1 Typical differences between conventional and non-conventional machining [60]

Conventional Machining	**Non-Conventional Machining**
1. Material removal by macroscopic chip-formation	1. Material removal by microscopic chip-formation
2. There is a physical tool present	2. There may not be a physical tool present
3. Cutting tool is harder than workpiece	3. Cutting tool is not necessarily harder than workpiece
4. Direct contact of tool and workpiece	4. May not require physical contact between tool and workpiece
5. Material is removed by the action of shear cutting forces - energy domain is mechanical	5. Different energy domains such as thermal, mechanical, chemical, and electrochemical are used for material removal

The ever–changing demands of manufacturing industries for their sustainability in this competitive environment has stimulate the process of advance material's development to augment the industrial needs. Super alloys, ceramics, fiber composites, carbides, stainless steels, titanium and cladded material are some of the examples of such kind of advanced materials. These materials offer immense advantages in contrast to the conventional materials in terms of strength, wear resistance, resistance to degradation, strength to weight ratio etc. and has various applications such as in aerospace, nuclear, dies and molds, automobile, tools and chemical plants etc.[61]. Although, these materials offer variety of advantages but the machinability of these material with reasonable accuracy is a big challenge owing to their higher wear resistance, brittleness and low machinability with conventional means. Additionally, the requirement of high surface finish and accurate formation of complex intricate shapes are simply impossible with the traditional machining processes [62]. Therefore, non-traditional machining processes have been developed to cater with the situation which include abrasive water jet machining (AWJM), plasma arc machining (PAM), electric discharge machining (EDM) and chemical machining (CHM) etc. Some of the specific considerations that demand the use of non-traditional machining processes are [63]:

- Machining of very hard and brittle materials
- Machining of complex geometries and delicate components
- Machining of parts requiring high surface finish and tight tolerances
- Machining of parts without inducing residual stresses or producing burrs
- Mass production of microelectronic components and integrated circuits

Non-conventional machining processes are broadly classified into three categories based on the type of energy involved in the material removal process. The detailed classification is described in Figure 3.1 [64]. A brief summary pertaining to these processes is mentioned hereafter.

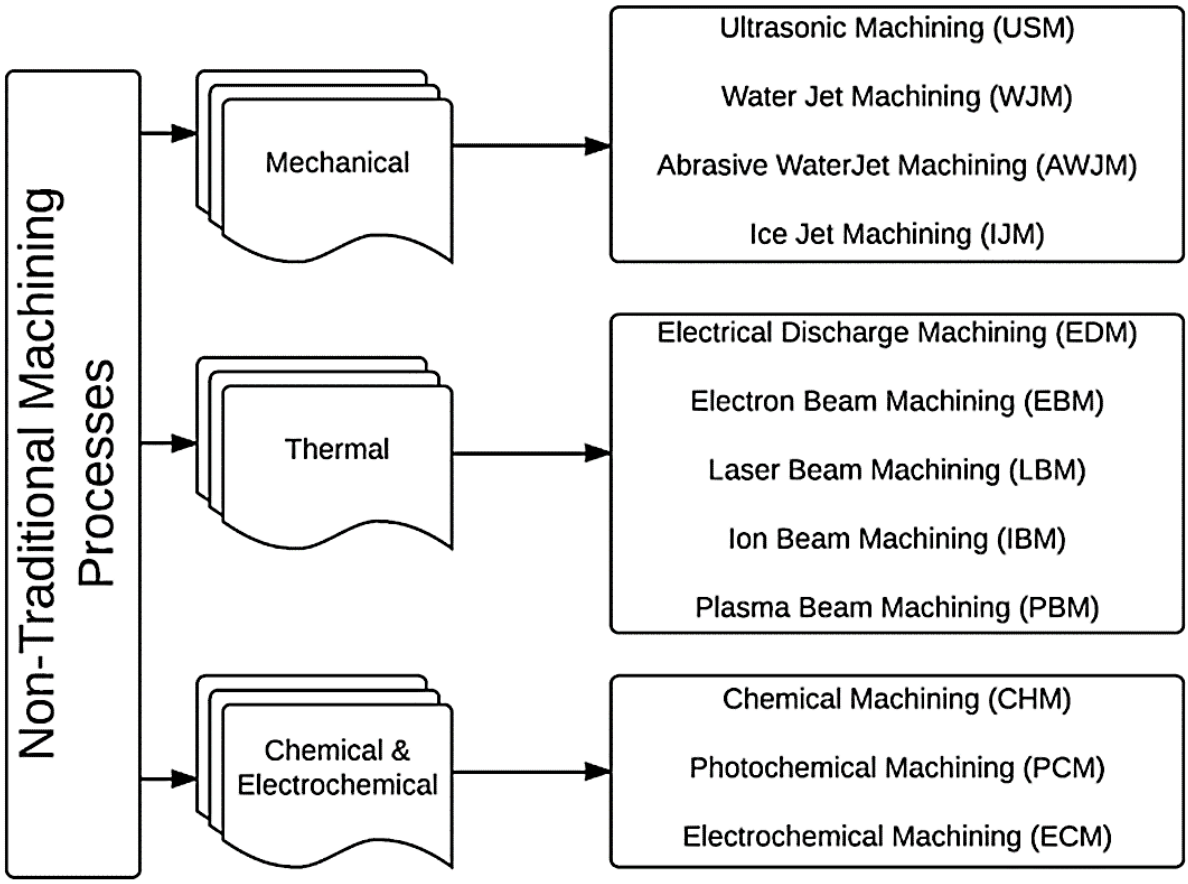

Figure 3.1 Classification of non-traditional machining processes [64]

3.2 Mechanical non-traditional machining processes (MNTM)

The basic source responsible for the material erosion process is the mechanical energy in mechanical non-traditional cutting processes. Ultrasonic machining (USM), water jet machining (WJM), abrasive water jet machining (AWJM) and ice jet machining are the common examples of non-conventional machining processes in which mechanical energy is the sole source of material removal. The schematic illustration that how these processes works is presented in Figure 3.2.

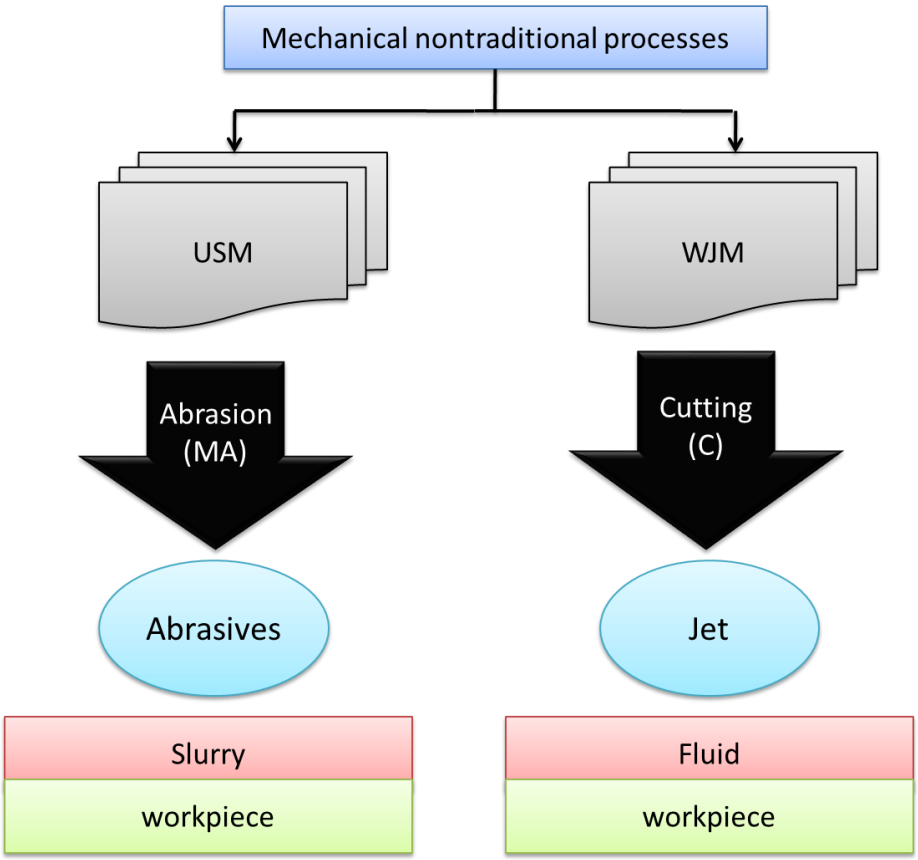

Figure 3.2 Schematic illustrations of MNTM processes [65]

3.3 Thermal non-traditional machining processes

In thermal non-traditional machining processes (TNTM), thermal energy is primarily responsible for the material removal. Electric discharge machining (EDM), laser bean machining (LBM), ion beam machining (IBM), electron beam machining (EBM) and plasma beam machining (PBM) are the typical examples of non-traditional cutting methodologies that use thermal energy to remove the material. The description of the working of these processes is shown in Figure 3.3. In EDM and PBM plasmas channel is formed that is accountable for the transfer of heat energy to the target material for its melting and vaporization. Whereas, in case of EBM, IBM and LBM electrons, protons and ions are the sources for heat transfer respectively as elaborated in Figure 3.3. The amount of material removed is mainly dependent on the amount of heat transfer that is in turn controlled by selection of the process parameters.

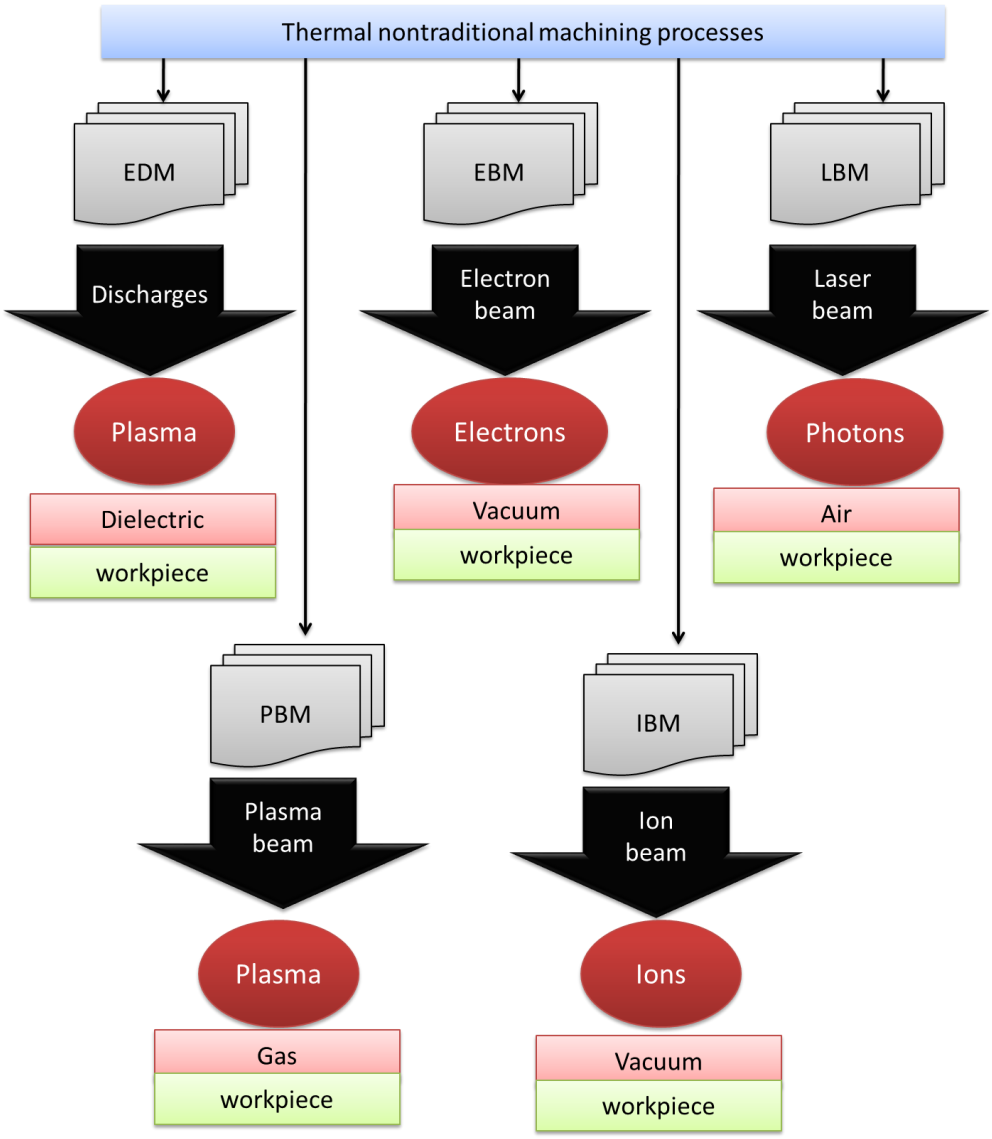

Figure 3.3 Schematics of TNTM processes [65]

3.4 Chemical and electrochemical non-traditional machining processes

Chemical reagent called as etchant is the principle source for material removal in the chemical non-conventional machining process whereas the process of electrochemical machining is an anodic dissolution of workpiece material in an electrolysis process. The working principle of this class of non-traditional machining process is schematically described in Figure 3.4.

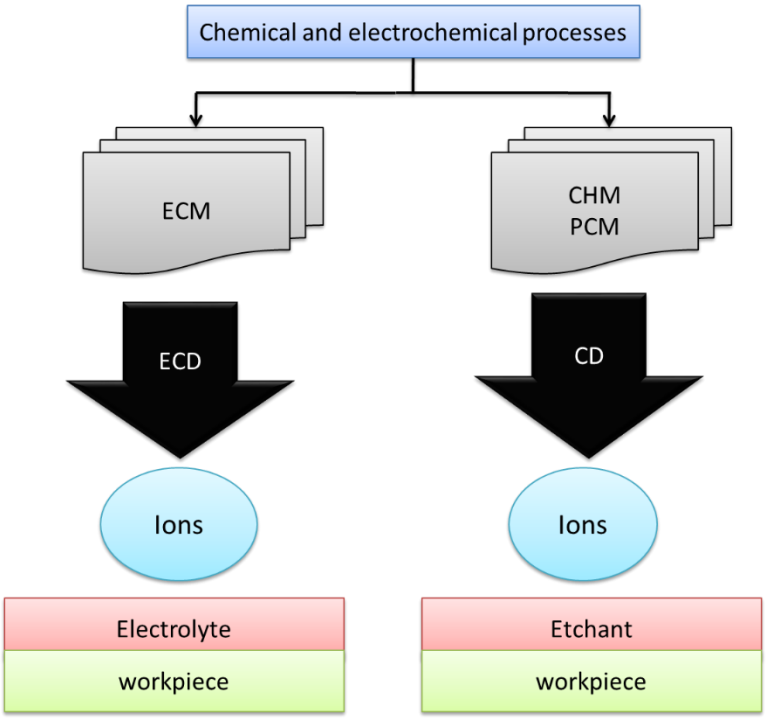

Figure 3.4 Schematics of chemical and electrochemical machining [65]

Some of the general characteristics of the above mentioned non-conventional machining processes are tabulated in Table 3.2.

Table 3.2 General characteristics of non-traditional cutting processes [66]

Process	**Characteristics**	**Process Parameters and typical material-removal rate (MRR) or cutting speed (CS)**
Chemical machining	Shallow removal on large flat or curved surfaces; blanking of thin sheets; low tooling and equipment cost; suitable for low production runs	CS: 0.0025-0.1 mm/min
Electrochemical machining	Complex shapes with deep cavities; highest rate of material removal among other nontraditional processes; expensive tooling and equipment; high power consumption; medium-to-high production quantity	Voltage: 5-25 volts; Current: 1.5-8 A/mm2; CS: 2.5-12 mm/min, depending on current density

Electrochemical grinding	Cutting off and sharpening hard materials, such as tungsten-carbide tools; also used as a honing process; higher removal rate than grinding	Current: 1-3 A/mm2; MRR: 25 mm3/s per 1000 A
Water-jet machining	Cutting all types of nonmetallic materials; suitable for contour cutting of flexible materials; no thermal damage; noisy	Varies considerably with material
Abrasive water-jet machining	Single or multilayer cutting of metallic and nonmetallic materials	CS: Up to 7.5 m/min
Abrasive-jet machining	Cutting, slotting, deburring, etching, and cleaning of metallic and nonmetallic materials; tends to round off sharp edges; hazardous	Varies considerably with material
Electric discharge machining	Shaping and cutting complex parts made of hard materials; some surface damage may result; also used as a grinding and cutting process; expensive tooling and equipment	V: 50-380 volts; Current: 0.1-500 A; MRR: Typically 300 mm3/min
Wire electric discharge machining	Contour cutting of flat or curved surfaces; expensive equipment	Varies with material and thickness
Laser-beam machining	Cutting and hole making on thin materials; heat-affected zone; does not require a vacuum; expensive equipment; consumes much energy	CS: 0.50-7.5 m/min
Electron-beam machining	Cutting and hole making on thin materials; very small holes and slots; heat-affected zone; requires a vacuum; expensive equipment	MRR: 1-2 mm3/min

3.5 Selection of non-traditional machining process

Selection of an appropriate non-traditional process for a particular situation is considered as a challenging task. An adequate knowledge of the machining process and material properties is essential to attain the desired output. Number of factors are under consideration while selecting a suitable non-conventional machining process for a specific job which include power consumption, material removal rate, machining process capability and the process economics [61]. A comparative analysis of the narrated non-traditional cutting processes are presented in for deciding the suitable process for the present research wok.

3.5.1 Comparison of power consumption and material removal rate

Adnan Akkurt [67] classify different non-traditional machining processes on the basis of power consumption and material removal rate. The classification is described in Figure 3.5. It has been noticed that

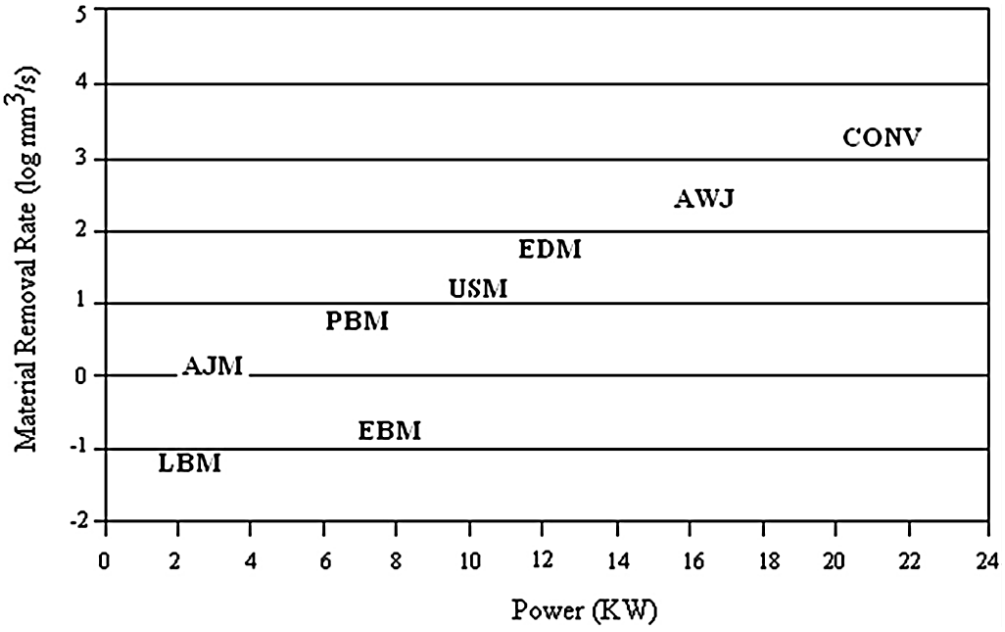

Figure 3.5 Comparison of non-traditional machining processes (NTMPs) in terms of power and material removal rate [67]

Abrasive water jet cutting process yields the maximum material removal rate among the commonly available non-traditional machining processes (NTMPs) followed by EDM. Although abrasive water jet provides the maximum material rate but the machined surface is subjected to striations. On the other end material removal rate of EDM is comparable with that of abrasive water jet and additionally the cut quality is appreciable. However, the exact choice of the non-conventional process is not only dependent on the said two attributes.

3.5.2 Machinability comparison of NTMPs for different materials

Another important factor for non-conventional machining process selection is machinability performance of the particular process for the selected material. A. Akurt [68] compared different NTMPs in terms of machinability performance while machining variety of material commonly subjected to non-conventional cutting. The results of comparison are presented in Table 3.3.

Table 3.3 Machinability comparison of NTMPs during cutting of different materials [68]

Process	**Aluminium**	**Steel**	**Super Alloy**	**Titanium**	**Refractory Materials**
USM	Poor	Fair	Poor	Fair	Good
AJM	Fair	Fair	Good	Fair	Good
ECM	Fair	Good	Good	Fair	Fair
CHM	Good	Good	Fair	Fair	Poor
EDM	Fair	Good	Good	Good	Good
EBM	Fair	Fair	Fair	Fair	Good
LBM	Fair	Fair	Fair	Fair	Poor
PAM	Good	Good	Good	Fair	Poor

It has been found that the machining performance of EDM process is adequate during cutting of the above-mentioned materials except plastics which lies in the category of insulators. Specifically, the cutting performance of EDM has been considered reasonably good as per the results mentioned in Table 3.3.

The comparison of the above narrated NTMPs in terms of machining characteristics like tolerance, surface finish, depth of surface damage etc. is presented in Table 3.4. Moreover, the comparison of EDM with plasma arc and gas cutting which are commonly used cutting methods for cladded materials is presented in Table 3.5.

Table 3.4 Machining characteristics of NTMPs [69]

Process	MRR (mm^3/min)	Tolerance (μm)	Surface finish (μm)	Depth of surface damage (μm)	Power (watts)
USM	300	7.5	0.2-0.5	25	2,400
AJM	0.8	50	0.5-1.2	2.5	250
ECM	15,000	50	0.1-2.5	5.0	1,00,000
CHM	15	50	0.5-2.5	50	----
EDM	800	15	0.2-1.2	125	2,700
EBM	1.6	25	0.5-2.5	250	150(average) 2,000 (peak)
LBM	0.1	25	0.5-1.2	125	2 (average)
PAM	75,000	125	Rough	500	50,000

Table 3.5 Comparison of thermal processes used for the cutting of cladded materials

Process	Surface finish	Depth of heat affected zones	Surface integrity	Requirement of subsequent of finishing operation	Material thickness limitation
EDM	good	smaller	better	not required	no issue
Plasma Arc	poor	high	poor	required	yes
Gas cutting	very poor	very high	poor	required	yes

Keeping in view the type of workpiece material (stainless-clad steel) considered and its application requirements, it has been found that EDM is quite a suitable machining option. The detailed description of EDM process, its variants and the effects of various control factors on the response attributes is elaborated in the forthcoming sections.

3.6 Electric discharge machining (EDM) process

EDM is basically a thermoelectric cutting process. In this process workpiece material is eroded due to the series of discrete electric sparking which occur between the electrode and the workpiece surface. The temperature of these sparks can rise upto 12000°C. Such a high temperature provides an intense localized heating that results into melting and vaporization of the target material. The melted debris produced during this cutting methodology are then removed by the flushing dielectric fluid [71-73]. The complete description of EDM process is shown in Figure 3.6.

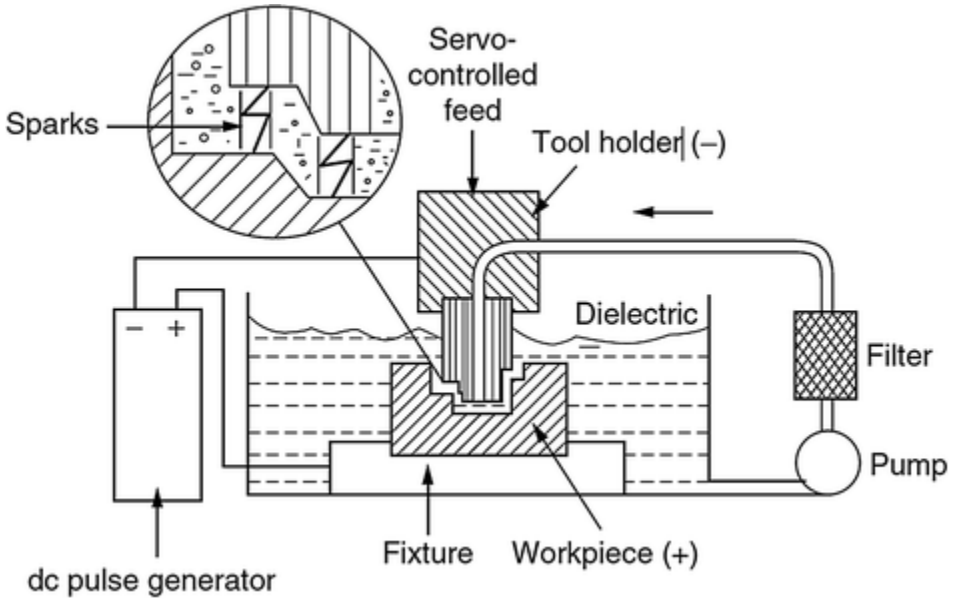

Figure 3.6 Schematic of EDM process [73]

3.6.1 Recent trends in EDM

DSEDM has proved to be a viable cutting technique in various application related to manufacturing. Different domains of this cutting methodology are under investigation in order to improve the working efficiency of DSEDM. The research domains pertaining to this process can be classified into four major classes like powder mixed EDM (PMEDM), dry EDM (DEDM), ultrasonic vibration assisted EDM (UEDM) and micro EDM (MEDM) [74].

3.6.1.1 Powder mixed EDM (PMEDM)

The use of DSEDM has been increased in industry because of its various advantages such as high surface finish and formation of intricate shapes. But the problem of tool wear, recast layer formation and low material removal rates cause a contrary effect on the performance of DSEDM. The machining performance of DSEDM can be improved by using powder mixed dielectric fluid. Actually, the use of powder increases the spark gap which in turn stabilize the machining process. The process of DSEDM has a tendency to machine a mirror like surface. The process performance is greatly influenced by the type, size and quantity of powder mixed in dielectric fluid.

Wong et al. [75] reported that mixing of powder into dielectric has a positive effect on the distribution of electrical discharges i.e. discharged distribution become uniform. This uniformity in discharge distribution permits to attain highly polished surface. It was also concluded that specimen composition also played a pivotal role in determining the surface quality. In another study, it was revealed that the use of powder (silicon) can significantly reduce the time required to achieve the mirror like surface [76]. The process of PMEDM can also be applied for the surface modification. R. Toshimitsu et al. [77] narrated that the cut surface of D53 steel has become hardened and corrosion resistant when machined through PMEDM. This increase in the said material properties was due to the penetration of Cr into the surface.

The powder material is also of significant importance with regard to the machining characteristics of the PMEDM. Talla et al. compared the performance of three types of powder materials namely; aluminium, graphite and silicon during cutting of Inconel 625. Material removal rate was noticed to be maximum when cutting was done using Al powder upto 6 g/l concentration level. Graphite powder provides better cutting performance at higher concentration levels. The highest surface finish was obtained by using the silicon powder. Moreover, maximum micro hardness and minimum radial overcut was observed by using the silicon powder. The smaller value of electrical and thermal conductivity is the basic reason for providing the said effects. On the other end higher thermal conductivity of graphite is likely to reduce the surface micro-cracking. As maximum heat is carried away by the graphite powder due to its higher thermal conductivity. Hence, micro-cracking reduces.

3.6.1.2 Dry EDM (DEDM)

Generally, in DSEDM kerosene oil is used as a dielectric that has a detrimental effect on the environment. The toxic fumes generated during the cutting process is really a critical concern regarding the health of the operator [78]. DEDM process was developed to handle the environmental concern. This process offers various advantages in contrast to the DSEDM like, reduction in cost of waste management, compacting size of EDM as need of dielectric fluid tank is no more there, residual stresses and reaction forces produced during the process are minimal as highlighted in Figure 3.7.

Figure 3.7 Benefits of dry EDM [79]

In DEDM process, a high pressure gas is used as a dielectric medium. The electrode used in DEDM has a hole in it through which dielectric is provided in the spark gap. The shape of the electrode is just like a thin walled pipe. As the electrode achieved the spark gap, plasma channel is formed. Consequently, target material gets melted and vaporized due to localized heating generated by plasma channel. The complete description of the process is demonstrated in Figure 3.8.

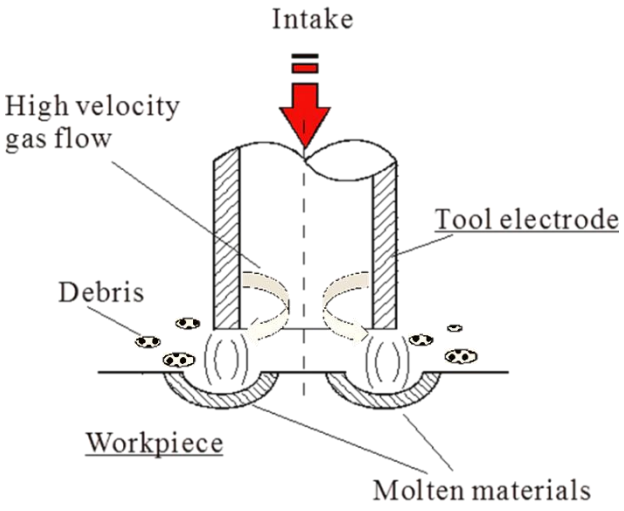

Figure 3.8 DEDM process schematic [80]

The comparison of DEDM milling with oil EDM milling has shown that not only material removal rate has been increased by using DEDM but also this technique reduces the tool wear as described in Figure 3.9 [81].

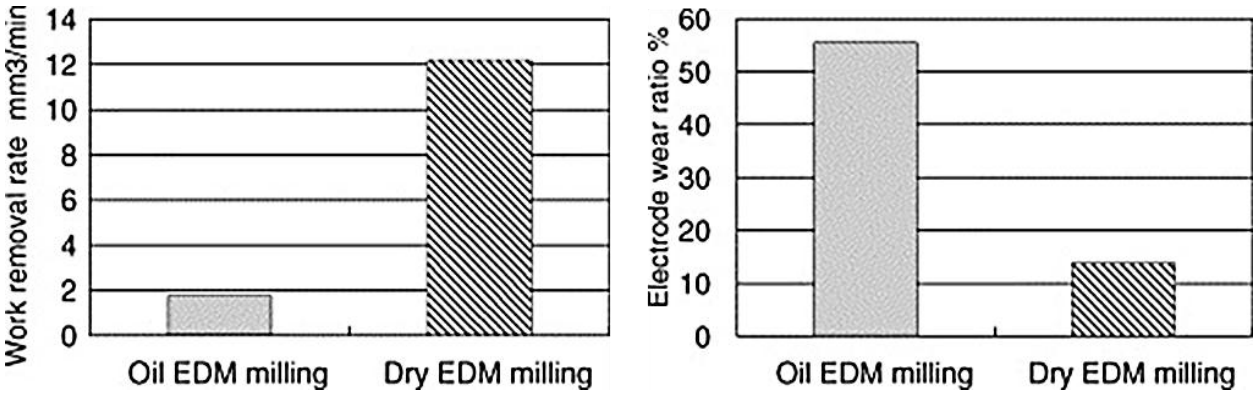

Figure 3.9 Comparison of DEDM and oil EDM milling [81]

The material removal rate can be further improved in DEDM by providing the oxygen gas into the sparking gap. The supply of oxygen is provided through a small hole in the electrode. The presence of oxygen enlarge the discharge crater volume and also promote the discharge occurring frequency [82]. Govindan et al. reported that electrode rotational speed, discharge current and gap voltage were the significant control factors with respect to material removal rate in the mentioned cutting process. Furthermore, it was also stated that tool wear is approximately negligible in DEDM [83]. The potential of DEDM has also been tested for micro machining. Material removal rate in micro DEDM is much better in comparison to the traditional EDM which uses kerosene as dielectric. The only limitation of DEDM process is that it cannot be used for accurate machining of deep holes. As with the increase in the depth of the hole the evacuation of melted debris become difficult. The melted debris that were not removed from the spark gap complicates the machining process [84].

3.6.1.3 Ultrasonic vibrations assisted EDM (UEDM)

Although the process of EDM has many advantages but the formation of recast layer deteriorates the quality of machined surface. The debris that are not cleaned effectively by the dielectric fluid are the fundamental source of this phenomena. The amount of material removal also reduces due to re-deposition of melted debris [85]. Ultrasonic vibrations are induced in tool electrode to minimize this problem. The prime role of these vibrations is to facilitate the ejection of molten material through an effective dielectric circulation. UEDM process is specifically considered quite suitable for obtaining higher surface finish at a lower discharge energy [86]. Jahan et al. mentioned that vibrations induced in workpiece has also a positive impact on cut quality. Furthermore, amplitude and frequency of vibrating workpiece were found to be the vital control parameters in defining the optimal cutting conditions [87] . Workpiece vibration can increase the cutting speed thrice as compared to the cutting speed without workpiece vibrations [88]. The schematic illustration of the working principle of UEDM is presented in Figure 3.10.

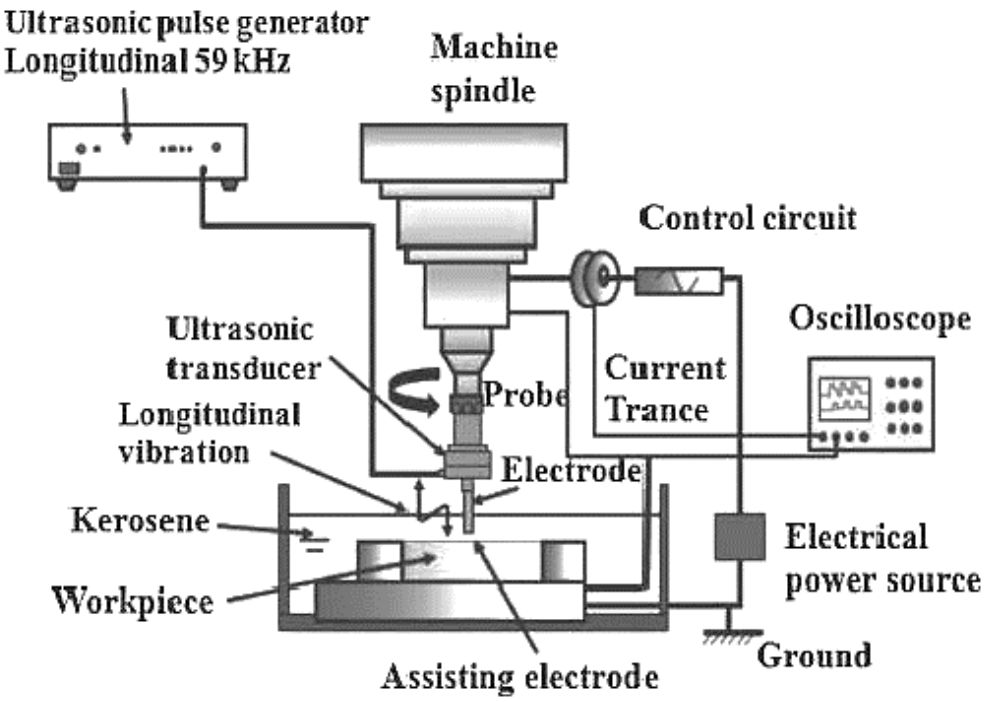

Figure 3.10 Schematic of UEDM process [89]

Manwangi et al. [89] studied the effect of dielectric fluid and workpiece vibrations on material removal rate, tool wear rate and surface roughness. Results revealed that vibrations has a positive impact on the said responses. Moreover, the use of deionized water provides the maximum material removal rate. However, surface finish produced by deionized water dielectric was observed to be inferior in comparison to the finish produced by kerosene oil. Also the tool wear rate was seemed to be higher in the case when deionized water was used as dielectric as depicted in Figure 3.11 and Figure 3.12.

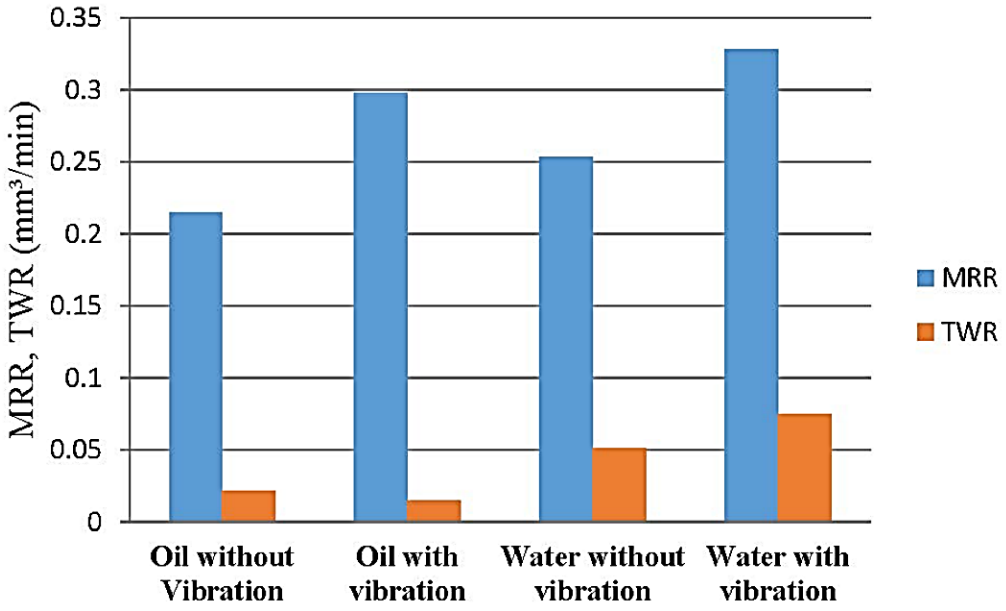

Figure 3.11 Effect of workpiece vibrations and dielectric medium on MRR & TWR [89]

Vibrations imparted to the tool electrode was also proved beneficial regarding the evacuation of machining debris for the spark erosion zone. Additionally, electrode vibrations also improves the machining stability [90]. The surface finish and material removal rate are further enhanced if ultrasonic vibrations has been coupled with tool rotation [91].

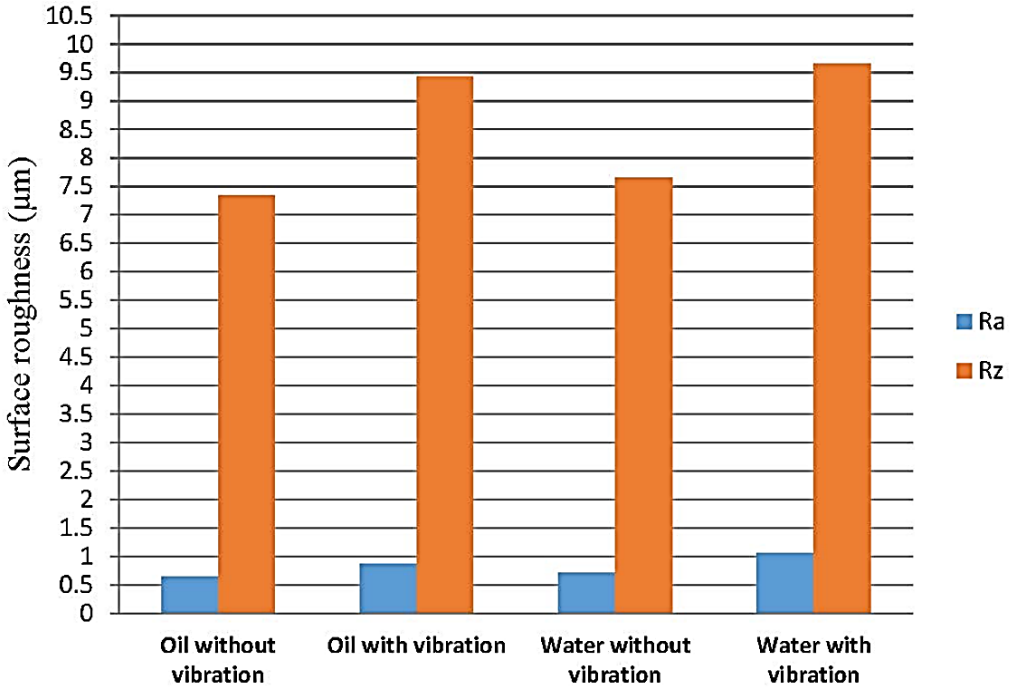

Figure 3.12 Effect of workpiece vibrations and dielectric medium on surface roughness [89]

3.6.1.4 Micro EDM (MEDM)

The process of EDM has not only been useful but it has proved to be equally good at micro level as well. The intricate micro features that were considered impossible to develop with conventional EDM can be precisely machined using this cutting methodology[92]. The working principle of MEDM is alike as that of ordinary EDM with the only difference that it has an RC relation type generator. The role of this generator is to provide the low spark energy so that small amount of material gets eroded from the target material [93-94]. The illustration of the setup of MEDM is presented in Figure 3.13. The process of MEDM is controlled by number of parameters. Various researches were conducted in the past to evaluate the effect of different factors on the machining performance of MEDM.

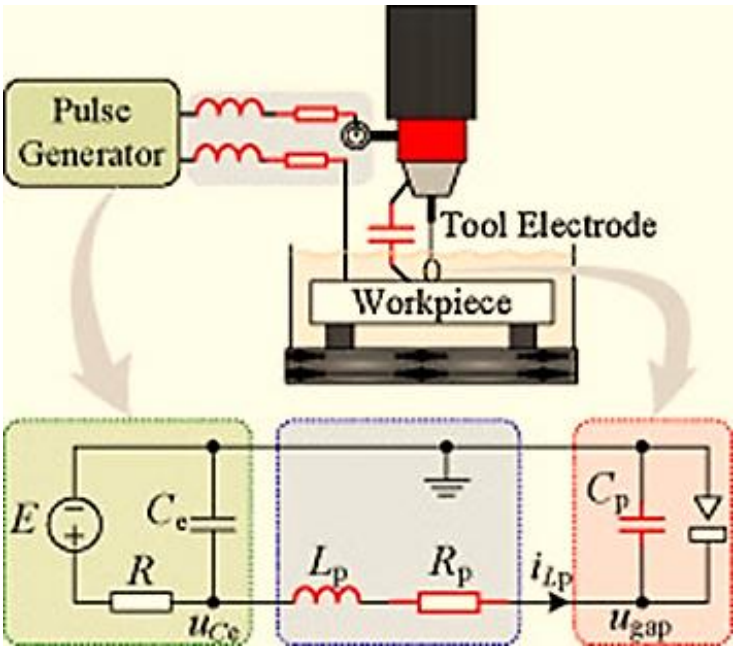

Figure 3.13 Schematic of MEDM circuitry [92]

Rasheed et al. [95] studied the impact of MEDM parameters on the material removal rate, tool wear rate and surface finish. It has been noted that material removal rate and surface finish of the machined part were mainly dependent on capacitance, material of the tool electrode and the discharge voltages. Moreover, lower discharge energy resulted into smaller tool wear and fine surface finish. The maximum material removal rate was provided by the tungsten electrode material during machining of NiTi SMA workpiece material. However, brass electrode yields the minimum surface roughness. The efficiency of micro EDM is further enhanced if it coupled with the ultrasonic vibrations [96]. Actually, the induction of vibrations tends to improve the flushing of melted debris and therefore machining efficiency increases. The machining efficiency is increased by about 60 times without causing a noticeable increase in the tool wear. The induction of ultrasonic vibrations in EDM has yielded a valuable effect in micro drilling as well. Holes having a diameter lesser than 200 μm and depth to diameter ratio of 15 can be precisely drilled using UEDM [97]. The accuracy of holes has been improved if vibrations are induced in workpiece rather than in the tool electrode [98].

3.7 Variants of EDM process

The process of EDM is broadly classified into two categories i.e. die-sinking EDM (DSEDM) and wire EDM (WEDM). This classification is based on the type of electrode. If the electrode is a female of the impression of the cavity to be produced, it is termed as DSEDM whereas if a wire electrode is used for machining, this type is known as WEDM. Both the variants are presented in Figure 3.14.

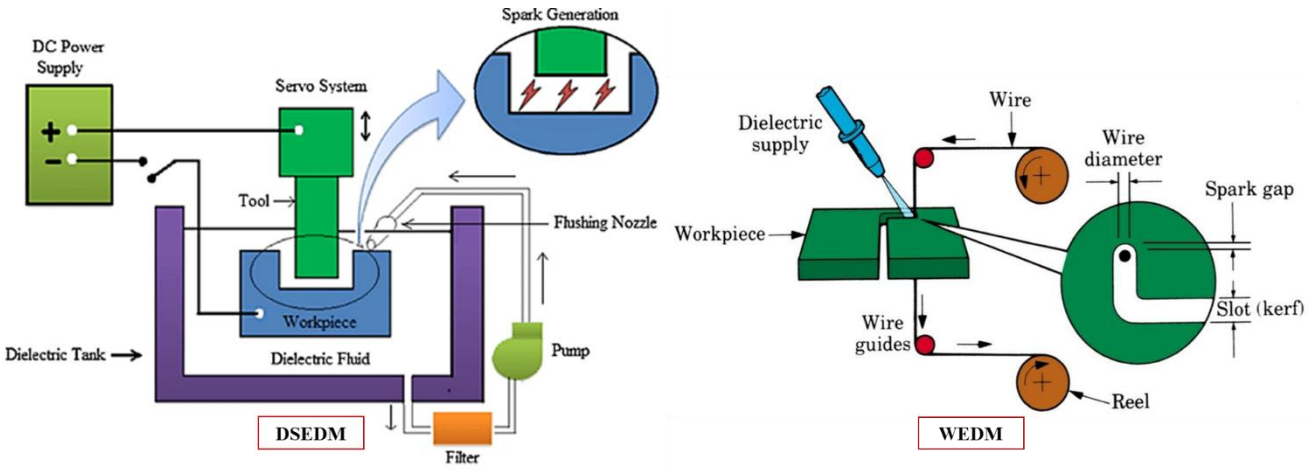

Figure 3.14 Schematics of DSEDM and WEDM[99][100]

3.7.1 Die-sinking EDM (DSEDM)

DSEDM is a widely used non-traditional machining process ion manufacturing industry today especially, in dies and molds. The target material is shaped into desired geometry by the thermal erosion of material. Parts requiring high finish as that of aerospace and automobiles are machined with the aid of this cutting process [101-102].

The DSEDM cutting methodology was introduced by two scientists B.R Lazarenko and N.I Lazarenko in 1940. Later on in 1967 first EDM equipment was developed by the scientists of Soviet Union [103]. In DSEDM both the workpiece and the electrode are immersed into a dielectric fluid. The material is removed through thermal erosion process.

The thermal energy required for the material erosion is being provided by the discrete sparks occur between the electrode and the workpiece material. This gap (between electrode and the workpiece) is termed as spark gap and is usually in the range of 0.005 – 0.05 mm [104-106]. The formation of electrical sparks in the spark gap tends to produce the localized heating. The temperature produced by these sparking is sufficiently high. As a result the target material is melted and vaporized. The melted debris produced during the cutting process are then flushed away by the circulating dielectric fluid. The dielectric fluid is usually oil and kerosene oil [107]. The process is completely demonstrated (schematically) in Figure 3.15. The only limitation of the process is that both workpiece and the electrode material should be conductor of electricity.

The process of DSEDM is controlled by number of parameters which include electrical parameters (pulse frequency, pulse on time, pulse off time etc.), non-electrical parameters (electrode lift time, working time etc.), powder based parameters (powder density, grain size etc.) and electrode based parameters as elaborated in Figure 3.16 [108]. The correct choice of these parameters is essential to ensure the desired surface quality. Therefore, parametric optimization is still a hot area in EDM research. The involvement of large number of input parameters and stochastic nature of the process really demands the optimal parametric combination to maximize the process output [109] . Some of the applications of DSEDM are mentioned in Figure 3.17.

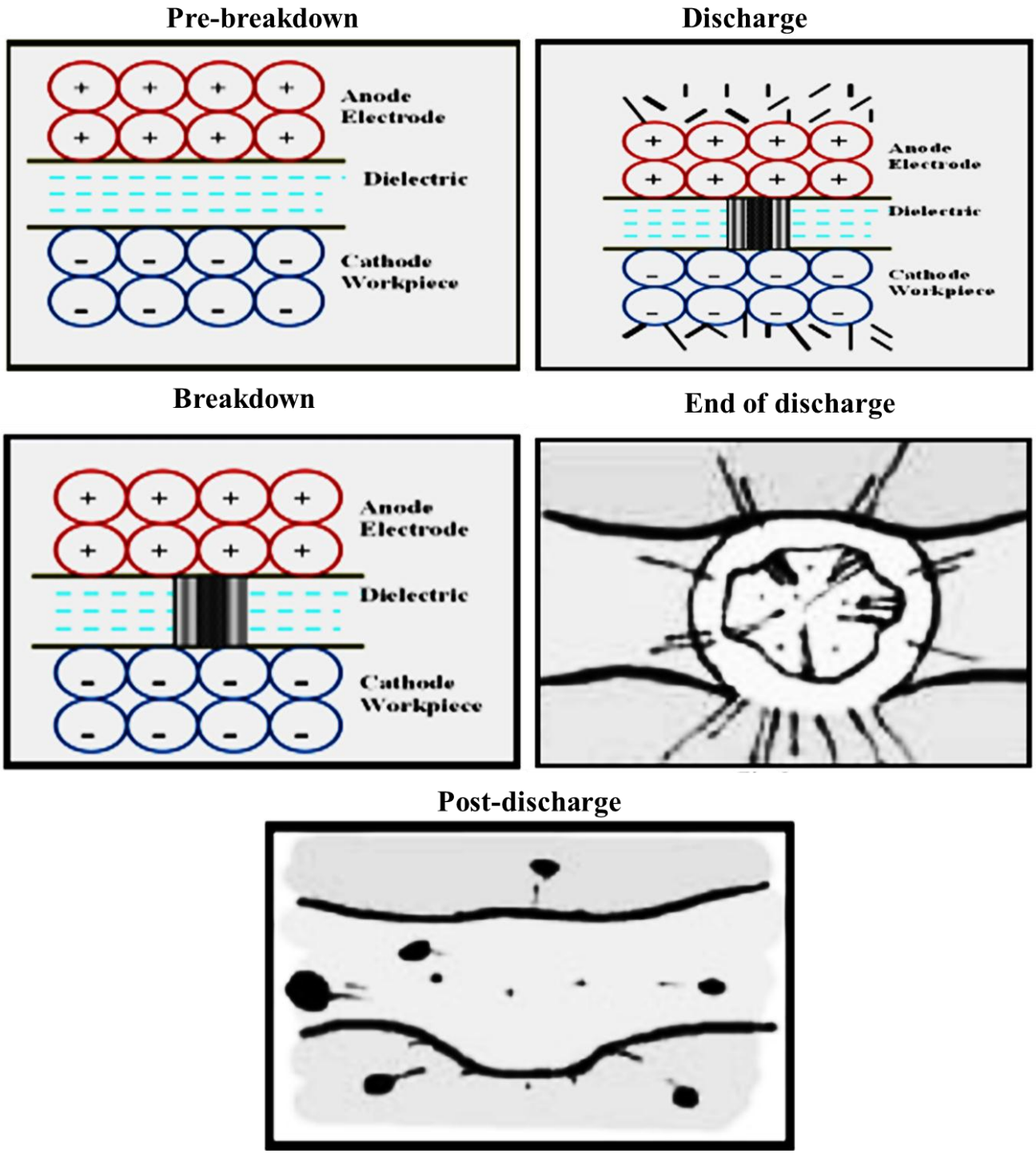

Figure 3.15 Description of DSEDM process [107]

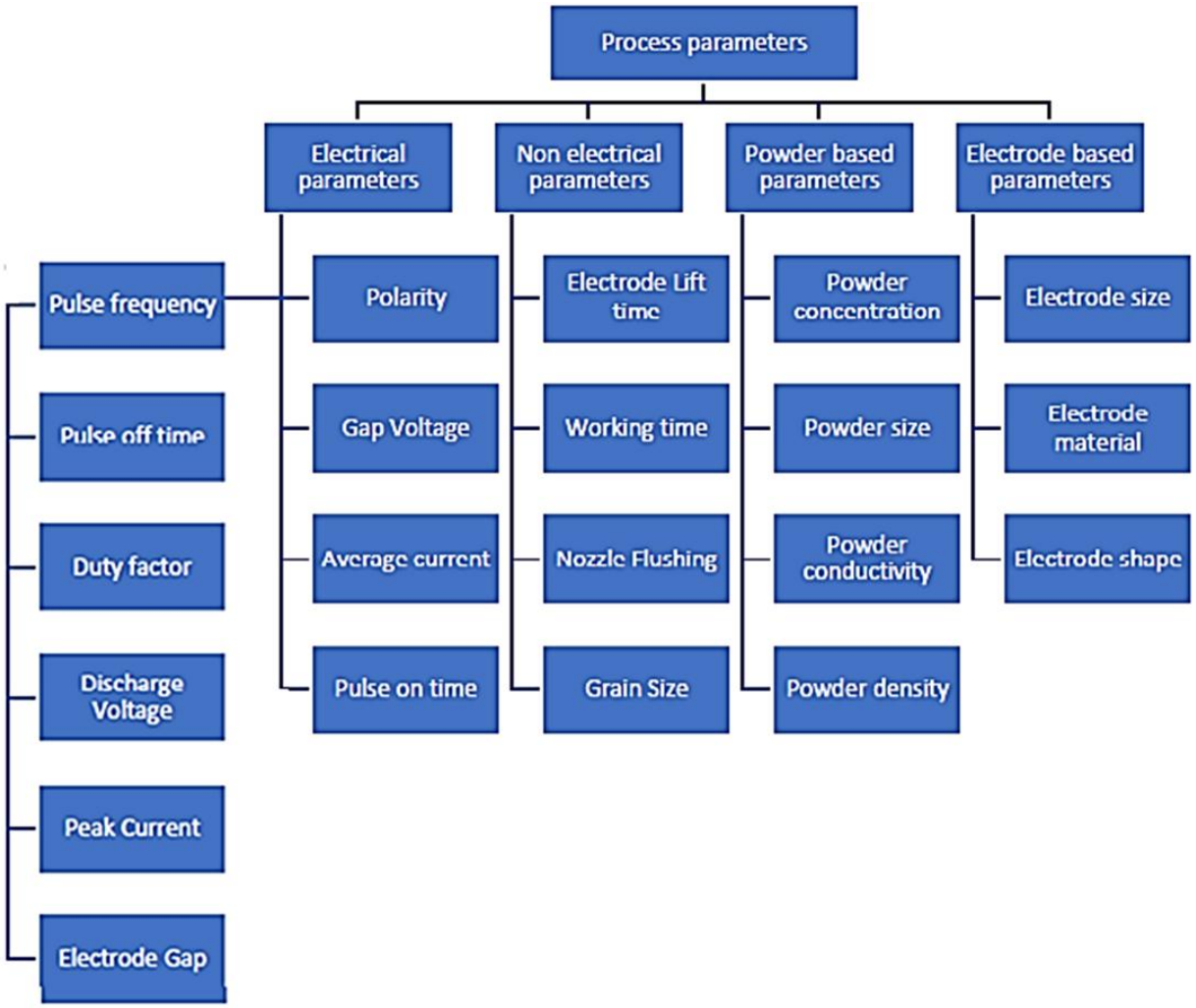

Figure 3.16 DSEDM process parameters [108]

Figure 3.17 DSEDM applications [110]

3.7.2 Wire electric discharge machining (WEDM)

WEDM is basically the modification of DSEDM. In this variant of EDM, electrode is a thin wire instead of a solid electrode as that was in DSEDM. The formation of sharp corners that were difficult to machine through ordinary EDM can be conveniently machined with this cutting mechanism. The formation of recast layer and depth of heat affected zone has also been smaller in case of WEDM. Surface finish provided by WEDM has also been superior in contrast to that of formed in DSEDM. These inherent advantages of WEDM makes it a more attractive option as compared to DSEDM.

In 1960's the technique of WEDM was introduced in the manufacturing sector and then gained a popularity of a promising cutting methodology for machining harder, wear resistant and high strength materials. The formation of intricate shapes that was a huge challenge with the conventional means can be precisely produced with the aid of WEDM [8]. The non-contact nature of the process eliminates the chances of vibrations, mechanical stresses and chatter which are prominent issues associated with conventional machining processes [9].

This cutting technique has been widely applied in various industries like in dies & molds, chemical, medical, aerospace and automotive. The working principle of this cutting technique is quite alike as that of DSEDM with the only difference that in WEDM continuously moving brass wire electrode has been used instead of a solid electrode. The continuous feeding of the brass wire electrode thus improves the surface quality as each time fresh wire electrode come in contact with the target material. Whereas, in case of DSEDM this is not the case. A single electrode undergoes repetitive sparks due to which the electrode surface gets eroded and subsequently reduces the cut quality. Therefore, the use of WEDM process has become more demanding in industry. In wake of the above motioned reasons WEDM has been found more appropriate for the current study.

Presently, the research carried out in the field of WEDM can be broadly classified into two distinct categories i.e. process monitoring, control and process optimization [111].

3.8 Process monitoring and control

The success of WEDM process mainly rely on effectiveness of the monitoring and control system. The complex nature of WEDM process imparts cutting instability. Although, parametric optimization minimizes the chances of cutting instability but still issue of cutting stability persist. Actually, the chance of unpredictable and transient conditions during WEDM cutting process are always there. Therefore, an effective adaptive control system must be in placed to ensure effective monitoring of the ongoing cutting process [112]. Generally, two types of adaptive control systems are used i.e. fuzzy adaptive control system and self-tuning adaptive control system. An overview about both systems is described in this part.

3.8.1 Fuzzy control system

In fuzzy adaptive control system usually proportional controllers are used for servo feed control mechanism. The prime responsibility of this system is to maintain a safe sparking gap during machining. However, the output of the controller has also been influenced by the machine parametric settings [113]. To improve the performance of the aforementioned control system various models were developed which include, explicit statistical models, mathematical models and algorithms [114-117]. Liao et al. introduced the discrimination system of pulse in order to quantitatively monitor the machining conditions and pulse train [118]. On the other end, these systems have a limitation that sparking gap will not be maintained if unexpected disturbance occur [119]. In another research work, fuzzy controller based on the discharge pulse characteristics has been designed. The noise associated with the discharge pulse was isolated from the pulse with the aid of online monitoring system of the pulse. The ignition delay discernment for each of the discharge pulse was also applied. The developed control system was observed to be adequate in terms of improving the machining performance of WEDM operation [120].

The fuzzy logic can also be a helpful tool in achieving the optimal combination of machining parameters as well [121]. Additionally, fuzzy controller does not require complex mathematical models for interpreting the dynamic behaviour of WEDM operation [122].

Yilmaz et al. [123] stated that the use of fuzzy logic is not limited to the controller application in WEDM. It can be a useful tool for the selection of control factors in WEDM as well. Shabgard et al. [124] has also witnessed that fuzzy logics can be successfully applied for the selection of control factors in electric discharge machining process.

3.8.2 Self-tuning adaptive control system

Self-tuning adaptive control system was developed to make the cutting process of WEDM more robust. The main theme of this system was to make the WEDM equipment to automatically adjust in accordance with the varying height of workpiece and spark gap. The purpose of this online monitoring was to ensure that cutting action can take place smoothly without any wire breakage. As frequent wire breakage is always undesirable because it reduces the surface quality and also the productivity of the process is compromised [125].

Zhang et al. [126] developed a technique for on-line monitoring of WEDM process. This system helps to identify and segregate the discharge pulses into five categories, like open circuit, spark, transient arc, arc, and short circuit. Based on the recognition of the type of discharge pulse the adaptive control system adjusts its output to improve the machining stability.

Another way to minimize the inherent problem of wire breakage is through determining the unstable discharge pulse ratio along with discharge energy on micro level time scale. The WEDM parameters like discharge voltage, pulse off time and peak current were considered in this study. The aforesaid factors were considered responsible for determining the dynamic behaviour of the process. Machining feed rate and surface finish were seen to be upgraded by employing the developed control method [127].

Cabanes et al. [128] designed a system based on discharge parameters (discharge energy, peak current, and ignition delay time). This control mechanism detects instability in the cutting process by comparing the values of discharge parameters at a particular instant with the predefined reference values of aforementioned parameters. Any irregularity observed in the process was communicated by an alarm triggering.

In another study, spark distribution phenomena was investigated using high speed camera based on the presumption that spark distribution has a vital role in governing instability in WEDM. Experimental results revealed that higher value of servo voltages and pulse off time yield a uniform distribution of spark. Lower wire speed was also seemed to have a positive impact on spark distribution [129].

Hoang and Yang introduced a new methodology for ensuring the safe sparking gap to reduce the chances of wire rupture. This approach was based on the relative movement of wire electrode and workpiece. This control strategy provides a real-time estimation of cutting rate and height of workpiece by approximating discharge parameters such as discharge current, voltage and frequency. Additionally, the effect of workpiece vibrations on flushing of debris was also investigated. It was noticed that not only machining stability has been increased but the cutting time has also been shortened by applying the purposed method [130].

Another control strategy was devised by Caggiano et al. [131] to enhance the machining stability. In this control mechanism voltages and current signals form the spark gap were used to envisage the cutting constancy. Any abnormality occurring in the spark gap would alter the signal, showing that an undesirable situation arises. The information regarding the spark discharges (spark frequency, short circuit ratio, ignition delay time) were also extracted from the received signals. Surface defects can also be approximated with the aid of developed model. Artificial neural network analysis revealed that there exists a strong relationship between signal features and surface imperfections [132].

3.9 Process optimization

This section provides an overview about the effect of different process parameters on commonly used response attributes like productivity, cut quality and dimensional accuracy. In the present study, cutting speed/ cutting rate accounts for the productivity aspect whereas, cut quality and dimensional accuracy are determined in terms of surface roughness and spark gap.

The process of WEDM is controlled by number of parameters. A slight change in any parameter may led to change the process output in a complex manner. The problem is not completely solved yet and therefore, the area of process optimization is still a prominent research area in the field of WEDM. It's quite essential to find the optimal parametric combination to obtain the desired level of performance characteristic to justify the process economics.

Researchers have tried different experimental design techniques and process modeling methods to optimize the machining performance of WEDM. However, the influence of parameter with regard to the selected response attribute must be evaluated before finding the optimal level. The detail of the effects of different WEDM parameters on the selected output variables is described in forthcoming sections.

3.9.1 Effect of WEDM input parameters on cutting speed/cutting rate

Numerous researches have been reported in the past related to this important response characteristic while cutting variety of materials using WEDM. Bobbili et al. [133] studied the effect of six WEDM input parameters namely, pulse on-time, pulse off-time, servo voltage, wire feed, flushing pressure and wire tension on cutting rate during WEDM high strength armor steel. Cutting rate was found to be increased with the increase in pulse on-time while reverse seemed to be true for off-time and servo voltage. In another study, carried on WEDM of Nimonic C-263 super alloy using multi-cut strategy, on-time, off-time and servo voltage were found to be the most influential process parameters for cutting rate [134]. Cutting rate was also observed to be affected by arc off-time, servo voltage, wire feed and wire tension in WEDM of tungsten [135]. M. P. Gopal et al. [136] reported that pulse on-time and reinforcement percentage were the two most influential parameters that affect cutting rate during WEDM of hybrid metal matrix composite (Mg/BN/CRT). In another research the impact of WEDM input parameters on cutting speed during machining of titanium was evaluated. The study concluded that pulse on-time, pulse off-time and servo voltage were the most contributing factors for cutting speed [137]. Pulse on-time was proved to be the most influential factor for cutting speed in case of machining AISI D3 tool steel [138]. Vikram Singh et al. [139] reported that pulse on-time, pulse off-time and servo voltage were the significant factors for cutting rate in WEDM of AISI D2 steel. Cutting speed increases with the increase in pulse on time and decreases with the increase in pulse off-time and servo voltage in wire electric discharge cutting of Ti-6-2-4-2 Alloy [140]. The cutting performance of zinc coated wire in terms of cutting speed was evaluated for machining high speed steel (M2, SKH9) in another research work. Results revealed that pulse peak current, pulse duration, pulse off period and wire feed were the influential parameters for selected response characteristic [141].

It was also reported that surface quality reduces as cutting rate increases. An increase in cutting rate was observed with the increase in dielectric fluid pressure whereas reverse seemed to be true in case of wire tension, linear velocity of wire and dielectric electrical conductivity in WEDM of ASP30 steel [142]. Machining feed rate was also seemed to have a significant effect on cutting rate. Increase in feed rate resulted in increasing the cutting rate [143]. Cutting rate was also observed to be influenced by pulse off-time, power, and pulse frequency in WEDM of high strength low-alloy (HSLA) steel [144]. The effect of wire diameter on cutting rate in WEDM was investigated in another research work. The study concluded that smaller diameter wire found to be the most effective for increasing the cutting rate [145].

3.9.2 Effect of WEDM input parameters on surface roughness

N. Tosun stated that surface finish that accounts for the final quality of the machined part is of supreme importance among the other performance characteristics [146]. Surface roughness is an important machining attribute that accounts for the surface finish of the machined component. A high quality surface finish tends to improve corrosion resistance, wear resistance and fatigue strength of the target material [147]. Therefore in the current research work, the cutting performance of the WEDM has been investigated in terms of surface roughness that mainly influence the machined surface properties.

Noticeable research work has been carried out in the past to improve the surface finish in WEDM of various materials. The effect of six WEDM parameters on the surface roughness was investigated by Ravindranadh Bobbili et.al. [133] in WEDM of high strength armor steel. Surface roughness was found to increase with the increase in pulse on-time whereas increase in pulse off-time and servo voltage reduces the surface roughness. The other parameters such as wire feed, wire tension and dielectric pressure have no significant effect on surface roughness in WEDM of high strength armor steel. In another study on WEDM of 572-grade 50 HSLA steel, it was reported that pulse on time, pulse off time, peak current have a significant effect on surface roughness. It was also revealed that pulse on-time was the most contributing factor for controlling the surface roughness [148].

G. Selvakumar et al. [138] & P. Raju et al. [149] also witnessed that pulse on-time was the most influential factor for surface roughness during WEDM of AISI D3 tool steel and 316L stainless steel respectively but in another research work carried out on WEDM of 316L it was found that pulse on-time and servo voltage were the significant factors for surface roughness [150]. However, pulse on–time and pulse off-time have shown little influence on surface roughness in WEDM of Nimonic C-263 super alloy. It has also been reported that surface roughness can be reduced by using multi-cut strategy.

Furthermore, it was observed that the multi-cut strategy also minimized the thickness of recast layer [134]. R. T. Yang et al. [135] reported that flushing pressure and pulse on-time were the significant factors for controlling the surface roughness of wire electric discharge machined specimen. In another study carried out on WEDM of SAE 4140 steel by N. Tosun et al. [146], the impact of four WEDM input parameters namely; open circuit voltage, pulse duration, wire feed and dielectric pressure on surface roughness was evaluated.

Surface roughness found to increase with the increase in pulse duration, open circuit voltage and wire feed whereas increase in dielectric pressure reduces the surface roughness. K. Kumar et al. [141] studied the effects of six WEDM parameters on surface roughness and cutting rate using zinc coated brass wire while machining high speed steel (M2, SKH9). Results revealed that pulse peak current, pulse duration, pulse off period and wire feed were the influential parameters for both response characteristics. It was also reported that surface quality reduces as cutting rate increases. In another research work, the effect of wire diameter on surface roughness was evaluated in WEDM of Inconel 706 [35, 145]. It was found that smaller diameter wire resulted into smaller value of surface roughness.

Vikram Singh et al. [139] described that surface roughness was found to be mainly dependent on pulse on-time and servo voltage while cutting AISI D2 steel. In another study, the impact of six WEDM input parameters namely; pulse on-time, pulse off-time, peak current, wire feed, wire tension and servo voltage on surface roughness was investigated. The study concluded that pulse on-time was the most contributing factor for surface roughness [137]. Similar trend of pulse on-time was narrated by another researcher in WEDM of D2 tool steel [151]. In another investigation carried out on WEDM of stainless steel (304), it was concluded that surface roughness of machined specimen was influenced by pulse on-time, wire feed. However the percentage contribution of pulse on-time was found to be larger [152]. Pulse on-time was found to have an inverse relationship with surface roughness in WEDM of duplex stainless steel (2205) [153].

3.9.3 Effect of WEDM input parameters on spark gap

Spark gap is basically a measurement of the material got wasted during WEDM. The dimensional accuracy of the finished part is primarily dependent on this aspect [154]. However, the magnitude of spark gap is mainly controlled by the kerf width produced during machining [155]. Increase in kerf width always causes a correspondent increase in spark gap.

Numerous studies have been conducted previously to address this important accuracy issue. Liao et al. reported that spark gap was observed to be mainly controlled by pulse on-time. A high value of pulse time produced wider slot [156]. Hoang and Yang evaluated the impact of four control variables namely; open voltage, feed rate of wire electrode, air pressure and capacitance on the kerf size in dry micro-WEDM of titanium alloy. All of the selected control factors were proved to be significant despite open voltage with regard to kerf size. Moreover thickness of the workpiece also significantly influence kerf size [157].

Prasad et al. [158] formulated mathematical models for reducing the kerf width. Those models were blend of global optimization approach and harmony search algorithm. The size of kerf was also seemed to be affected by the deformation in the wire electrode. The increase in wire deformation lead to widen the cut slot. The amount of deformation induced in the wire electrode is dependent on the selection of input control factors and the target material [159].

The most important stimulus with regard to the spark gap is the vibrations generated in the moving wire electrode. These vibrations promote the sideways sparking and consequently spark gap has been increased. Wire tension was demonstrated as a major control parameter for controlling the amount and amplitude of vibrations induced in the wire electrode. Furthermore, high magnitude of vibrations was resulted into unstable machining [160]. Kamei et al. claimed that workpiece position can also affect the amplitude of vibrations produced during WEDM [161]. Nishikawa also witnessed the dependency of kerf size on wire vibrations [162]. Sivanaga et al. [163] investigated the impact of workpiece thickness and current on spark gap. It was noted that spark gap increases both with current and thickness of workpiece. This was attributed to the fact that increase in the aforesaid parameters (current and workpiece thickness) likely to produce vibrations of higher amplitude that widens the slot width. Garg et al. [164] evaluated the impact of six WEDM control factors on spark gap. Increase in wire tension was found to have a positive impact on the spark gap. All the other parameters were shown an inverse relationship. Mathematical model for the prediction of spark gap was also made using desirability approach.

In another research carried out on WEDM of titanium it was concluded that peak current, servo voltages and pulse on/off time have a significant role in determining the amount of spark gap [165]. In addition to that a micro-model was also made that can predict the spark gap.

Manna et al. [166] stated that wire feed, wire tension and servo voltages significantly affect the magnitude of spark gap.

Though number of researchers tried to investigate the effect of process parameters and identify possible parametric combinations to minimize the spark gap but still the level of effort devoted in this area is not up- to the mark. Still there is need to explore WEDM performance with this perspective as little work has been reported in this regard.

3.9.4 Summary

It is evident from the literature review that WEDM has emerged as a capable machining process for cutting difficult-to- cut materials. The quality of cut of WEDM is comparable to any other unconventional machining methodology even better in many cases. The potential of WEDMM has been explored for cutting variety of different materials such as, titanium and its alloys, Inconel 718, Monel alloy, stainless steels, ceramics, tool steels, metal matrix composites [7-17]. But machining performance of the aforementioned cutting mechanism is still to be evaluated for cladded materials' machining. No literature has been reported in this regard. Moreover, the issues pertaining to the conventional cutting processes of stainless-clad steel like poor surface finish, larger heat affected zones and workpiece wrapping are presumably minimized by using the WEDM process.

Therefore, a research work has been planned to evaluate the cutting efficiency of WEDM for machining of stainless-clad steel. Cutting speed, surface roughness and spark gap are the selected responses. The selection of these responses is based on their industrial importance. Inspite of studying the common parametric effects the focus has been shifted to envisage the impact of wire diameter, layer thickness of individual layer, workpiece orientation and pressure ratio on the selected responses.

Chapter 4

Experimental Design & Infrastructure

This chapter explains the justification of using an experimental design technique, provides an overview of various experimental design techniques and a rationale of selecting the Taguchi's experimental design technique for present research work. The selection of process parameters and their levels along with the justification is also elaborated in this part of the study. The details pertaining to the infrastructure used for this work is also mentioned herein.

4.1 Need for experimental design

Experimental design technique (DOE) is a statistical tool that guides for the choice of experiments execution in an efficient manner [167]. Following are the reasons that advocate the use of experimental design techniques [168]:

- These techniques provide the best way to cope with experimental variation in a systematic way.
- DOE also helps to identify small/ limited number of experiments that can essentially serve the purpose of investigation.
- Experimental settings can be selected to optimally cover the region of interest of a factor by using the DOE techniques.
- Factor interactions can also be studied using DOE techniques
- Experimental errors can be handled

4.2 Experimental design techniques

Experimental design techniques are extensively applied in research owing to the inherent advantage of showing inter-relationship between the control factors and response attributes. There exists variety of different techniques for experimental design like classical DOE or factorial design, randomized complete block design (RCBD), Latin squares, response surface methodology, Taguchi's experimental design etc. However, in engineering applications mostly factorial design, response surface methodology and Taguchi's experimental design is used for experimental design.

Therefore, in the current study only the said designs are discussed for evaluating the most suitable design for the experimentation. The details of these design methodologies are described in the forthcoming sections. The progress of various DOE techniques is described in Figure 4.1.

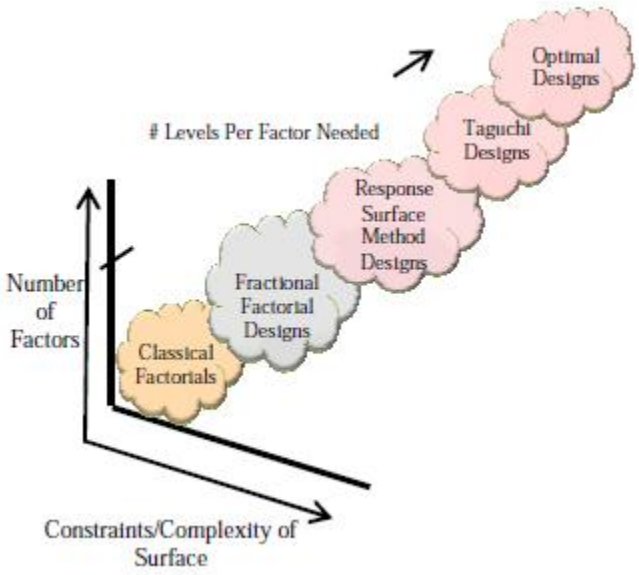

Figure 4.1 Progress of DOE methods [168]

4.2.1 Factorial design

Factorial designs are specifically used to thoroughly investigate the effects of parameters and their interactions on the response characteristic. In many of the processes, factor's interactions play a pivotal role in controlling the value of selected response variable that cannot be observed without the aforementioned experimental design technique.

In this technique, the value of responses are recorded against all possible combinations of levels of input parameters. Each combination is actually representing the condition at which responses are measured/recorded. Experimental condition is termed as a "run" whereas the value of response recorded is known as "observation", the results of full factorial design are considered more reliable as all possible combinations are considered. But the experimentation as per this technique is always costly and sometimes unaffordable [169] . The total number of experiments as per the said design can be calculated by the following relationship.

$$N = L^K \qquad (1)$$

Where N is the total number of experiments, L accounts for levels of parameters and k represents the number of parameters involved in the study. Examples pertaining to this design are presented in Figure 4.2.

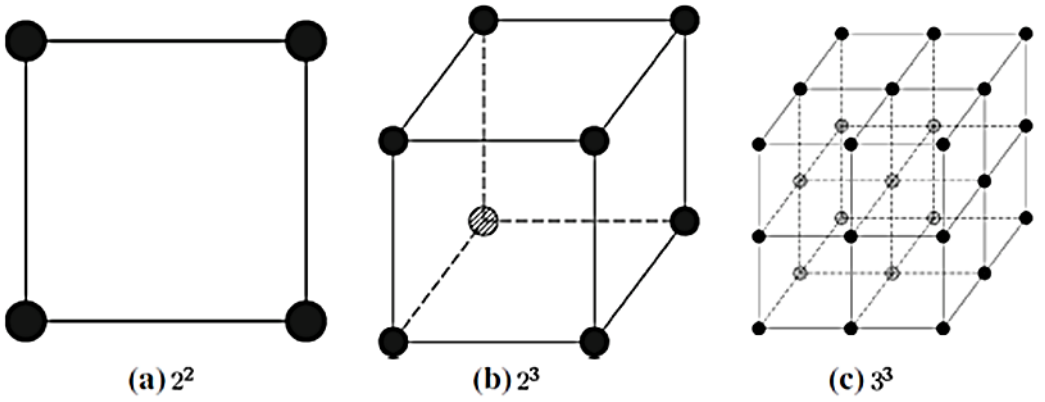

Figure 4.2 Full factorial design examples [167]

When the number of parameters are increased and also factors contain more levels then execution of experiments as per full factorial design might not be feasible. In these scenarios, one of the following experimental design technique may be employed:

- Half factorial
- Fractional factorial

Both the mentioned techniques are basically the modifications of full factorial design technique rather a subset of full factorial design. But the reliability of the results obtained as per the above mentioned techniques is mainly dependent of the right choice of control factors combinations.

The samples chosen for these methodologies must be balanced or orthogonal. Therefore, it is difficult to use these techniques (half factorial and fractional factorial) in many practical applications as it is challenging to judge the appropriate combinations of parameters to obtain the desired process outcome [167].

4.2.2 Response surface methodology

Response Surface Method (RSM) is basically a blend of mathematical and statistical methods to examine the control factors interactions and the impact of parameters and their interactions on the value of the selected response attribute. This experimental design technique was first introduced by G. E. P. Box and K. B. Wilson in 1951. The foremost theme of this design methodology is to employ a set of designed experiments to achieve an optimal value of response variable. Box and Wilson had developed DOE through RSM by using first-degree polynomial model and recognized that the model is simply an approximation and is easy to estimate and apply. The model can also be applied fairly in those situations even when little information is known about the process. RSM is found to be useful for modeling and analyzing experiments in which a response attribute is controlled by several independent control factors.

RSM is used to fit the developed model to the desired model if random input parameters are involved in the study. It also allows to apply linear or quadratic models to describe the response characteristic as a function of the independent control factors and then identifies the optimal settings of input parameters. The relationship between input parameters with regard to the selected response variable can also be quantified with the aid of this experimental design methodology [170].

In RSM experimental design techniques following two design are commonly used:

- Central composite design
- Box-Behnken design

Central composite designs (CCDs) which are also termed as Box-Wilson designs, are applied to calibrate the full quadratic models described in Response Surface Models.

CCDs are classified into three categories namely; circumscribed, inscribed and faced. The geometries pertaining to three aforementioned categories are presented in Figure 4.3.

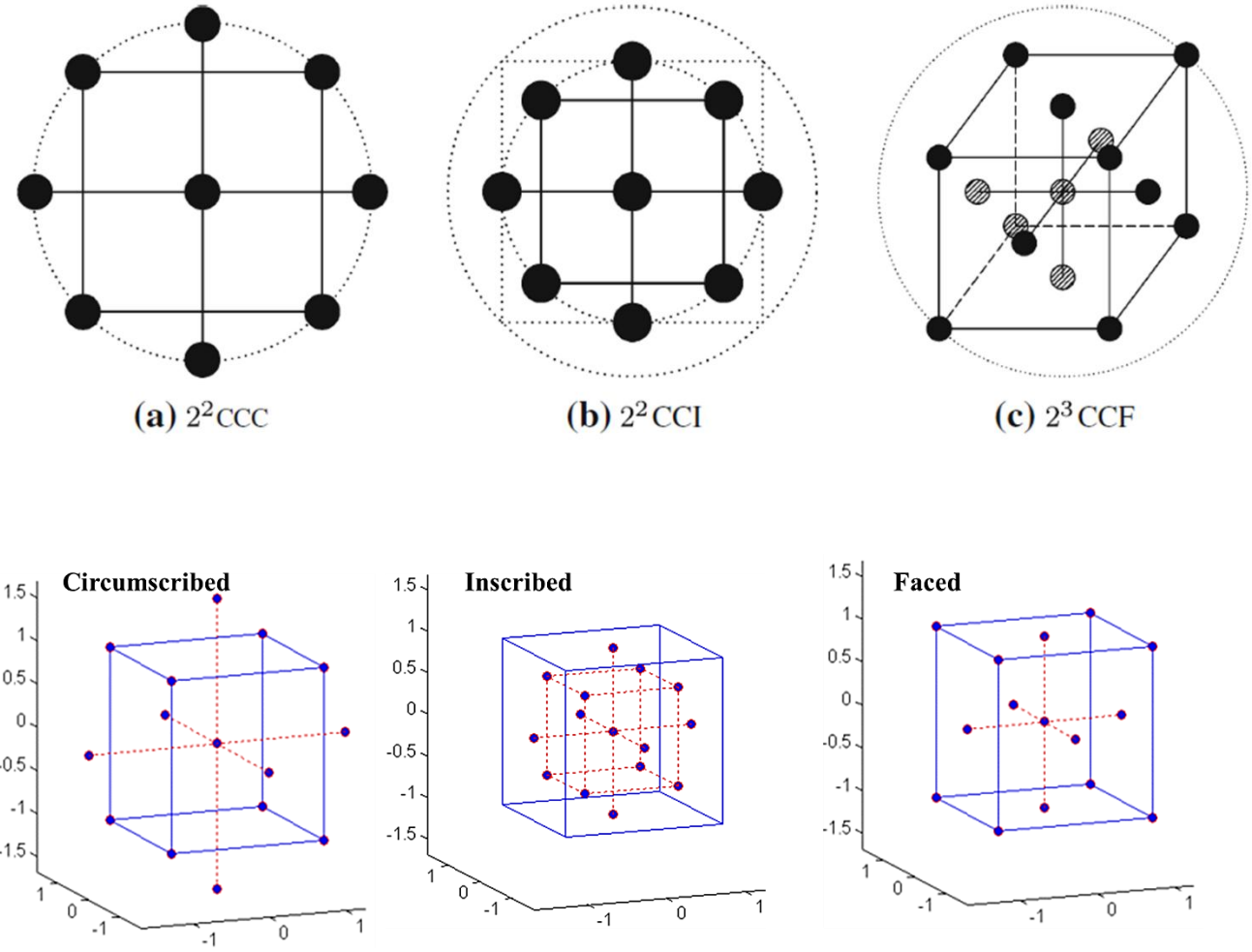

Figure 4.3 Geometries of CCDs [167][168]

All the above mantioned designs consists of a factorial design (represented by corners of cube) alonwith center and star points owing to which second order effects are evaluated. The selection of the type of CCD is based on the number of factors and the desired properties. Some of the imporatnt properties regarding the applocation of the said design are described in Table 4.1.

Table 4.1 Comparison of CCDs [168]

Design	Rotatable	Factor Levels	Uses Points Outside ±1	Accuracy of Estimates
Circumscribed (CCC)	Yes	5	Yes	Good over entire design space
Inscribed (CCI)	Yes	5	No	Good over central subset of design space
Faced (CCF)	No	3	No	Fair over entire design space; poor for pure quadratic coefficients

Another experimental technique that lies under the RSM methodology is Box-Behnken designs. These are applied for the calibration of full quadratic models. The main advantage of Box-Behnken designs over the CCD is that it requires fewer experimental runs and also these are rotatable. But the mentioned designs have a limitation that these are only applicable for small number of factors (four or even less than four). Only extreme factor combinations are examined as per these design without incorporating the corners of the design space as shown in Figure 4.4. The drawback associated with these designs is the poor estimation of extreme points [168].

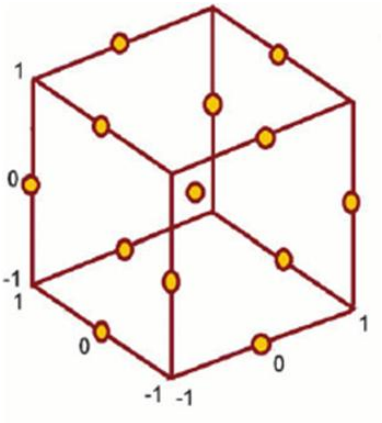

Figure 4.4 Box-Behnken design [171]

4.2.3 Taguchi's experimental design

Taguchi's experimental design technique was developed by Genichi Taguchi in order to improve the off-line total quality control. This method adopts the stratergy of making the process robust aginst the variations imparted due to uncontrollable factors (noise factors) with approperiate selection of controllable factors [172]. This design methodology uses special frcational factorial designs known as orthogonal arryas [173]. These array are actually representing the minimum set of experiments. These arrays are classified into two catagories; inner arrays and outer arrays. For the design based on th econtrollable factors inner arrays are used and for the design based on noise factors outer arrays are used. Sometimes both the arrays are mixed up togther as per the requirement. These arays are termed as mixed arrays. An exapmle of mixed array is described in Figure 4.5. The selection of these arrays is based on the number of factors and their levels as presented in Table 4.2. A performance statistics called signal-to-noise ratio (S/N) was used as a performance statistics by Taguchi for the evaluation of process robustness [174].

Table 4.2 Orthogonal array selection table [167]

Number of variables	Number of levels			
	2	3	4	5
2, 3	L4	L9	LP16	L25
4	L8	L9	LP16	L25
5	L8	L18	LP16	L25
6	L8	L18	LP32	L25
7	L8	L18	LP32	L50
8	L12	L18	LP32	L50
9, 10	L12	L27	LP32	L50
11	L12	L27	N./A.	L50
12	L16	L27	N./A.	L50
13	L16	L27	N./A.	N./A.
14, 15	L16	L36	N./A.	N./A.
from 16 to 23	L32	L36	N./A.	N./A.
from 24 to 31	L32	N./A.	N./A.	N./A.

S/N ratio accounts for the deviation of the response attribute from the desired value of the selected output characteristic [175]. Taguchi's defined six S/N ratio like, smaller the better, larger the better, nominal the better, logarithmic the better etc. Depending upon desired value of the selected response variable these S/N ratios are selected.

For instance smaller the better S/N ratio is used in case of surface roughness as a smaller value is the desired outcome [176]. Three S/N ratios are quite common among the said S/N ratios namely; larger the batter, smaller the better and nominal the better [177].

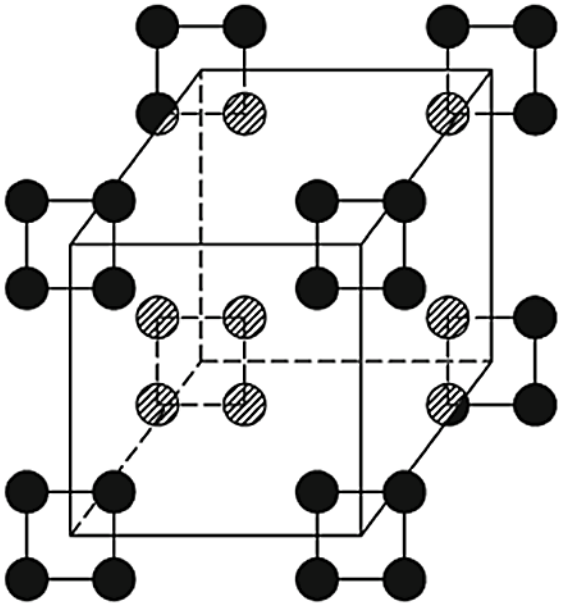

Figure 4.5 Example of Taguchi's mixed array design

Following relationships are used in order to compute the said S/N ratios [151, 178-179].

Larger the better

$$\boldsymbol{\eta_{ij} = -10log(1/n \sum_{k=1}^{n} \frac{1}{Y_{ij}^2})} \qquad \textbf{(4.1)}$$

Smaller the better

$$\boldsymbol{\eta_{ij} = -10log(1/n \sum_{k=1}^{n} Y_{ij}^2)} \qquad \textbf{(4.2)}$$

Nominal the better

$$\boldsymbol{\eta_{ij} = -10\, log\left(\frac{1}{n} \sum_{k=1}^{n} \frac{\mu^2}{\sigma^2}\right)} \qquad \textbf{(4.3)}$$

Here, $\mu = (\frac{1}{n}) \sum_{k=1}^{n} Yij$; $\sigma = (\frac{1}{n-1}) \sum_{k=1}^{n} (Y_{ij} - \mu)^2$ and n accounts for number of experiments whereas Y_{ij} is representing response variable.

It is important to mention that this design technique requires balanced/orthogonal parametric combinations which in turn is an added advantage in contrast to the fractional factorial design [180]. This robust experimental design methodology enables industrial sector to significantly reduce the product development cycle time. As a result costs are reduced, raising the profit margins [181] .

This design technique is generally carried out in four steps that are planing, execution, analysis and finally the validation of the optimal settings of input parameters as described in Figure 4.6.

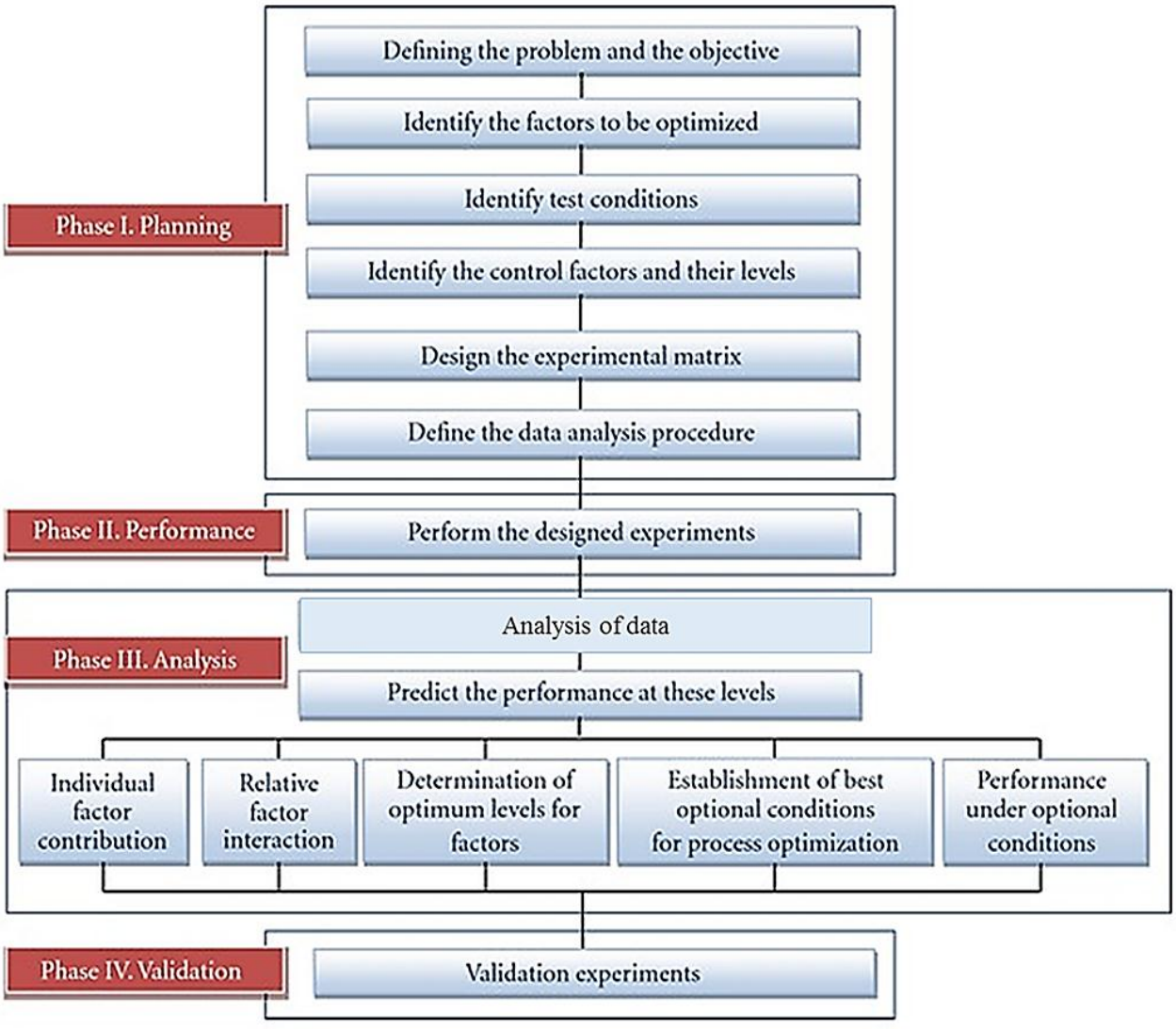

Figure 4.6 Phases of Taguchi's experimental design [182]

Taguchi's experimental design technique results into an improved product quality because it emphasizes that mean value of a response attribute should be close to the desired target value despite of a value within the specific limits. Moreover, this experimental design strategy is straightforward and can easily be applied in many engineering applications. This is a powerful but simple experimental design technique that has a capability to narrow down the scope of a research project [168]. In addition to the above mentioned advantages, the fewer number of experimental runs is the major benefit of this robust technique as mentioned in Figure 4.7. It is worthy to note that other experimental design techniques require more number of experiments that not only consume more time but also a cost addition in terms materials and equipment utilization. For instance, if there are seven control factors each having three levels, full factorial design demands 2,187 experimental runs in a single replicate. Half factorial suggests 1094 experiments whereas central composite design requires 160 experiments for a single trial. In the present study there is an involvement of eight control factors so the number of experiments increased further which is not only difficult to conduct but also quite expensive. Moreover, WEDM process in itself is considered expensive. Therefore, Taguchi's experimental design technique best suits to the situation.

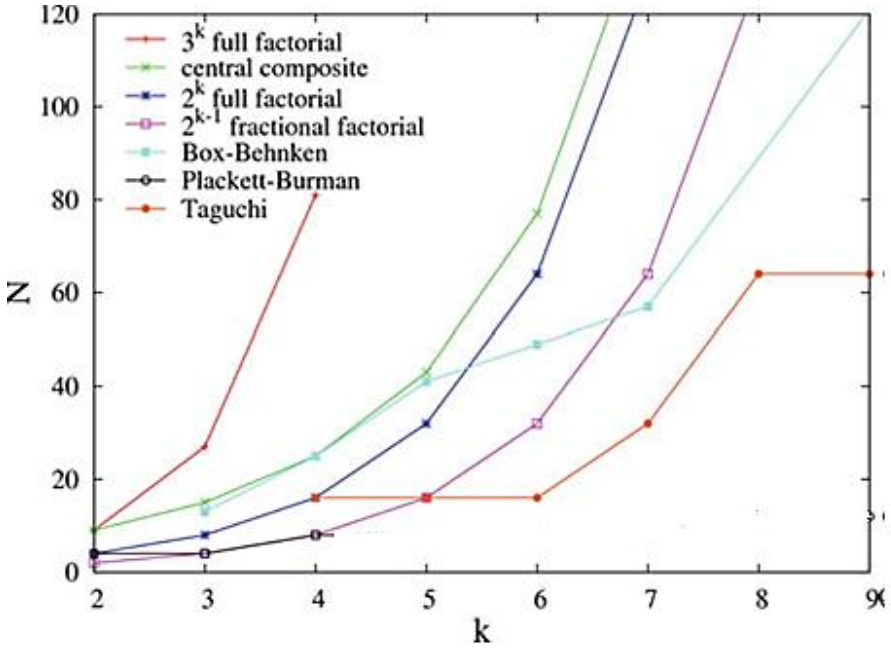

Figure 4.7 Required number of experiments as per selected DOE technique [167]

4.3 Considerations for the selection of experimental design

Following are the main consideration for the selection of appropriate experimental design technique:

- Cost
- Time involved in experimentation
- Factors & their levels
- DOE objective
- Number of experiments

These considerations are also presented in Figure 4.8 and Figure 4.9.

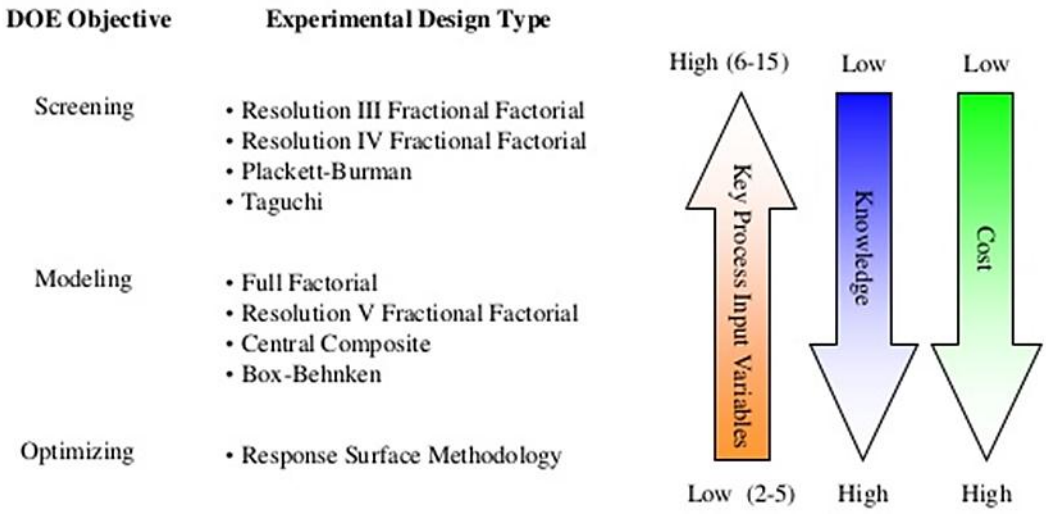

Figure 4.8 Considerations for experimental design selection [183]

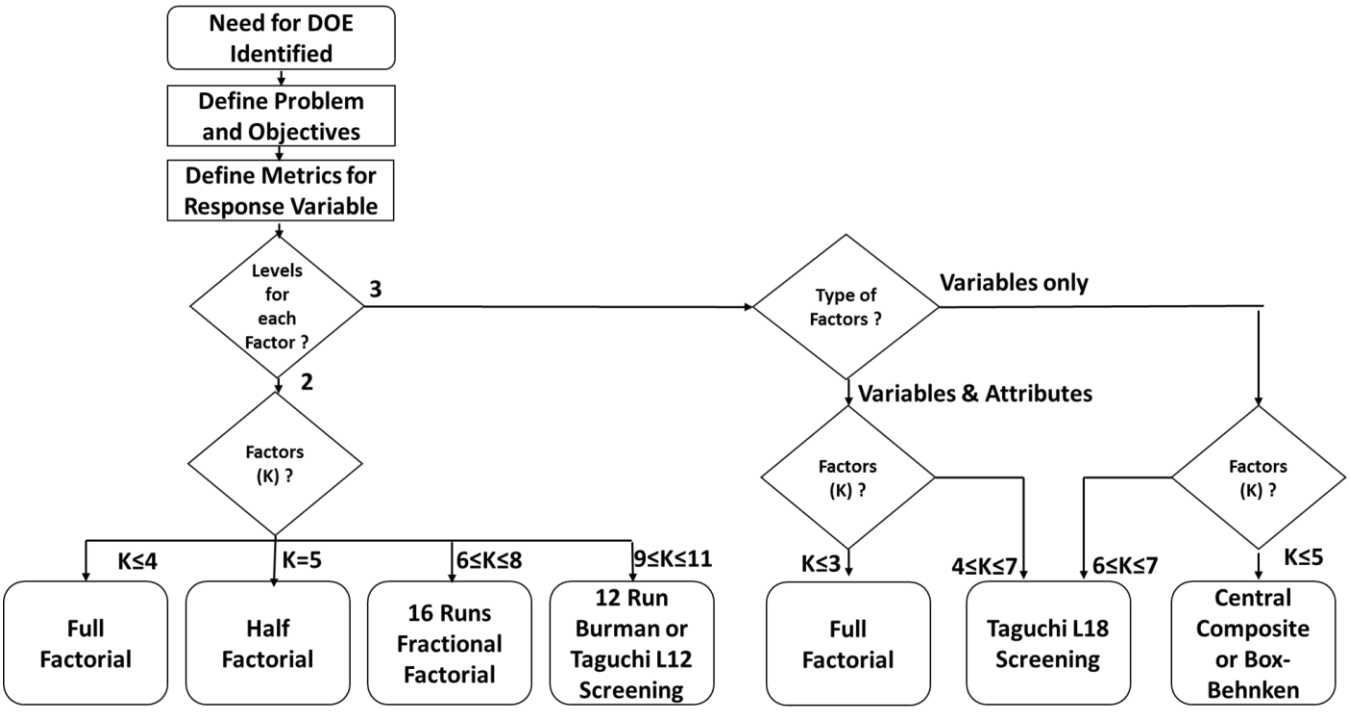

Figure 4.9 Decision tree for experimental design selection [183]

4.4 Response attributes selection

Response characteristics selected in the present study include cutting speed, surface roughness and the spark gap. All the narrated responses are taken keeping in view their significance with regard to the industrial requirements. For instance, cutting speed accounts for the productivity aspect, surface roughness defines the cut quality/ surface finish whereas spark gap is responsible for determining the dimensional accuracy of the machined part.

4.5 Selection of parameters and their levels

As mentioned earlier that the aim of this research work is to evaluate the potential of WEDM for cutting stainless-clad steel material in terms of the narrated responses. Keeping in view the selected response attributes, eight input parameters like orientation of workpiece (Or), mild steel layer thickness (LT_{MS}), pressure ratio (Pr), stainless steel layer thickness (LT_{SS}), servo voltage (Sv), Wire feed (F_w), pulse on-time (P_{ON}) and wire diameter ($D_{w)}$ have been selected for determining their effect on the selected responses. The control factors pertaining to the WEDM process such as, servo voltage (Sv), wire feed (F_w), pulse on-time (P_{ON}) and wire diameter ($D_{w)}$ have been selected in current study owing to the rationale that literature reveled that these parameters significantly affect the selected performance characteristics (cutting speed, surface roughness and spark gap) in WEDM [11, 139, 141-142, 144-145, 148-149, 184-185]. However, the workpiece related parameters like workpiece orientation (Or), layer thickness of individual layer (LT_{SS} and LT_{MS}) and pressure ratio of dielectric fluid are taken due to the reason that their effect is still to be explored on the selected responses in WEDM.

Preliminary experimentation has been performed in order to select appropriate levels of control factors. Wire breakage is a quite commonly occurring phenomena associated with WEDM process that not only has a detrimental effect on the cut quality but also prolongs the machining time. Therefore, a due consideration has been devoted to this problem during preliminary experimentation and those levels of parameters have been taken for mature experimentation that minimize the chance of wire breakage.

Moreover, the experimental runs in which wire breakage occur were not considered true and repeated. Based on the literature and the preliminary experimentation results input parameters and their levels have been finalized. The details of control factors and their level values are shown in Table 4.3.

Table 4.3 Control factors and their level values

Levels (j)	**Parameters (i)**							
	Or	LT_{SS}	LT_{MS}	D_W	Pr	SV	P_{ON}	F_W
	Workpiece orientation*	SS layer thickness (mm)	MS layer thickness (mm)	Wire diameter (mm)	Pressure ratio	Servo voltage (V)	Pulse ON-time (µs)	Wire feed rate (mm/s)
1	A	2	6	0.2	0.7	30	3	60
2	B	3	7	0.25	1	40	4	140
3	---	4	8	0.3	1.3	50	5	220

*Workpiece orientation "A" means stainless steel layer lies at the top while in orientation "B" mild steel layer faces the top as described in Figure 4.10.

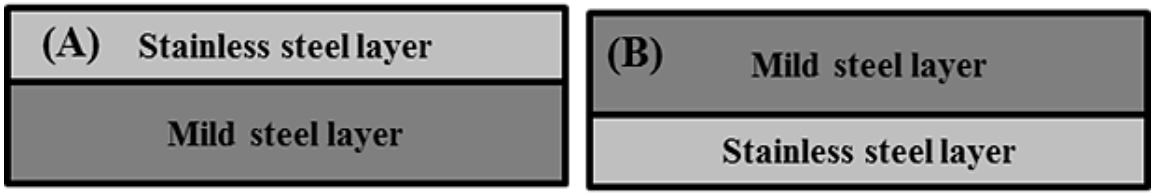

Figure 4.10 Workpiece orientations

Keeping in view the no of input parameters selected for current research work and their level values it has been found that Taguchi's experimental design technique most suited for the current study.

The time and the cost involved during experimentation is the main reason for the selection of this design as other design yield quite a large no of experimental run that are not practically possible. Additionally the accuracy of the Taguchi results have also been proved to be comparable to the other design techniques like factorial design and response surface methodology [172, 186].

4.5.1 Selection of orthogonal array

The selection of orthogonal array is based on the number of input parameters and their levels. As in the current scenario there are eight control factors namely; workpiece orientation (Or), stainless steel layer thickness (LT_{SS}), mild steel layer thickness (LT_{MS}), wire diameter (D_W), pressure ratio (Pr), servo voltages (SV), pulse on time (P_{ON}) and wire feed (F_W). Each factor has three levels except workpiece orientation (Or) which has two levels. L18 orthogonal array has been found suitable for experimental design as per the number of factors and their levels for current research work.

4.5.2 Experimental design table

As mentioned in the previous section that L18 orthogonal array is found to be suitable which means that eighteen experimental runs are to be performed and the details of which is tabulated in Table 4.4.

Table 4.4 Taguchi L18 orthogonal array

Exp. No.	**Or**	**LT_{SS} (mm)**	**LT_{MS} (mm)**	**D_W (mm)**	**Pr**	**SV (V)**	**P_{ON} (µs)**	**F_W (mm/s)**
1	A	2	6	0.30	0.7	30	3	60
2	A	2	7	0.20	1.0	40	4	140
3	A	2	8	0.25	1.3	50	5	220
4	A	3	6	0.30	1.3	40	5	140
5	A	3	7	0.20	0.7	50	3	220
6	A	3	8	0.25	1.0	30	4	60
7	A	4	6	0.20	1.0	30	5	220
8	A	4	7	0.25	1.3	40	3	60
9	A	4	8	0.30	0.7	50	4	140
10	B	2	6	0.25	1.0	50	3	140
11	B	2	7	0.30	1.3	30	4	220
12	B	2	8	0.20	0.7	40	5	60
13	B	3	6	0.20	1.3	50	4	60
14	B	3	7	0.25	0.7	30	5	140

15	B	3	8	0.30	1.0	40	3	220
16	B	4	6	0.25	0.7	40	4	220
17	B	4	7	0.30	1.0	50	5	60
18	B	4	8	0.20	1.3	30	3	140

Experimentation has been performed under L18 orthogonal array with three replications in a randomized manner. The details pertaining to the experimental runs of three replicates are presented in Table 4.5.

Table 4.5 Details of experimental runs of three replicates

Exp. No.	**Or**	**LT_{SS} (mm)**	**LT_{MS} (mm)**	**D_W (mm)**	**Pr**	**SV (V)**	**P_{ON} (µs)**	**F_W (mm/s)**
1.	A	2	6	0.30	0.7	30	3	60
2.	A	2	7	0.20	1.0	40	4	140
3.	A	2	8	0.25	1.3	50	5	220
4.	A	3	6	0.30	1.3	40	5	140
5.	A	3	7	0.20	0.7	50	3	220
6.	A	3	8	0.25	1.0	30	4	60
7.	A	4	6	0.20	1.0	30	5	220
8.	A	4	7	0.25	1.3	40	3	60
9.	A	4	8	0.30	0.7	50	4	140
10.	B	2	6	0.25	1.0	50	3	140
11.	B	2	7	0.30	1.3	30	4	220
12.	B	2	8	0.20	0.7	40	5	60
13.	B	3	6	0.20	1.3	50	4	60
14.	B	3	7	0.25	0.7	30	5	140
15.	B	3	8	0.30	1.0	40	3	220
16.	B	4	6	0.25	0.7	40	4	220
17.	B	4	7	0.30	1.0	50	5	60
18.	B	4	8	0.20	1.3	30	3	140
19.	A	2	6	0.30	0.7	30	3	60
20.	A	2	7	0.20	1.0	40	4	140
21.	A	2	8	0.25	1.3	50	5	220
22.	A	3	6	0.30	1.3	40	5	140
23.	A	3	7	0.20	0.7	50	3	220
24.	A	3	8	0.25	1.0	30	4	60
25.	A	4	6	0.20	1.0	30	5	220
26.	A	4	7	0.25	1.3	40	3	60

27.	A	4	8	0.30	0.7	50	4	140
28.	B	2	6	0.25	1.0	50	3	140
29.	B	2	7	0.30	1.3	30	4	220
30.	B	2	8	0.20	0.7	40	5	60
31.	B	3	6	0.20	1.3	50	4	60
32.	B	3	7	0.25	0.7	30	5	140
33.	B	3	8	0.30	1.0	40	3	220
34.	B	4	6	0.25	0.7	40	4	220
35.	B	4	7	0.30	1.0	50	5	60
36.	B	4	8	0.20	1.3	30	3	140
37.	A	2	6	0.30	0.7	30	3	60
38.	A	2	7	0.20	1.0	40	4	140
39.	A	2	8	0.25	1.3	50	5	220
40.	A	3	6	0.30	1.3	40	5	140
41.	A	3	7	0.20	0.7	50	3	220
42.	A	3	8	0.25	1.0	30	4	60
43.	A	4	6	0.20	1.0	30	5	220
44.	A	4	7	0.25	1.3	40	3	60
45.	A	4	8	0.30	0.7	50	4	140
46.	B	2	6	0.25	1.0	50	3	140
47.	B	2	7	0.30	1.3	30	4	220
48.	B	2	8	0.20	0.7	40	5	60
49.	B	3	6	0.20	1.3	50	4	60
50.	B	3	7	0.25	0.7	30	5	140
51.	B	3	8	0.30	1.0	40	3	220
52.	B	4	6	0.25	0.7	40	4	220
53.	B	4	7	0.30	1.0	50	5	60
54.	B	4	8	0.20	1.3	30	3	140

4.6 Infrastructure

The details pertaining to the infrastructure required for the present research work is described in this section. The procedure of experimentation and the response measurement is also explained herein.

4.6.1 CNC wire EDM

CNC wire electric discharge machine (G 43S) is used for doing the experimentation as shown in Figure 4.11 .

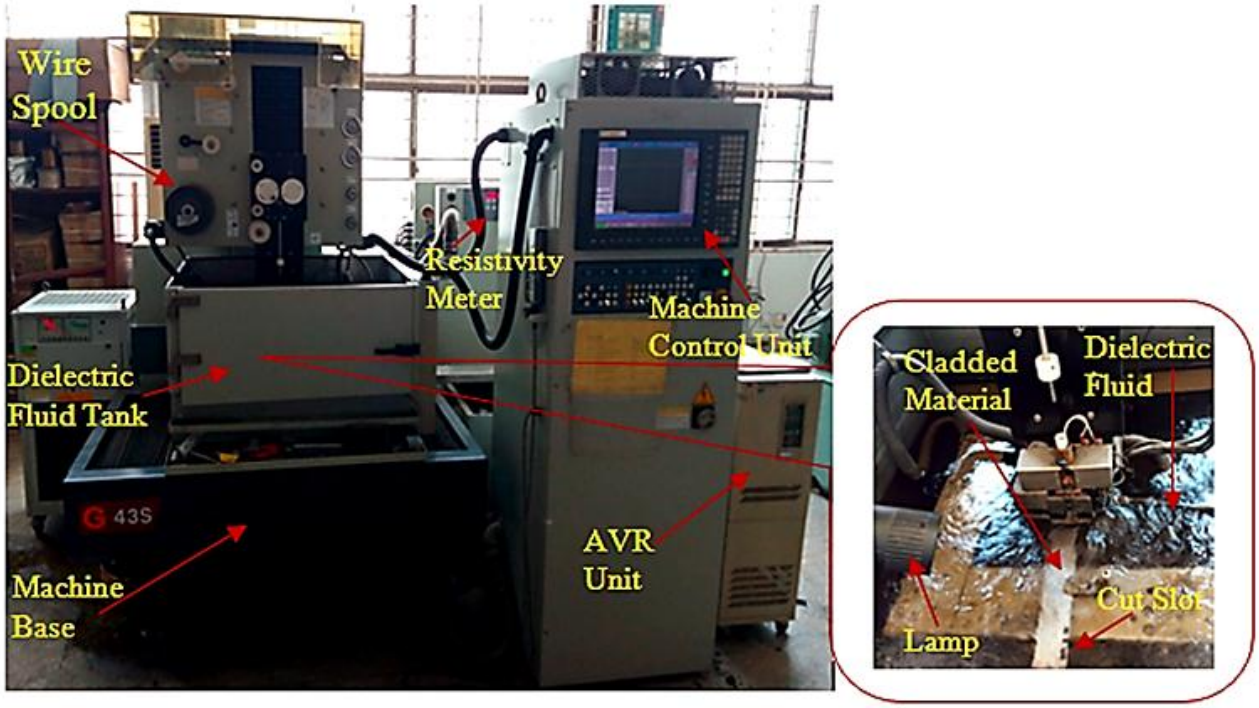

Figure 4.11 CNC wire EDM (G 43S)

Before doing the final experimentation, following arrangement have been made. Based on the results of preliminary experimentation it has been noticed that machine has a warm up time of about 15 minutes.

Therefore, CNC wire cut machine has given a due warm up time before doing the experiments. Another important consideration while performing the experiments is the perpendicularity of the specimen on the work table as it directly effects the dimension of the machined component. In other words, dimensional accuracy of the part produced through WEDM has been compromised. So, the perpendicularity of the workpiece with respect to the machine table has been also assured with the aid of Set Square before doing the experiments. Moreover, the resistivity of the dielectric fluid is consistently monitored and kept maintained during experimentation as it has a direct impact on the cutting efficacy in WEDM. In the present research work 24 mm length was machined in each experimental run.

Upon completion of every experiment, the cut specimen has been immediately removed from the machine tank. Later on the surface of the machined specimen has been cleaned and dried. The dried sample is than subjected to measurements.

4.6.1.1 Measurement of cutting speed

The cutting speed during WEDM of cladded material has been recoded directly from the controller of the machine during each experimental run. Moreover, to assure the authenticity of the results a stop watch has been used to approximate the time of cut for a predefined cut length of 24 mm through the experiments. In this manner the cutting speed during every experiment has also been calculated manually by dividing the cut length by the measured time of cut. Both the results of the selected response have observed to be in good agreement.

4.6.2 Surface texture meter

Upon completion of experiments according to the Taguchi's experimental design technique (L18), the surface roughness (Ra) of the machined specimen has been measured with the aid of Surtronic surface roughness tester (S128) as presented in Figure 4.12 .

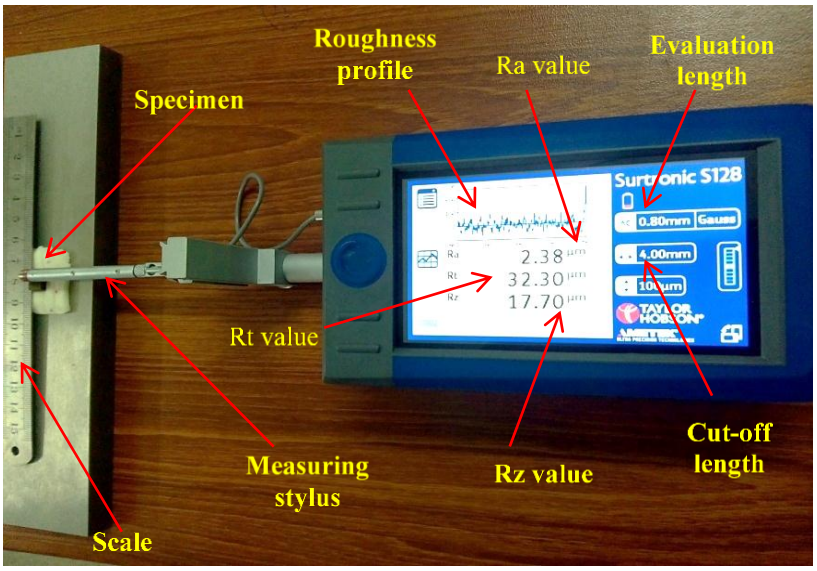

Figure 4.12 Measurement of surface roughness using Surtronic surface texture meter (S 128)

For the measurement of the said response parameter, evaluation length has been set at 4 mm whereas a cut off length of 0.8mm have been used to find the surface roughness of machined cladded sample. Calibration of the surface texture meter is quite a critical consideration that has a direct effect on the measurement of surface roughness. Therefore, surface roughness tester has been calibrated by using the standard specimen provided by the manufacturer before taking the roughness measurements. Surface roughness of both the layers of cladded specimen have been found in terms of arithmetic averages (Ra) which is a frequently used parameter for the assessment of surface roughness.

4.6.3 Coordinate Measuring Machine (CMM)

Coordinate measuring machine (Model: CHEN WEI CE-450DV) has been used for the measurement of spark gap as described in Figure 4.13.

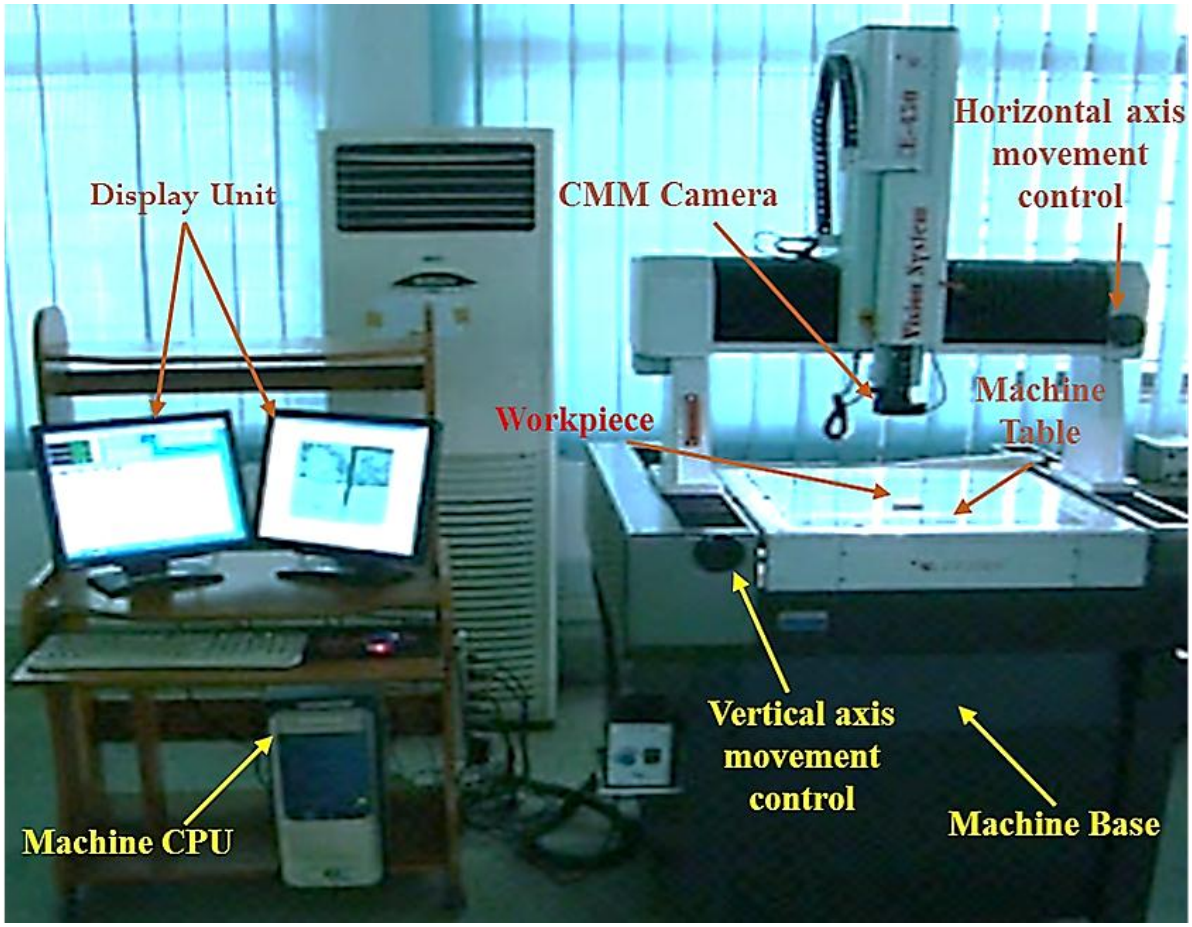

Figure 4.13 Coordinate measuring machine

Spark gap is basically account for the amount of overcut that is being produce during wire electric discharge machining due to the sideways sparking between the wire electrode and the target material as demonstrated in Figure 4.14. This gap is unavoidable as wire has to maintain a safe distance in order to minimize the chance of short circuiting but this gap is always undesirable as it affects the accuracy of the machined part. The attainment of the exact dimension in the machined part becomes challenging task owing to this accuracy concern. Keeping in view the importance of this issue, an attempt has been made to minimize that gap so that the effect on the final dimensions may be negligible.

In other words, the dimensional accuracy of the final part is within the permissible limits of acceptability. The measurement of spark gap has been recorded with the aid of coordinate measuring machine (CMM).

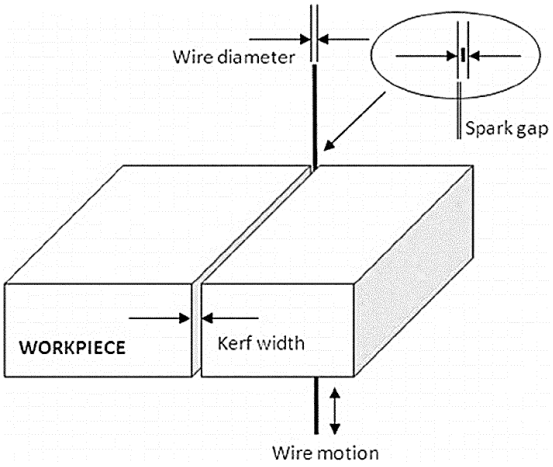

Figure 4.14 Schematic illustration of spark gap produced in WEDM

Initially, the kerf width of the machined specimen has been measure at three different points along the thickness of the kerf and then averaged. Additionally, the value of standard deviation has also been calculated to assess that whether the mean is a true representative of the data or not. The value of standard deviation thus obtained for all the experiments is of quite small magnitude. This shows that mean is a true representative of the data in the present case. After finding the average value ok kerf width spark gap has been calculated by the following relationship [163].

$$\boldsymbol{Spark\ gap} = \frac{\boldsymbol{K_W - D_W}}{\boldsymbol{2}} \qquad (\boldsymbol{4.4})$$

Here, K_W accounts for the averaged kerf width and D_w is representing the value of diameter of brass wire electrode used for the experimentation.

4.6.4 Scanning Electron Microscope (SEM)

Scanning Electron Microscope (Model: TESCAN VEGA 3) is used to evaluate the surface quality of the machined surface as presented in Figure 4.15.

Figure 4.15 Scanning electron microscope

WEDMed samples have been placed in the vacuum chamber of the SEM for examining the micro-features (micro-cracks, craters, melted re-deposits etc.) formed at the cut surface without any sample preparation. However, samples were mirror polished and etched subsequently for finding the recast layer thickness. An SEM micrograph of the cut surface is presented in the below Figure 4.16.

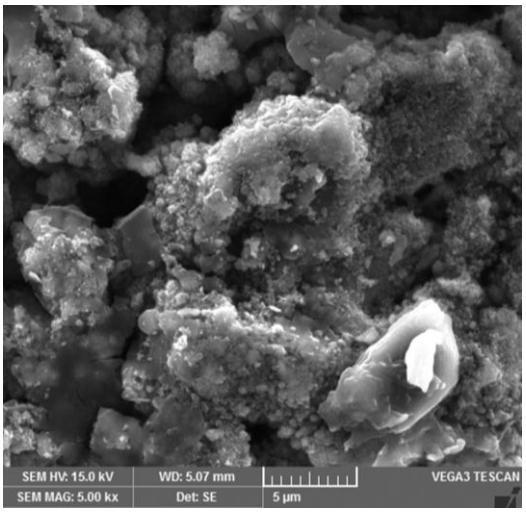

Figure 4.16 SEM micrograph of machined surface

Chapter 5

Results and Discussion

This chapter includes the results of experimentation, statistical analysis of the results and detailed discussion. Stainless-clad steel strips have been machined through wire electric discharge machining process. Experimentation has been performed as per Taguchi's experimental design technique. Following section elaborates about the experimental arrangements followed by experimental results, comprehensive statistical analyses and discussion on selected response attributes such as cutting speed, surface roughness of individual layer and spark gap.

5.1 Experimental results of cutting speed

The results pertaining to the narrated response have been described in Table 5.1. The results obtained during experimentation were then subjected to statistical techniques for comprehensive investigation of the effects of input factors on the cutting speed.

Table 5.1 Experimental results of cutting speed

Exp. No.	Or	LT_{SS} (mm)	LT_{MS} (mm)	D_W (mm)	Pr	SV (V)	P_{ON} (µs)	F_W (mm/s)	Cutting Speed (mm/min)
1	A	2	6	0.30	0.7	30	3	60	2.07
2	A	2	7	0.20	1.0	40	4	140	2.38
3	A	2	8	0.25	1.3	50	5	220	2.15
4	A	3	6	0.30	1.3	40	5	140	2.32
5	A	3	7	0.20	0.7	50	3	220	1.99
6	A	3	8	0.25	1.0	30	4	60	2.07
7	A	4	6	0.20	1.0	30	5	220	2.31
8	A	4	7	0.25	1.3	40	3	60	1.66
9	A	4	8	0.30	0.7	50	4	140	1.50
10	B	2	6	0.25	1.0	50	3	140	1.87
11	B	2	7	0.30	1.3	30	4	220	2.01
12	B	2	8	0.20	0.7	40	5	60	2.59
13	B	3	6	0.20	1.3	50	4	60	2.22
14	B	3	7	0.25	0.7	30	5	140	2.55
15	B	3	8	0.30	1.0	40	3	220	1.42
16	B	4	6	0.25	0.7	40	4	220	2.04
17	B	4	7	0.30	1.0	50	5	60	1.87
18	B	4	8	0.20	1.3	30	3	140	1.68

5.1.1 Analysis of variance (ANOVA) for cutting speed

First of all, Analysis of Variance (ANOVA) has been carried out to identify the significant control factors with respect to the selected response. As ANOVA is considered as an important statistical oftenly employed to access the significant control factors with regard to the defined response characteristic. In ANOVA, significance of a factor is determined at a particular defined confidence interval that is usually taken as 95% (α=0.05). The control factor having a p-value less than the predefined alpha value is rated as significant factor for a particular response attribute. Additionally, F-value is another check to screen out the significant factor. If any input parameter holds a high F-value this shows that a slight change in that process parameter can yield a noticeable change in the response feature [187]. In the current research work, both the said measures have opted to evaluate the influential input parameters for cutting speed at a confidence interval of 95%. The results of the analysis for the selected response during WEDM of stainless-clad steel workpiece material are described in Table 5.2. In the said Table, "DF" stands for degree of freedom, "Seq SS" stands for sequential sum of squares, "Adj SS" stands for adjusted sum of squares and "Adj MS" is representing adjusted mean square.

The results of ANOVA clearly indicate that four input control factors namely; stainless steel layer thickness LT_{SS} (0.024), mild steel layer thickness LT_{MS} (0.048), wire diameter D_W (0.027) and pulse on-time P_{ON} (0.011) holds a p-value lesser than the defined alpha value (α=0.05) and also the F-value of these factors have found to be higher in comparison the rest of the control factors as shown in Table 5.2. Hence, the above mentioned four input parameters come out to be the significant control factor with respect to the selected response characteristic in WEDM of the cladded material. It is also of worth noting that the value of the R-sq (adj) has observed to be 95.87%. The value of R-sq (adj) is actually represents that how accurately developed model fits the data and explain the variation of the process. As in the present case, the developed model has a high value of R-sq (adj) that validates the suitability of the purposed model.

Table 5.2 Results of ANOVA for cutting speed in WEDM of cladded material

Sr. No.	Source	DF	Seq SS	Adj SS	Adj MS	F-value	P-value
1	Or	1	0.002	0.002	0.002	0.50	0.555
2	LT_{SS}(mm)	2	0.366	0.366	0.183	40.01	**0.024**
3	LT_{MS}(mm)	2	0.181	0.181	0.091	19.82	**0.048**
4	D_W(mm)	2	0.330	0.33	0.165	36.04	**0.027**
5	SV (V)	2	0.106	0.106	0.053	11.60	0.079
6	F_W(mm/s)	2	0.026	0.026	0.013	2.88	0.257
7	Pr	2	0.066	0.066	0.033	7.21	0.122
8	P_{ON} (µs)	2	0.798	0.798	0.399	87.16	**0.011**
9	Error	2	0.009	0.009	0.005		
	Total	17	1.886				
	Model Summary:		S = 0.068	R-Sq = 99.51%		R-Sq(adj) = 95.87%	

Afterwards, the percentage contribution of the control factors has also been calculated. The percentage contribution of all the selected input parameters for narrated response variable has been shown in Figure 5.1.

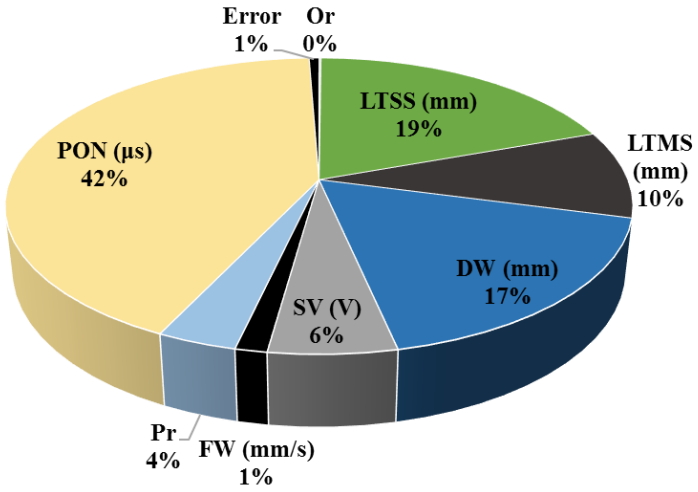

Figure 5.1 Percentage contribution of parameters for cutting speed

The value of percentage contribution of pulse on-time (P_{ON}) is observed to be maximum in controlling the cutting in comparison to other factors i.e. 42% approximately during WEDM of cladded specimen. Stainless steel layer thickness (LT_{SS}) is proved to be the second most contributing factor with the percentage contribution of 19% followed by wire diameter (D_W), mild steel layer thickness (LT_{MS}) having percentage contributions as 17% and 10%, respectively. It is worth noting that the combined effect of layer thickness comes out to be 29%. The percentage contribution of error comers out to be ~ 1% that is quite a small magnitude highlighting that the purposed model explains the variation of the process fairly well thus validates the model adequacy.

5.1.2 Analysis of parametric effects

ANOVA has envisaged the significant control factors for cutting speed as described in the previous section. The next phase is to perceive the trend of input control factors with respect to the response attribute during WEDM of the stainless-clad steel specimen. Main effects plot analysis technique is applied to identify the trend of input factors for the cutting speed. The results of the analysis are shown in Figure 5.2.

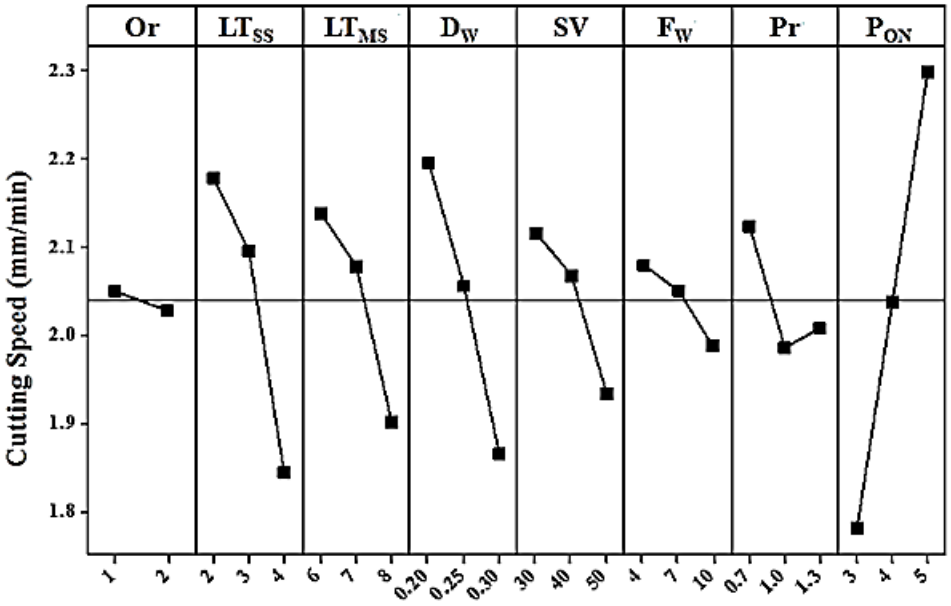

Figure 5.2 Main effects plot analysis for cutting speed

5.1.2.1 Effect of workpiece orientation (Or)

The effect of orientation of workpiece on cutting speed is observed to be quite minimal (ANOVA results indicate this factor as insignificant for cutting speed) as depicted from the Figure 5.2. The workpiece orientation "A" (stainless steel layer faces the top) found to be the preferred orientation in contrast to the orientation "B" (mild steel layer at the top) with respect to the selected response. Although, the impact of workpiece orientation is not appreciable but still there exist about 2% improvement in the cutting speed if workpiece is placed in such a way that stainless steel layer faces the top i.e. orientation "A". In the aforementioned orientation, a fresh wire comes in contact with the stainless steel, starts performing the cutting action and then it enters the next layer of mild steel to complete the machining of stainless-clad steel specimen.

5.1.2.2 Effect of layer thickness (LT_{SS} and LT_{MS})

The layer thickness of individual layer has found to have an inverse relationship with cutting speed i.e. increase in the layer thickness results into decrease in the cutting speed. Actually, by increasing the thickness of individual layer the overall thickness of specimen is increased that offers a larger contact area. Thus, adequate amount of heat is required for vaporization of this larger target. Therefore, machining action is prolonged in producing the requisite amount of heat which in turn reduces the cutting speed. It is observed that an increase in the stainless steel layer thickness from 2 to 4mm, the cutting speed decreases from 2.17 to 1.84 mm/min (~ 17.7% reduction in cutting speed). However, in case of mild steel layer, the increase in layer thickness form 6 to 8mm, cutting speed lowers down from 2.14 to 1.902 mm/min (approximately 12.5% reduction).

It is important to mention that during WEDM of cladded specimen the impact of stainless steel layer thickness LT_{SS} (holds a percentage contribution of about 19%) on cutting speed is more in comparison to LT_{MS} (having a contribution of ~10%) as per the ANOVA results presented in Table 5.2.The percentage contribution of stainless steel layer (LT_{SS}) is about two folds in contrast to the mild steel layer thickness (LT_{MS}).

It is attributed to the fact that the electrical conductivity (12.35 x 10^3 ohm^{-1} cm^{-1}) and thermal conductivity (17W/m K) of stainless steel is lower as compared to mild steel layer (as shown in Table 2.3) and also stainless steel has higher density (8.07 g/cm^3).

Actually, the amount of discharge energy produced during machining is mainly accountable for the erosion of target material in WEDM. The dependency of the generation of the discharge energy is primarily on the electrical characteristics (mainly electrical conductivity) of the target material. Electrical conductivity of the target material plays a vital role in determining the cutting rate during WEDM process [188]. A similar kind of findings regarding the effect of workpiece electrical conductivity on cutting speed were reported in WEDM of Al/SiCp-MMC [189]. It was reported that cutting speed was observed to be high during cutting of Al-matrix workpiece material in contrast to Al/SiCp-MMC material owing to the reason that Al/SiCp-MMC holds a lower electrical and thermal conductivity that resulted into a lower cutting speed during WEDM. The higher electrical conductivity of the workpiece material is an indication of the high value of spark strength. The increased spark strength is always associated with higher erosion rates. Therefore, cutting rate promotes with the increase in the value of electrical conductivity of the workpiece material.

In the present case, mild steel layer (LT_{MS}) has a higher electrical conductivity than the stainless steel layer (LT_{SS}). Thus it experiences a more intense spark in contrast to the other layer which increases the material vaporization rate of mild steel surface (LT_{MS}). But, material erosion process takes more time in vaporizing the stainless steel surface (LT_{SS}) owing to the reason that its electrical resistivity is lower. Hence, a hindrance is being offered by the stainless steel layer to wire feed inside the workpiece material although a cut has been produced in the mild steel layer, thus playing a role of limiting control factor during machining of stainless-clad steel. That is the main reason, stainless steel layer (LT_{SS}) has a twice percentage contribution with regard to the cutting speed as compared to the mild steel layer (LT_{MS}).

5.1.2.3 Effect of wire diameter (D_W)

ANOVA has revealed that wire diameter (D_W) plays a significant role in controlling the cutting speed in WEDM of cladded material. The trend of this factor is alike as that of layer thickness i.e. increase in wire diameter (D_W) yields lower cutting speed as presented in Figure 5.2**.** Experimental results reveal that cutting speed increases from ~1.86 to ~2.2 mm/min as the value of wire diameter reduces from 0.3 to 0.2 mm (~17% improvement in cutting speed).

This is due to the reason that with the increase in wire diameter, the surface area of wire electrode exposed to the target material also increases. Therefore, it is not only requires more adequate amount of heat but also consumes more time as wider area of the target material is to be machined. Consequently, cutting speed reduces in case of larger diameter wire (D_W). A similar kind of finding regarding the effect of wire diameter on cutting speed was reported in WEDM of Inconel 706 [145].

5.1.2.4 Effect of servo voltage (SV)

Based on the findings of main effects plot analysis, it has been noticed that there exists an inverse relation between servo voltages (SV) and cutting speed. The increase in servo voltages results into lower cutting speed. Cutting speed increases from 1.93 to 2.12 mm/min as the servo voltages (SV) reduces from 50 to 30 V. Basically, the servo voltages (SV) are accountable for maintaining a safe sparking gap between electrode and the target material to minimize the chance of short circuiting.

As the value of the aforesaid factor increases, the distance between wire electrode and the target material also increases which depicts that the wire stays a bit farther from the workpiece surface thus, lesser amount of discharge energy is transferred to the target material. As a consequence, material vaporization process consumes more time. Which in turn reduces the cutting speed during WEDM of cladded material.

5.1.2.5 Effect of wire feed (F_W)

The effect of wire feed (F_W) on the cutting speed in WEDM of cladded material is similar as that of servo voltages (SV). Increase in wire feed (F_W) yields lower cutting speed owing to the reason that with the increase in the value of said factor the contact duration of the electrode and of workpiece material becomes short. Consequently, inappropriate sparking occurs that results into the reduction of cutting speed. For instance, cutting speed reduces from 2.08 to 1.98 mm/min (about 4.6% reduction in cutting speed) as the value of wire feed increases from 60 to 220 mm/s.

5.1.2.6 Effect of pressure ratio (Pr)

Pressure ratio (Pr) is actually the ratio of dielectric flushing pressures (dielectric flushing pressure of upper nozzle to the dielectric flushing pressure of the lower nozzle). It is evident from the main effects plot analysis that cutting speed improves if flushing pressure of the upper nozzle is kept higher in contrast to the flushing pressure of the lower nozzle. It has been noticed that there exists an increase of about 6.8% in cutting speed by using the said settings of flushing pressure i.e. Pr, 0.7.

It might be due to the reason that such combination of flushing pressures results into better flushing of melted debris. If the melted debris are not properly flushed away by the dielectric fluid this not only leads to the wire breakage but also prolongs the cutting duration. Therefore, pressure ratio (Pr) of 0.7 is likely to produce a cleaner cutting gap by efficiently flushing the melted debris that results into higher cutting speed.

5.1.2.7 Effect of pulse on time (P_{ON})

Pulse on time has been found to be the most influential control factor for cutting speed in WEDM of stainless-clad steel as depicted from Table 5.2. Cutting speed is revealed to have a direct relationship with the pulse on time (P_{ON}) i.e. increase in pluse on time (P_{ON}) results into higher cutting speed.

As the value of the said parameter increases from 3 to 5 μs, the cutting speed rises from about 1.8 to ~2.3 mm/min (about 28% improvement in cutting speed) as shown in Figure 5.2. Actually, the increase in the pulse on time (P_{ON}) tends to prolongs the spark duration that susequently produce more amont of discharge energy for material errosion.

The increase in the amount of discharge energy produced provides more heat for longer period of time to melt and vaporize the workpiece material. Hence, metal vaporization rate is enhanced which results into higher cutting speed. Although, cutting speed has found to increase with the rise in pulse on time (P_{ON}) value, but on the other end machined surface is subjected to deeper crateres at higher values of discharge energy. The depth craters is directly dependent of the amount of discharge energy produced. Figure 5.3 and Figure 5.4 represent the scaning electron micrographs (SEM) of machined surface subjected to two machining coditions in this regard.
In first case, cladded speciemn is machined at higher value of pulse on time ($P_{ON,}$ 5μs) whereas in the second case the cutting is performed at 3μs as presented in Figure 5.3 and Figure 5.4. It is clearly evident form the SEM micrographs recorded for the two scnarios i.e. at maximum pules on time ($P_{ON,}$ 5 μs) and at minimum pules on time ($P_{ON,}$ 3μs), that machined surface of claddded material exposed to higher value of the said parameter is more irregular having deeper craters in contrats to the machined surface produced at lower value of pulse on time (P_{ON}) as shown Figure 5.3 and Figure 5.4. The machined surface of stainless-clad steel is found to have craters, spherical modules and melted re-deposits. The formation of craters on the machined surafce is because of the reason that machined surafce is subjected to sucsessions of electric sparks whereas, surface tension of the molten material tends to form spherical modules on the cut surface in WEDM.

Moreover, the melted re-deposits are produced due to the solidification of melted debris that has not been flushed away by the dielectric flushing fluid.

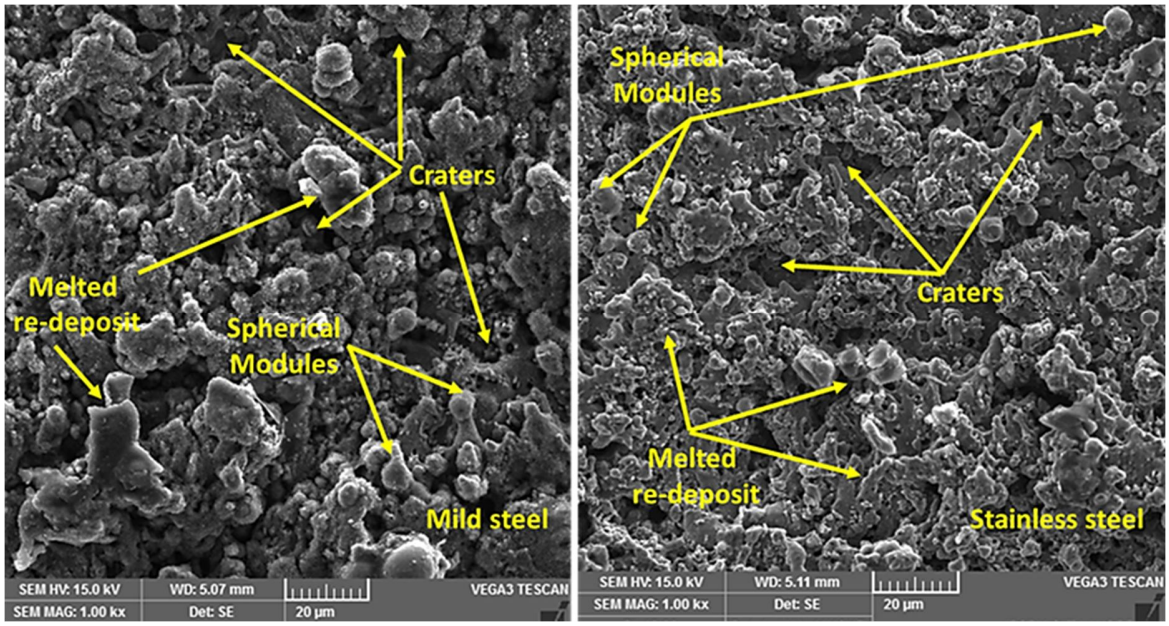

Figure 5.3 SEM micrograph of machined surface at 1000x using pulse on-time of 5µs

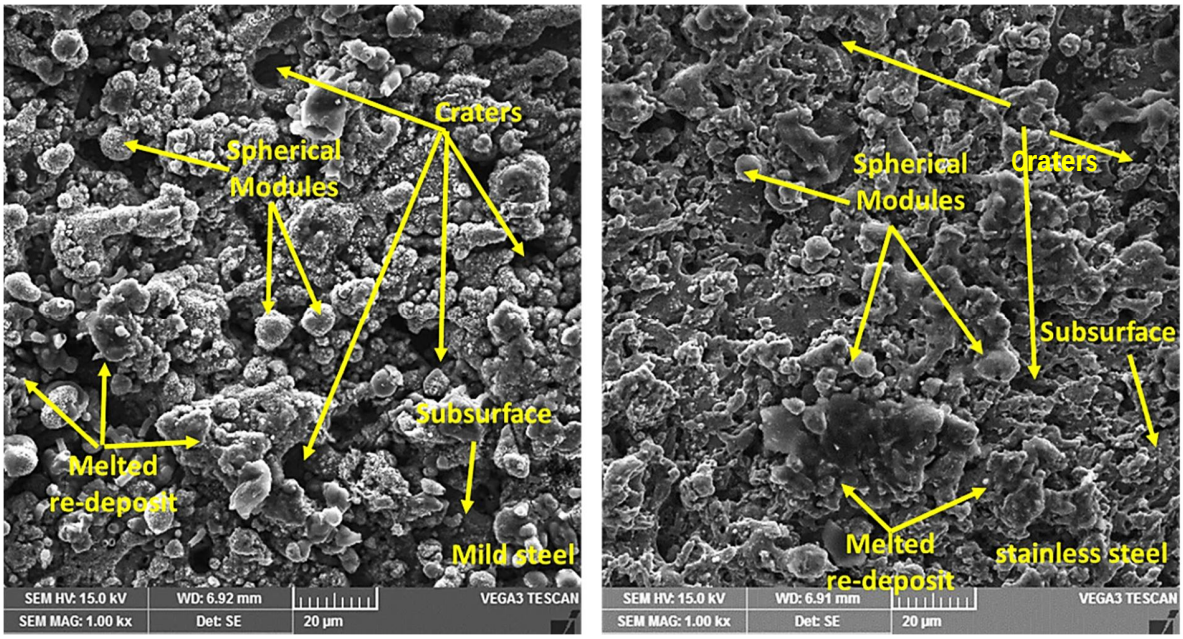

Figure 5.4 SEM micrograph of machined surface at 1000x using pulse on-time of 3µs

It is also interesting to mention that the surface texture of stainless steel layer seemed to be better as compared to the surface texture generated on the surface of mild steel layer at both the machining conditions. It is because of the fact that both the surfaces have different electrical conductivities. Due to this difference, both the surfaces are subjected to different spark strengths. As the electrical conductivity of mild steel is higher so it bears an intense spark. However, the spark produced in front of the stainless steel layer is of lesser intensity due to its lower electrical conductivity and higher resistivity in comparison to the other alternatives. Therefore, stainless steel surface contains shallow craters, smaller diameter spherical modules and smaller melted re-deposits in comparison to the mild steel surface as shown in Figure 5.4. A similar trend of pulse on time (P_{ON}) with respect to the selected response characteristic was also reported in another work carried out on WEDM of AISI D3 tool steel [138].

5.1.3 Contour plot analysis

Contour plot analysis is a statistical analysis that is carried out to screen out the optimal ranges of the significant control factors so that process yield can be optimized.

Figure 5.5 describes the contour plots of the four significant control factors namely; stainless steel layer thickness (LT_{SS}), mild steel layer thickness (LT_{MS}), pulse on time (P_{ON}), and wire diameter (D_W) as screened out by ANOVA analysis for the prescribed response variable.

The optimal range of the significant control factors has been shaded in blue color in all the contour plots provided in Figure 5.5. Figure 5.5 (a-c) show the contour plots among the pulse on time (P_{ON}) versus stainless steel layer thickness (LT_{SS}), layer thickness of mild steel (LT_{MS}), and diameter of wire electrode (D_W), respectively. It is observed from the contour plots that cutting speed has been improved if pulse on time (P_{ON}) is selected within 4.5-5 μs, about 2-3mm thickness of stainless steel (LT_{SS}) has been chosen, thickness of mild steel layer (LT_{MS}) is set at about 6mm and the diameter of the wire electrode is within 0.2-0.22 mm. Basically, the selection of the aforementioned parameters within that defined range tends to produce more discharge energy that eventually results into higher material vaporization rate. Consequently, cutting speed increases as material vaporization is a sort of decision factor for determining the cutting speed in WEDM.

It is observed form the contour plot of stainless steel layer thickness (LT_{SS}) versus wire diameter (D_W) that cutting speed is increased if wire diameter is selected within the range of ~0.2-~0.22 mm and layer thickness of stainless steel layer is set between 2-2.4 mm approximately as described in Figure 5.5(d). As this is a cladded material and both the layers are used in composite form, the optimal layer combination is either 2 mm layer thickness of stainless steel layer (LT_{SS}) and 8 mm layer thickness of mild steel layer (LT_{MS}) or 3 mm stainless steel layer thickness and 7 mm mild steel layer thickness as presented in Figure 5.5(e)**.** The contour plot Figure 5.5(f) between mild steel layer thickness (LT_{MS}) and wire diameter (D_W) further shows that wire diameter of 0.2 mm and about 6mm layer thickness of mild steel layer results into higher value of the selected response characteristic.

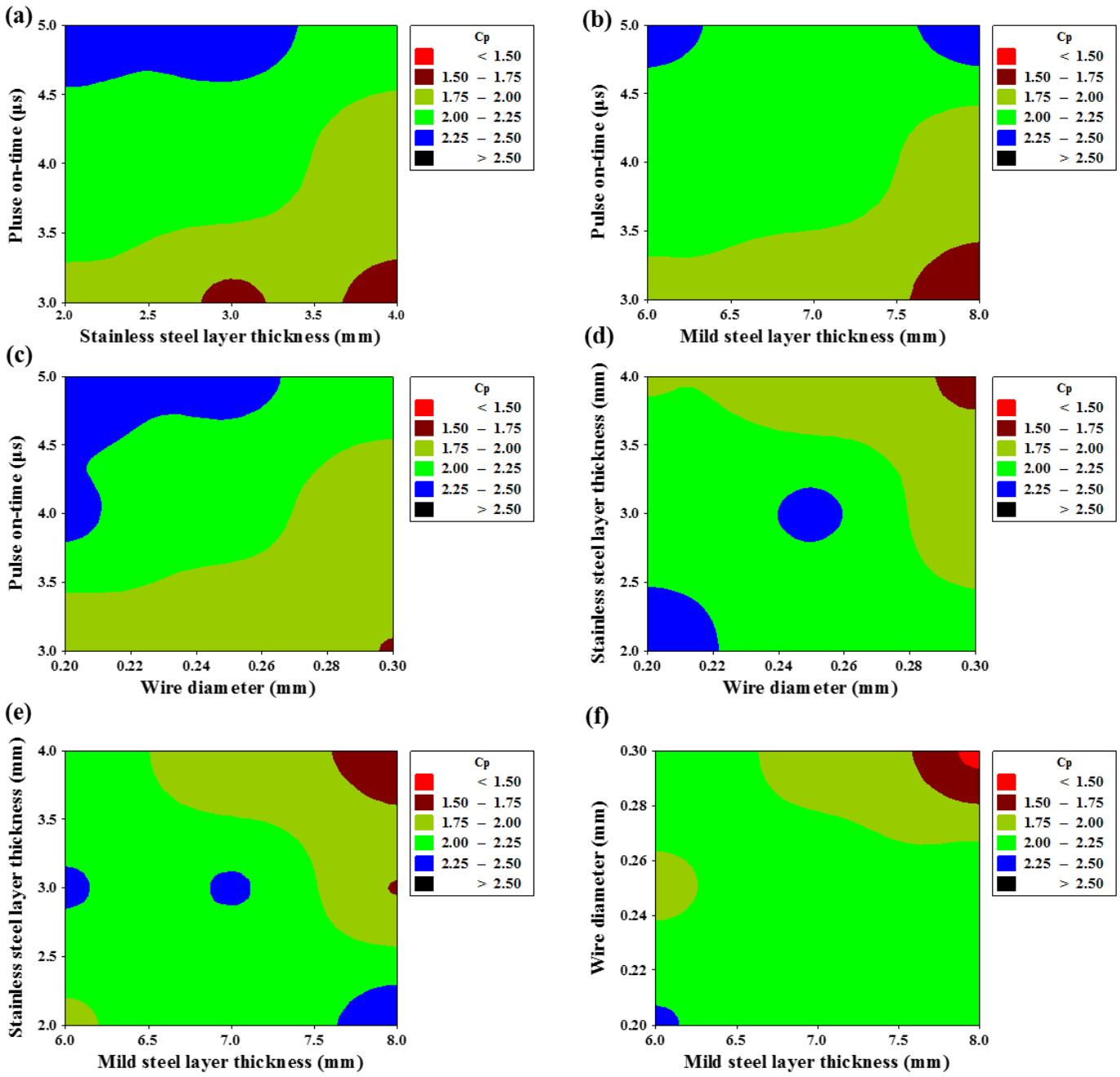

Figure 5.5 Contour plots for cutting speed; (a) P_{ON} Vs LT_{SS}, (b) P_{ON} Vs LT_{MS}, (c) P_{ON} Vs D_W, (d) LT_{SS} Vs D_W, (e) LT_{SS} Vs LT_{MS}, (f) W_D Vs LT_{MS}

5.1.4 Mathematical modeling

After evaluating the significance of control factors through ANOVA and perceiving their trends the next step is to establish a mathematical relationship of the response attribute with selected control factors. Multiple linear regression analysis technique has been used to find the relationship of control factors with the response variable. The fundamental relationship of the said model is described in Eq. 5.1.

$$\boldsymbol{Y = b_0 + b_1 X_1 + b_2 X_2 + \ldots + b_N X_N} \quad (5.1)$$

Here, "Y" represents the response attribute, X_1 ….X_N are representing the value of the predictor variables whereas b_o accounts for the regression constant if all the predictors are set at zero and b_1….b_N are the coefficients. These coefficients are presenting the predicted change in mean value of the selected response attribute per unit change in the predictor value. Only those factors have been used for developing the multiple liner regression model that were found to be statistically significant as per ANOVA results. The mathematical relationship of the selected response characteristic with the significant parameters is described in Eq. 5.2.

$$\boldsymbol{Cutting\ Speed = 3.16508 - 0.16775 LT_{SS} - 0.118333 LT_{MS} - 3.30333 D_W + 0.25791 P_{ON}} \quad (5.2)$$

Where "LT_{SS}", "LT_{MS}", "D_W", and "P_{ON}" are the layer thickness of stainless steel, layer thickness of mild steel, wire diameter and pulse on time, respectively. ANOVA has been carried out to validate the developed regression model at a confidence interval of 95%. The results of ANOVA are shown in Table 5.3.

Table 5.3 ANOVA for cutting speed for multiple linear regression

Source	DF	Seq SS	Adj SS	Adj MS	F	P
Regression	4	1.63	1.63	0.41	20.8	0.0000149
Error	13	0.26	0.26	0.02		
Total	17	1.89				

Based on the results of ANOVA, it has been observed that p-value of the purposed model is quite lower than the defined alpha value (α=0.05) and also the model has high F-value. Both of these values indicate that the developed model is statistically significant. Futhermore, normal probabilty plot of residuals has also been made as this plot is oftenly used to acess the adequacy of the developed regression model [190]. The normal probability plot of residuals for cutting speed as response variable is presented in Figure 5.6. Residual is defined as the difference between the recorded/observed value and the model fitted value of the response. Normal probability plot of residuals for cutting speed clearly shows that residuals are normally distributed. The difference between model predicted and observed value seemed to be quite minimal thus highlighting the adequacy of the devloped regression model.

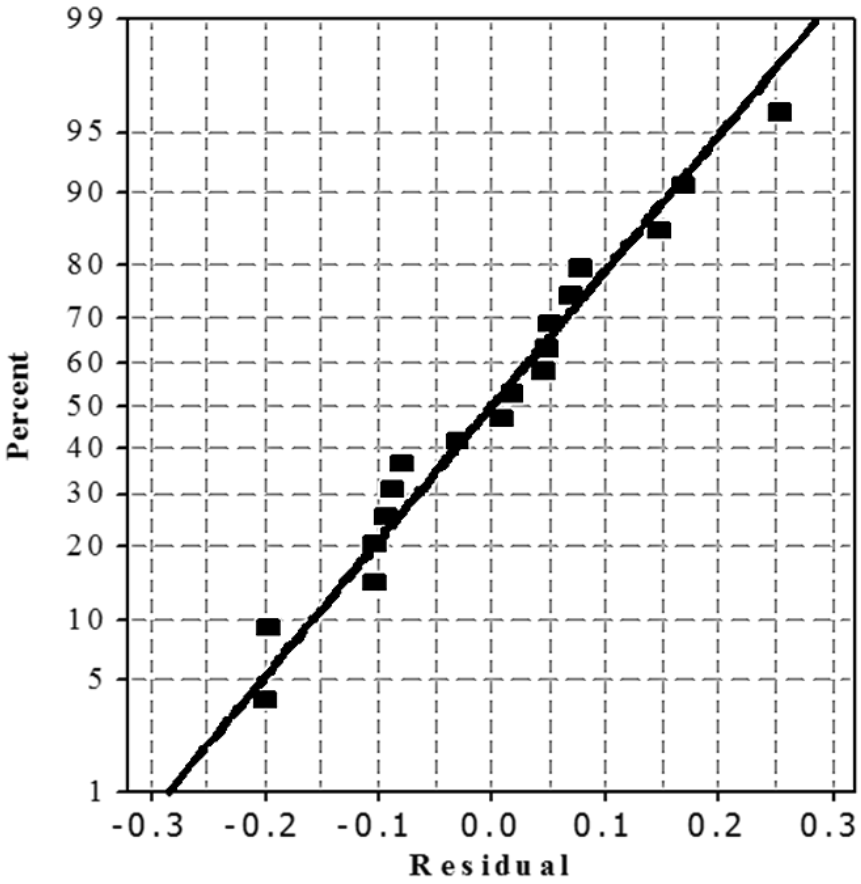

Figure 5.6 Normal probability plots of residuals for cutting speed

Another plot between residuals versus observation order has also been drawn as shown in Figure 5.7. The purpose of this plot is to evaluate that for which observation the magnitude of the residual is high and to identify the pattern of residual if exists. It is depicted from the Figure 5.7 that the magnitude of the residual is large for observation number 1, 3, 10 and 14. It was also noticed that the value of residual is positive in ten experimental runs whereas for the remaining experimental trials it is negative. The magnitude of residuals are approximately within the range of -0.2 – 0.2.

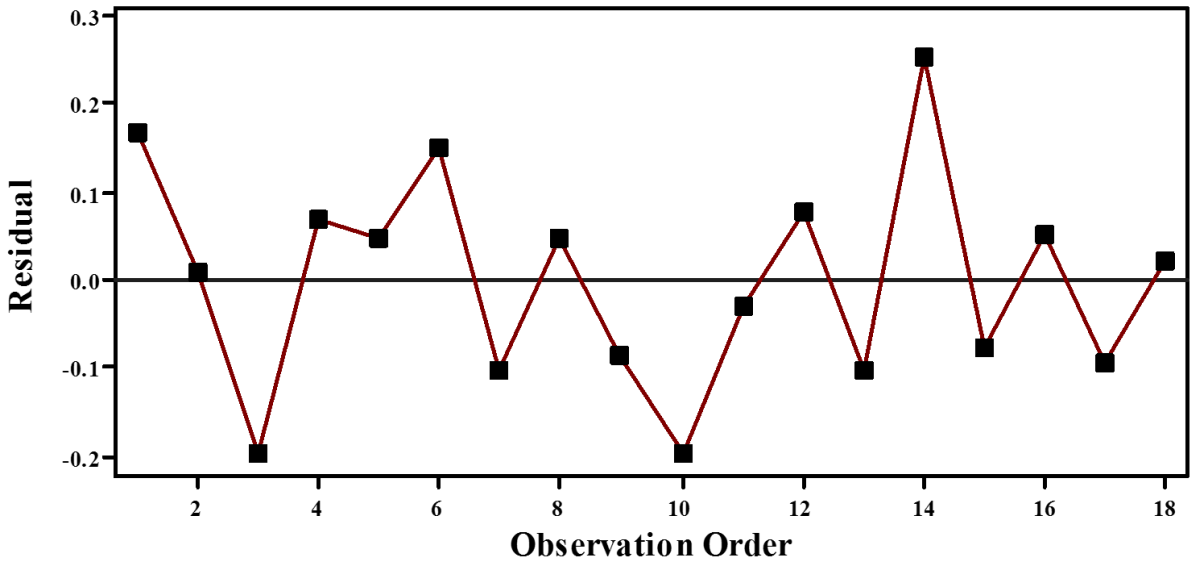

Figure 5.7 Residuals versus observation order

Additionally, the percentage error has also been calculated for all the experimental runs which are shown in Table 5.4. For calculating the percentage error initially difference between experimental and predicted values of cutting speed is calculated. Then this difference is divided by the predicted value of the cutting speed and multiplied by hundred which gives the percentage error. It is revealed that there exists an average error of about 4.8% between the experimental and predicted values of the cutting speed. The maximum error comes out to be 11% during 14^{th} experimental run and also in this experimental run the magnitude of the residual is maximum. The minimum error calculated between experimental and predicted values comes out to be only 0.1% that is fairly a small difference thus projecting the conformance of the developed model. The same has also been portrayed in Figure 5.8 where black line is representing the experimental values whereas predicted values are presented with red line. The two lines goes side by side throughout the experimentation. This validates the suitability of the purposed model.

Table 5.4 Percentage error in experimental and predicted cutting speeds

Exp. No.	Exp. Cutting Speed (mm/min)	Pred. Cutting Speed (mm/min)	% Error
1	2.07	1.9	8.8
2	2.38	2.3	0.3
3	2.15	2.3	8.4
4	2.32	2.3	3.1
5	1.99	1.9	2.5
6	2.07	1.9	7.8
7	2.31	2.4	4.3
8	1.66	1.6	2.9
9	1.50	1.6	5.5
10	1.87	2.1	9.6
11	2.01	1.9	0.1
12	2.59	2.5	3.1
13	2.22	2.3	4.4
14	2.55	2.3	11
15	1.42	1.5	5.2
16	2.04	1.9	0.1
17	1.87	2.0	4.8
18	1.68	1.7	1.2
	Average Percentage Error		4.8

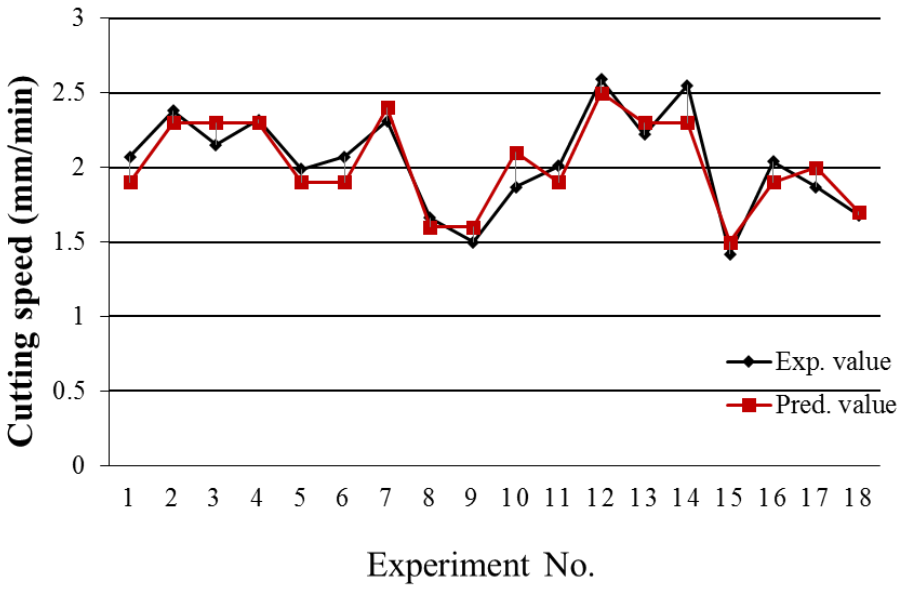

Figure 5.8 Comparison between exp. and pred. values of cutting speed

5.2 Experimental results of surface roughness of stainless steel layer

Upon completion of experiments according to the Taguchi's experimental design technique (L18), the surface roughness (Ra) of the machined specimen has been measured with the aid of Surtronic surface roughness tester (S128). Surface roughness of both the layers of cladded specimen have been found in terms of arithmetic averages (Ra) which is a frequently used parameter for the assessment of surface roughness and are presented in Table 5.5 and Table 5.7.

Table 5.5 Experimental results of surface roughness of stainless steel layer

Exp. No.	Or	LT_{SS} (mm)	LT_{MS} (mm)	D_W (mm)	Pr	SV (V)	P_{ON} (µs)	F_W (mm/s)	surface roughness (µm)
1	A	2	6	0.30	0.7	30	3	60	2.62
2	A	2	7	0.20	1.0	40	4	140	2.68
3	A	2	8	0.25	1.3	50	5	220	2.94
4	A	3	6	0.30	1.3	40	5	140	2.59
5	A	3	7	0.20	0.7	50	3	220	2.85
6	A	3	8	0.25	1.0	30	4	60	2.51
7	A	4	6	0.20	1.0	30	5	220	2.84
8	A	4	7	0.25	1.3	40	3	60	2.67
9	A	4	8	0.30	0.7	50	4	140	2.57
10	B	2	6	0.25	1.0	50	3	140	2.89
11	B	2	7	0.30	1.3	30	4	220	2.93
12	B	2	8	0.20	0.7	40	5	60	3.11
13	B	3	6	0.20	1.3	50	4	60	3.01
14	B	3	7	0.25	0.7	30	5	140	2.83
15	B	3	8	0.30	1.0	40	3	220	2.49
16	B	4	6	0.25	0.7	40	4	220	2.65
17	B	4	7	0.30	1.0	50	5	60	2.94
18	B	4	8	0.20	1.3	30	3	140	3.04

5.2.1 ANOVA of surface roughness of stainless steel layer

Analysis of variance has been performed to evaluate the significant control factors with respect to the surface roughness of the stainless steel layer. The confidence interval of 95% has been selected for caring out the ANOVA. The results of the analysis are presented in Table 5.6.

Table 5.6 ANOVA of surface roughness of stainless steel layer

Source	DF	Seq SS	Adj SS	Adj MS	F	P
Or	1	0.15	0.15	0.15	36.30	**0.03**
LT_{SS} (mm)	2	0.07	0.07	0.03	8.22	0.11
LT_{MS} (mm)	2	0.01	0.01	0.00	1.05	0.49
D_W (mm)	2	0.17	0.17	0.09	21.69	**0.04**
SV (V)	2	0.09	0.09	0.04	10.66	0.09
F_W (mm/s)	2	0.01	0.01	0.00	0.71	0.58
Pr	2	0.06	0.06	0.03	7.40	0.12
P_{ON} (µs)	2	0.07	0.07	0.04	9.20	0.10
Error	2	0.01	0.01	0.00		
Total	17	0.63				
Model summary: S = 0.0633772 R-Sq = 98.72% R-Sq(adj) = 89.11%						

The results of the aformetioned analysis depicts that two input parameters namely; workpiece orientation, Or (0.03) and diameter of the wire electrode, D_W (0.04) have a p-value lesser than the defined alpha value (α= 0.05) and also these control parametes holds a high F-value. This indicates that a slight change in the value of the mentioned control factors caused a noticeable change in the value of response attribute. In other words, the said input parameters are the significnat factors with respect to the surface roughness of the stainless steel layer in WEDM of stainless-clad steel workpiece material. The percentage contribution of input parameters has also been calcultedd based on the resluts of ANONA and is shown in Figure 5.9.

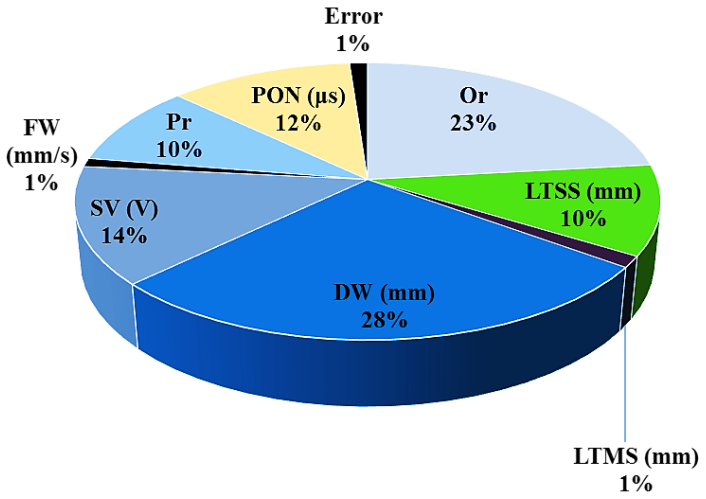

Figure 5.9 Percentage contribution of control factors for stainless steel layer surface roughness

The percentage contribution of the wire diameter (D_W) of brass wire is observed to be the maximum one i.e. 28%. The orientation of the workpiece (Or) is rated as the second prominent control factor for stainless steel layer surface roughness with a percentage contribution of 23% followed by servo voltages (SV), pulse on time (P_{ON}), layer thickness of stainless steel layer (LT_{SS}), pressure ratio (Pr), layer thickness of mild steel layer (LT_{MS}) and wire feed (F_W) with percentage contribution of 14%, 12%, 10%, 10%, 1% and 1%, respectively. The percentage contribution of the error is found to be quite minimal (~ 1%), thus projecting the feasibility of the purposed model. The same can also be seen from the model summary presented in Table 5.6. As the model has an R-Sq (adj) value of 89.11% that witnessed the model validity.

5.3 Experimental results of surface roughness of mild steel layer

The results pertaining to the surface roughness of the mild steel layer at an evaluation length of 4 mm and a cut-off length of 0.8 mm are tabulated in Table 5.7.

Table 5.7 Experimental results of surface roughness of mild steel layer

Exp. No.	Or	LT_{SS} (mm)	LT_{MS} (mm)	D_W (mm)	Pr	SV (V)	P_{ON} (µs)	F_W (mm/s)	surface roughness (µm)
1	A	2	6	0.30	0.7	30	3	60	2.90
2	A	2	7	0.20	1.0	40	4	140	2.80
3	A	2	8	0.25	1.3	50	5	220	2.84
4	A	3	6	0.30	1.3	40	5	140	2.76
5	A	3	7	0.20	0.7	50	3	220	2.99
6	A	3	8	0.25	1.0	30	4	60	2.66
7	A	4	6	0.20	1.0	30	5	220	2.97
8	A	4	7	0.25	1.3	40	3	60	2.71
9	A	4	8	0.30	0.7	50	4	140	3.05
10	B	2	6	0.25	1.0	50	3	140	2.75
11	B	2	7	0.30	1.3	30	4	220	3.00
12	B	2	8	0.20	0.7	40	5	60	3.19
13	B	3	6	0.20	1.3	50	4	60	3.02
14	B	3	7	0.25	0.7	30	5	140	3.04
15	B	3	8	0.30	1.0	40	3	220	2.51
16	B	4	6	0.25	0.7	40	4	220	2.92
17	B	4	7	0.30	1.0	50	5	60	3.04
18	B	4	8	0.20	1.3	30	3	140	3.17

5.3.1 ANOVA of surface roughness of mild steel layer

ANONA is performed after recording the measurements of surface roughness of mild steel layer at a confidence interval of 95% to evaluate the significant factors for the selected response characteristic. The results of ANOVA of mild steel layer are described in Table 5.8.

Table 5.8 ANOVA of surface roughness of mild steel layer

Source	DF	Seq SS	Adj SS	Adj MS	F	P
Or	1	0.08	0.08	0.08	38.36	**0.03**
LT_{SS} (mm)	2	0.07	0.07	0.03	15.68	0.06
LT_{MS} (mm)	2	0.02	0.02	0.01	4.06	0.20
D_W (mm)	2	0.18	0.18	0.09	41.04	**0.02**
SV (V)	2	0.07	0.07	0.04	16.34	0.06
F_W (mm/s)	2	0.00	0.00	0.00	0.87	0.54
Pr	2	0.11	0.11	0.06	26.51	**0.04**
P_{ON} (µs)	2	0.05	0.05	0.03	12.73	0.07
Error	2	0.00	0.00	0.00		
Total	17	0.59				
Model summary: S = 0.0464280			**R-Sq = 99.27%**		**R-Sq(adj) = 93.81%**	

As mentioned earlier that in ANOVA, any input parameter that has a p-value less than the defined alpha value is considered to be the significant parameter for the prescribed response variable. The results of ANOVA revealed that three input parameters, orientation of the workpiece, Or (0.03), wire diameter, D_W (0.02) of the used wire and pressure ratio, Pr (0.04) of the dielectric fluid hold a p-value lesser than the defined alpha value (α=0.05) and their F-value is also higher in contrast to the rest of the parameters as described in Table 5.8. Hence, these factors are proved to the significant control factors that plays a vital role in controlling the surface roughness of the mild steel surface in WEDM of selected workpiece material. The percentage contribution of input parameters is presented in Figure 5.10.

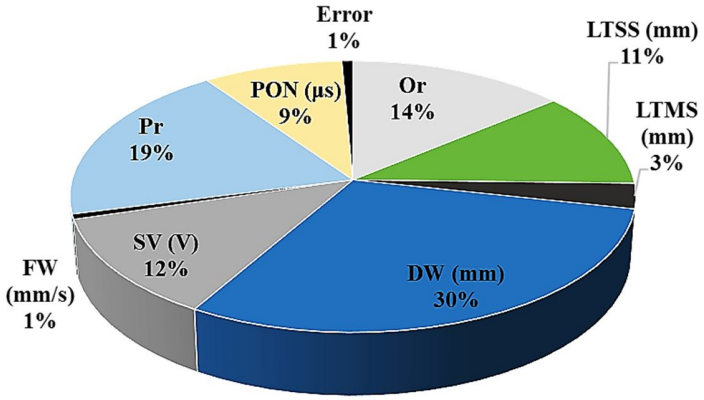

Figure 5.10 Percentage contribution of control factors for mild steel layer surface roughness

Based on the results of the analysis, it has been noticed that wire diameter (D_W) holds a maximum percentage contribution of 30% in controlling the roughness of mild steel surface in WEDM of stainless-clad steel specimen. It is important to mention that the said parameter is also proved to be the most contributing factor in controlling the surface roughness of the stainless steel layer as well. Pressure ratio (Pr) is observed to be the second most contributing factor with a percentage contribution of 19% with regard to the selected response. The orientation of the workpiece (Or) is rated as the third most contributing factor with a percentage contribution of 14%. The accumulative contribution of the narrated three input parameters come out to be 63% which means that these factors play a key role in determining the surface roughness of the mild steel layer. Among other parameters, percentage contribution of servo voltages, SV (12%), layer thickness of stainless steel layer, LT_{SS} (11%) and pulse on time, P_{ON} (9%) are prominent as compared to other control factors.

5.4 Parametric effects analysis of surface roughness

Main effects plot analysis has been performed in order to evaluate the trend of input parameters with respect to the selected response variable after evaluating the significance of parameters for the surface roughness of both the layers of cladded workpiece material using ANOVA.

The results of the main effects plot analysis for the surface roughness of both the layers i.e. stainless steel layer and mild steel layer are presented in Figure 5.11 and Figure 5.12 respectively.

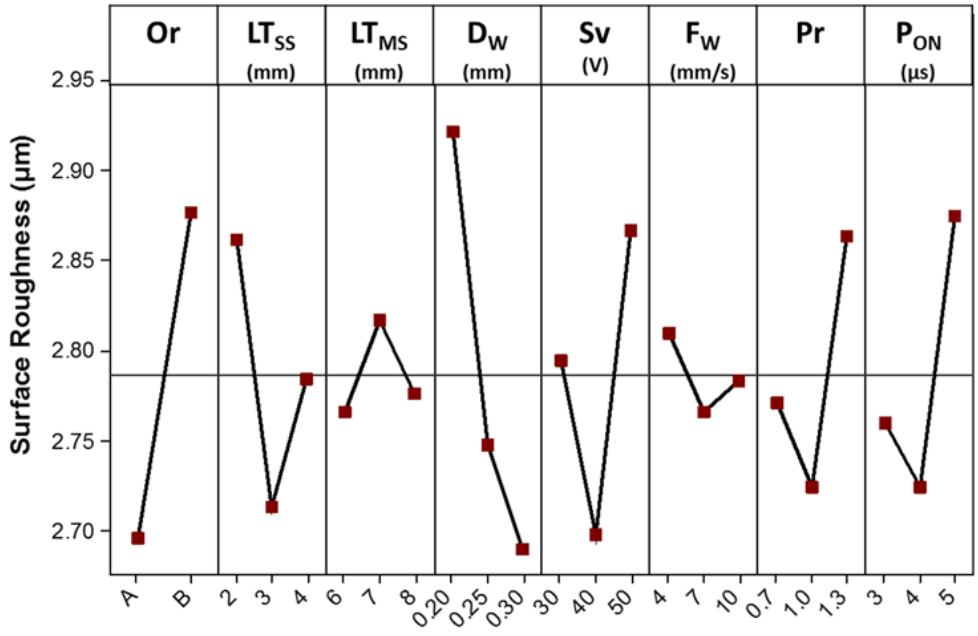

Figure 5.11 Effects of control factors on surface roughness of stainless steel layer

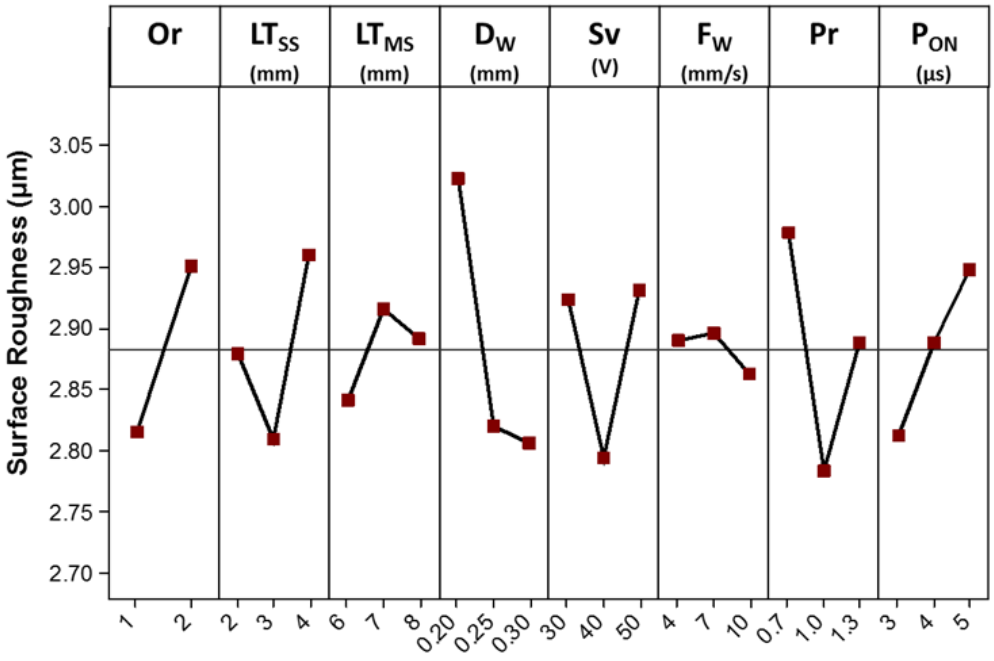

Figure 5.12 Effects of control factors on surface roughness of mild steel layer

5.4.1 Effect of workpiece orientation on surface roughness

It is observed that orientation (Or) "A" (stainless steel layer faces the top) of the cladded workpiece yields a better surface finish for both the layers in contrast to the other orientation (Or) "B" (mild steel layer lies at the top) as per main effects plot analysis presented in Figure 5.11 and Figure 5.12. It is attributed to the fact that stainless steel layer possesses higher hardness and has more density in comparison to the mild steel surface due to which it requires higher discharge energy for its machining. Actually, in WEDM, cutting of the target material has been carried out by the constantly moving wire electrode. The surface of this wire gets damaged because of experiencing multiple electric sparks as it moves downwards along the thickness of the workpiece to be machined.

Surface quality produced in WEDM is directly affected by the wire wear [146]. The increase in wire wear is always associated with a correspondent increase in the value of surface roughness of the machined part in WEDM. When the specimen is placed in orientation Or) "B" (mild steel layer lies at the top) a fresh wire electrode comes in contact with the mild steel surface and on the other end stainless steel surface is subjected to used wire electrode. The cutting efficiency of the used wire electrode is reduced and that's why it consumes more time to machine stainless steel surface as the density and the hardness of this layer is higher as compared to the other layer.

A Pramanik et al. [191] found that the availability of reinforced particles (having higher hardness, high density and high melting temperature) in the low melting matrix material cause a delay in machining of metal matrix composite in WEDM. Similarly, when stainless steel layer is subjected to cut by a deteriorated wire electrode, a delay is occurred although the surface of mild steel layer has already been machined. Therefore, the surface of mild steel layer is subjected to multiple sparking due to the delay caused by stainless steel surface. K. Kanlayasiri et al. [192] described that the phenomena of multiple sparking resulted into an increase in the value of surface roughness of the workpiece in WEDM. Therefore, surface finish of stainless steel layer reduces as it is machined by deteriorated wire electrode whereas surface roughness of mild steel layer increases as it suffers multiple sparking.

Hence, it is worthy to place the specimen in Orientation (Or) "A" where fresh wire electrode comes in contact with the stainless steel surface (A material having high density and higher hardness) and generates required amount of discharge energy to perform cutting action.

Although, the surface quality of the wire depreciates as the wire electrode moves downward along the thickness of cladded specimen but still amount of discharge energy produced is adequate enough to melt the mild steel surface that has high electrical conductivity, low density and lesser hardness as compared to stainless steel surface. Moreover, this way of placement of workpiece also minimize the chance of multiple sparking.

It is important to mention that the aforesaid control factor i.e. orientation of workpiece (Or) is also proved to be a significant control factor affecting the surface roughness of both layers (stainless steel layer and mild steel layer) according to the results of ANOVA presented in Table 5.6 and Table 5.8. Furthermore, it is revealed that the percentage contribution of the selected parameter (Or) in controlling the surface roughness of stainless steel layer is 23.25% and for mild steel layer the value of percentage contribution is 14%. This shows that the percentage contribution of workpiece orientation (Or) in controlling the surface roughness of mild steel surface is approximately 40% lesser as compared to its percentage contribution in controlling the surface roughness of stainless steel layer. Hence, the narrated input parameter is seemed to have more influence on the surface finish of stainless steel layer. The same is also depicted from the main effects plots described in Figure 5.11 and Figure 5.12.

The surface roughness profiles recorded for both the orientations, "A" and "B" have also witnessed the same i.e. the cut surface of cladded specimen is observed to have lesser surface irregularities imparted to both layers in orientation, Or "A" (stainless steel layer faces the top) in contrast to the other orientation, Or ("B" mild steel layer lies at the top) of the workpiece as demonstrated in Figure 5.13.

Additionally, scanning electron microscopic (SEM) analysis of the machined surface has also been carried to validate the aforementioned argument. Scanning electron microscope (SEM) images taken for both the orientations "A", "B" are shown in Figure 5.14. Figure 5.14 (a-b) accounts for the first case (specimen is placed in orientation "A") and the Figure 5.14 (c-d) represent the second case (cladded specimen is placed in orientation "B").

Based on the SEM micrographs it is observed that the machined surface contains melted re-deposits, craters and spherical modules. As described earlier, that melted redeposit are basically the re-solidified melted debris that were not flushed away by flushing dielectric fluid whereas succession of electric sparking occurs between electrode and workpiece material resulted into the formation of the craters on the cut surface in WEDM. The formation of the spherical modules on the machined surface is due to the surface tension of the molten material in the WEDM.

The magnitude of the surface irregularities found on the cut surface is smaller when the cladded specimen is positioned in orientation (Or) “A” (stainless steel surface lies at the top) as described in Figure 5.14. It is evident from the Figure 5.14 that the cut surface is likely to have spherical modules of larger diameter and also larger melted re-deposits on the surface of both layers if specimen is placed in such a way that mild steel layer faces the top (Orientation, Or “B”). The increase in the diameter of the spherical module is always associated with the increase in the value of surface roughness [193]. Also, the crater depth is observed to be lesser in orientation “A” in contrast to the other orientation (“B”) of the workpiece material. Consequently, surface roughness on both layer increases if workpiece is placed in orientation (Or) “B”.

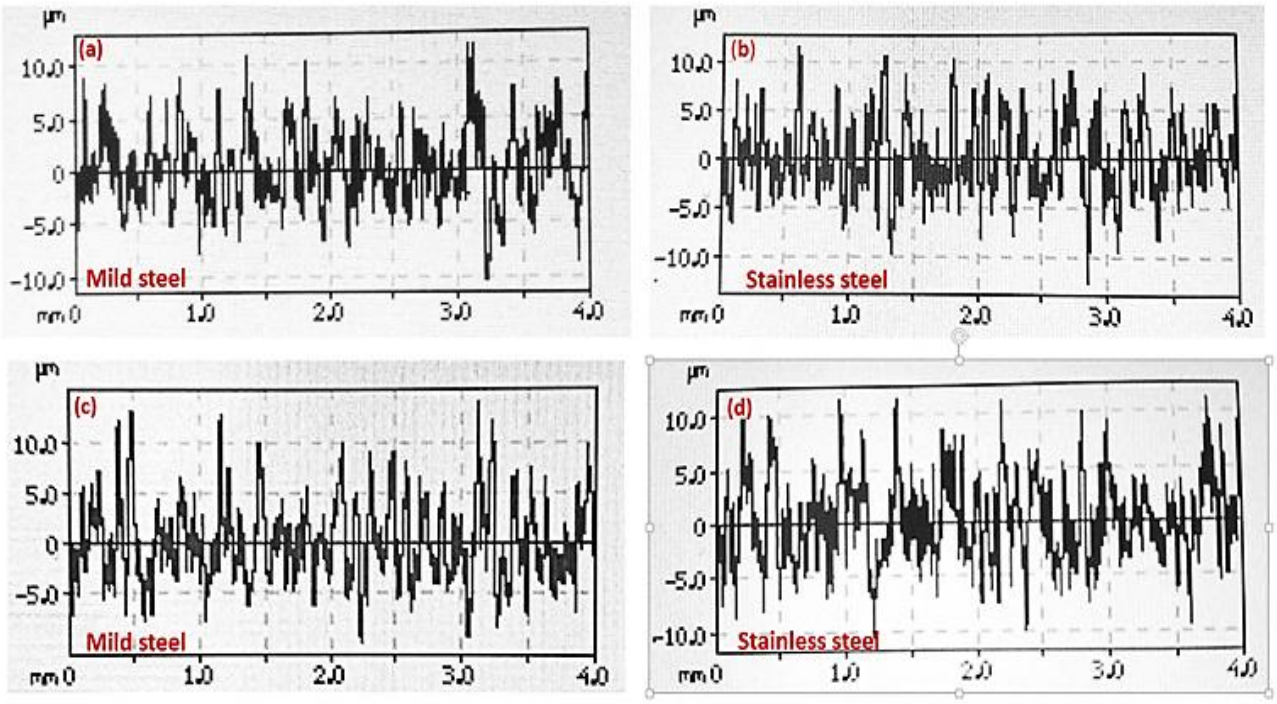

Figure 5.13; (a-b) surface roughness profiles of both layers in orientation “A” (c-d) surface roughness profiles of both layers in orientation “B”

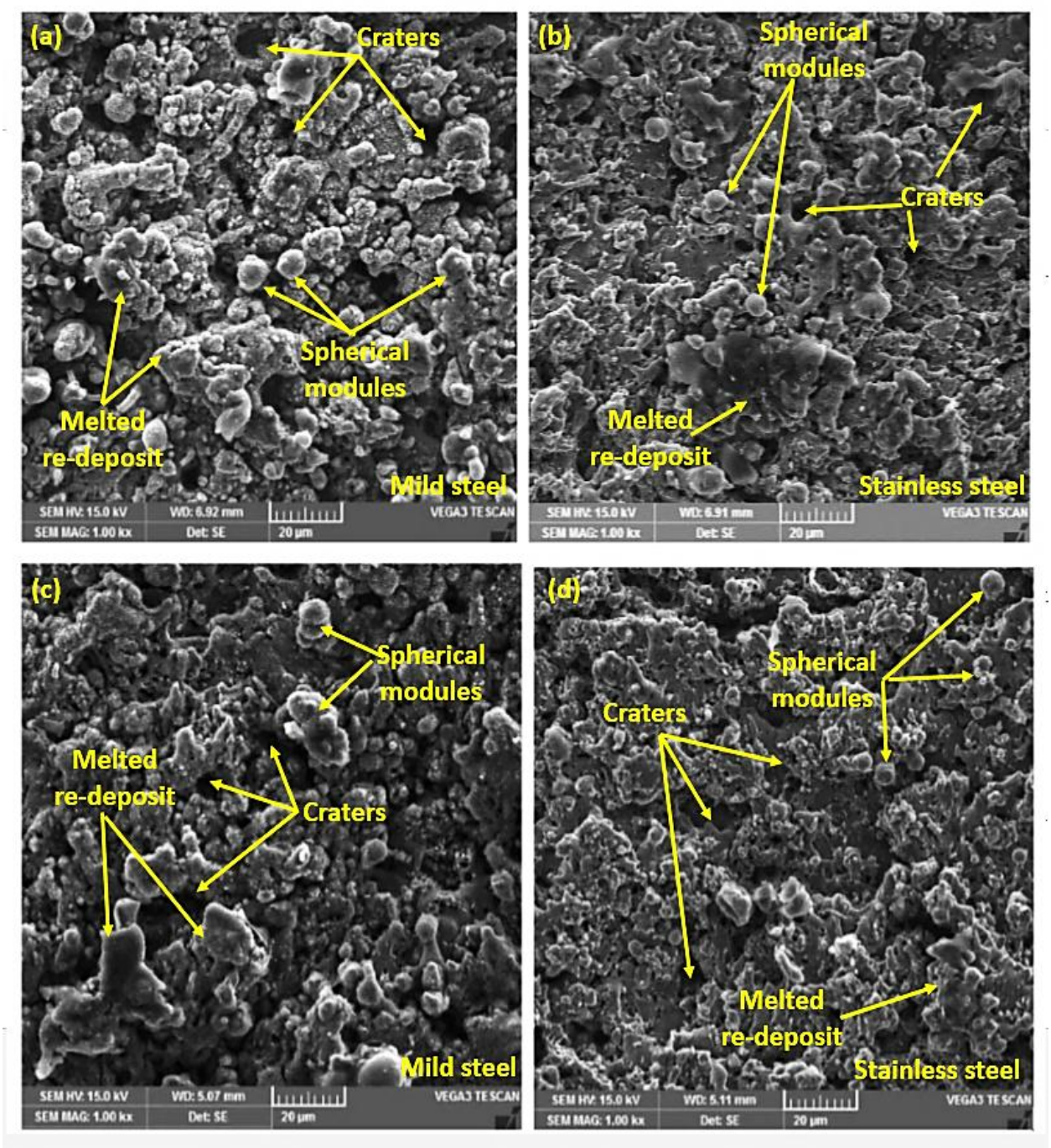

Figure 5.14; (a) SEM micrograph of mild steel layer in orientation "A" at 1000X, (b) SEM micrograph of stainless steel layer in orientation "A" at 1000X (c) SEM micrograph of mild steel layer in orientation "B" at 1000X (d) SEM micrograph of stainless steel layer in orientation "B at 1000x

It is also interesting to note that the surface of mild steel layer is subjected to deeper craters as compared to the stainless steel layer in both experimental runs that is primarily because of higher electrical conductivity ($58.52x10^3$ ohm^{-1} cm^{-1}) in comparison to the other layer ($12.35x10^3 ohm^{-1}$ cm^{-1}). Thus, an intense spark is produced at mild steel surface that subsequently, produces a deeper crater by removing more material that upholds the value of surface roughness of the said layer as highlighted in Figure 5.15 and Figure 5.16.

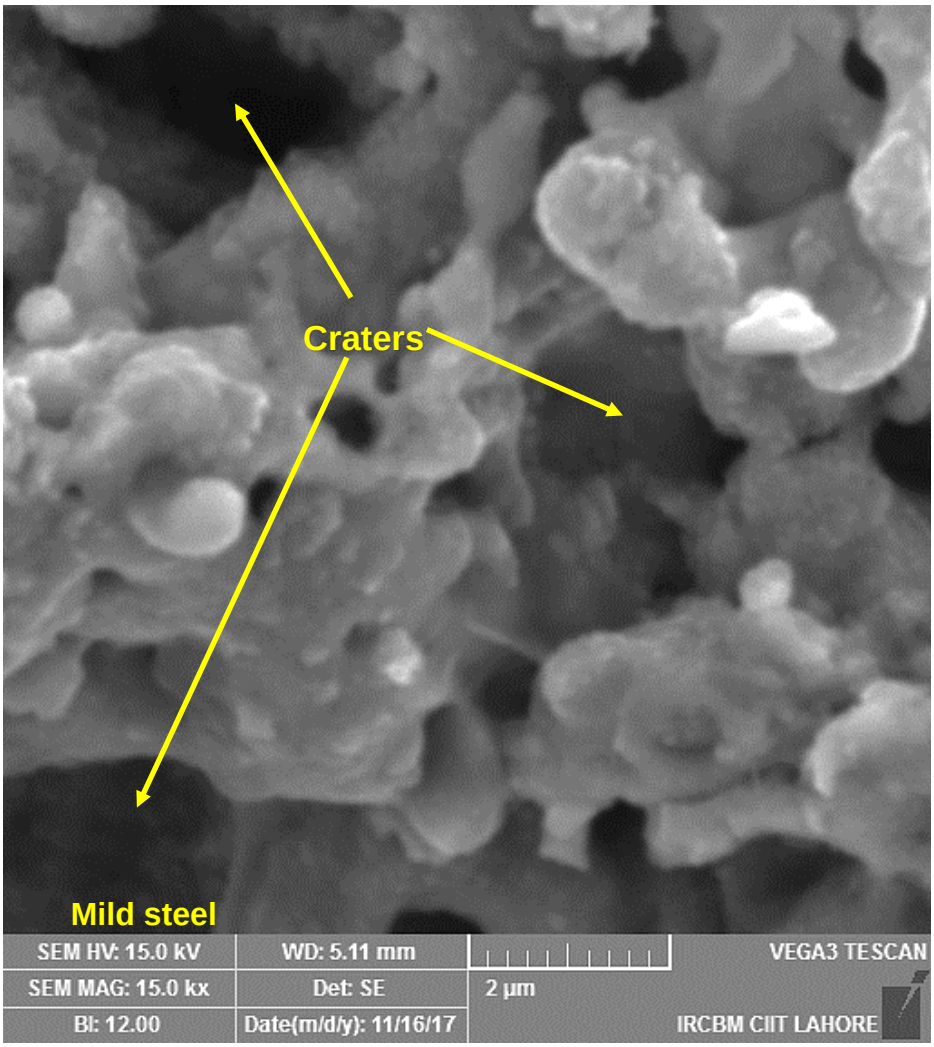

Figure 5.15 SEM micrograph of mild steel surface in Orientation "B" at 15000x

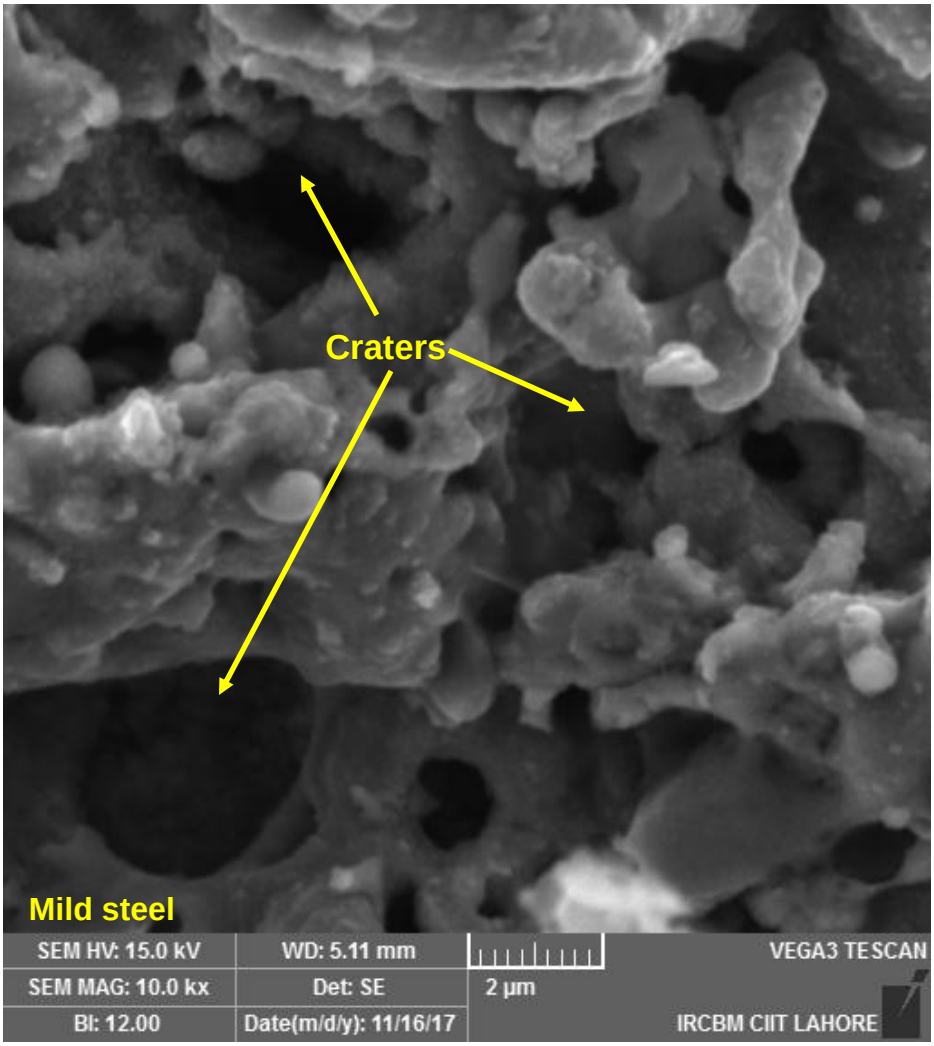

Figure 5.16 SEM micrograph of mild steel surface in Orientation "B" at 10000x

It is also worth noting that micro-cracks are observed in the recast layer formed at the surface of the mild steel layer when WEDM is performed by placing the workpiece in orientation “B” as shown in Figure 5.17. The formation of these micro-cracks are presumably due to the reason that the surface of mild steel layer is experiencing the phenomena of multiple sparking as in case of orientation “B” deteriorated wire electrode comes in contact with the stainless steel surface that consumes more time because of its low electrical conductivity, high density and higher hardness although a cut has already been produced in the mild steel layer.

Therefore, the surface of mild steel layer suffers the phenomena of multiple sparking that not only reduces the surface finish of the said layer but also resulted into the formation of micro-cracks in the recast layer.

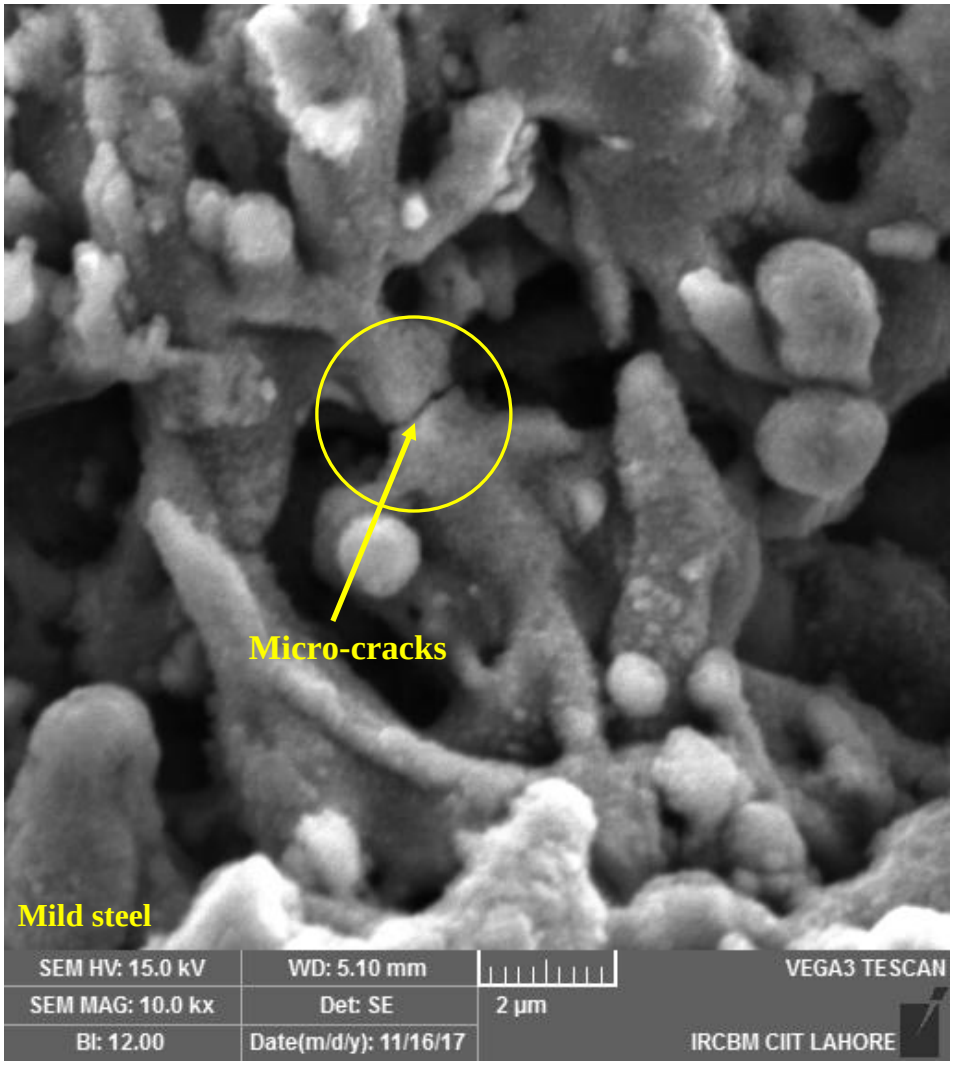

Figure 5.17 SEM image of mild steel layer machined in orientation "B" at 10000x

Hence, the placement of the workpiece in orientation “A” is validated to be a preferred orientation in order to have a better surface finish (lower surface roughness) based on aforementioned results and their discussion.

5.4.2 Effect of wire diameter (D_W) on surface roughness

The diameter of the wire electrode is found to have a significant effect on the surface roughness of both the layers on cladded material in WEDM as per ANOVA results presented in Table 5.6 and Table 5.8.

Beside the fact that diameter of wire electrode is significant parameter for surface roughness, the percentage contribution of the said factor for both the layers indicates that wire diameter is the most contributing input variable with respect to the surface roughness of the two layers of the stainless-clad steel workpiece material. The percentage contribution of the above mentioned input parameter (D_W) comes out to be 27.8% for controlling the roughness of stainless steel surface and in case of other layer, percentage contribution is found to be 30%. The value of the percentage contribution of diameter of wire electrode (D_W**)** is higher for mild steel layer that shows the said input factor is more influential with regard to roughness of mild steel layer in contrast to stainless steel surface. Higher value of electrical conductivity of the mild steel surface is the primary reason due to which it secured high value of percentage contribution. As described earlier, WEDM is a thermo-electric process whereby machining is performed by melting and vaporization of the target material and the amount of material removed is mainly dependent on the available discharge energy. Both wire diameter (D_W) and electrical conductivity of workpiece material play a key role in determining the amount of discharge energy. As wire diameter (D_W) is same for the two layers so the difference of discharge energies is mainly due to the electrical conductivities of both layers. As, the value of this factor is higher for mild steel layer that's why more discharge energy tends to be produced and subsequently more amount of material is being removed that is also associated with a change in the value of surface roughness. Therefore, mild steel layer surface roughness is more sensitive towards a change in the value of wire diameter or in other words wire diameter (D_W) holds more percentage contribution with the regard to mild steel surface roughness in comparison to the other layer. Moreover, the said input parameter is found to have an inverse relationship with respect to the roughness of both layer of cladded specimen as per the main effects plots represented in Figure 5.11 and Figure 5.12. The increase in wire diameter results into the reduction in value of the surface roughness of both the layers in WEDM of stainless-clad steel.

This is primarily attributed to the fact that with the increase in the wire diameter (D_W) the contact area between wire electrode and workpiece is increased that consumes more time as larger amount of material is to be machined and subsequently, cutting speed is reduced. This reduction in cutting speed in turns helped in the effective flushing of melted debris. Hence, the surface finish of the machined specimen got improved (surface roughness is reduced).

For instance, during 18th experimental (wire diameter; D_W = 0.2mm) run, the cutting speed was found to be 1.7 mm/min whereas the value of cutting speed was 1.5 mm/min (~12% lesser than the previously mentioned value of cutting speed) in case of 9th experiment. This reduction in cutting speed in turns provides better flushing of debris produced during machining. As a result, the surface finish of the machined part gets improved. The same has also been witnessed by the roughness profiles and SEM images of machined surface presented in Figure 5.13 and Figure 5.14 for the prescribed experimental conditions.

The SEM images of machined surface using the above mentioned experimental conditions have shown that the size of melted re-deposit is larger in the case when machining of cladded material is being carried out with 0.2 mm diameter wire (Figure 5.14, c-d) in comparison to the situation when cutting is done using larger wire diameter (Figure 5.14, a-b). It has also been noticed that diameter of the spherical modules found on the cut surface of both layers is lager when cutting is performed with the aid of smaller diameter wire (0.2 mm) in contrast to the other alternative. Additionally, the surface contains shallow craters while using lager diameter brass wire electrode as well.

A similar kind of findings about the effect of wire diameter (D_W) of electrode on the surface roughness of machined specimen were reported in another research work carried out on WEDM of mild steel [194].

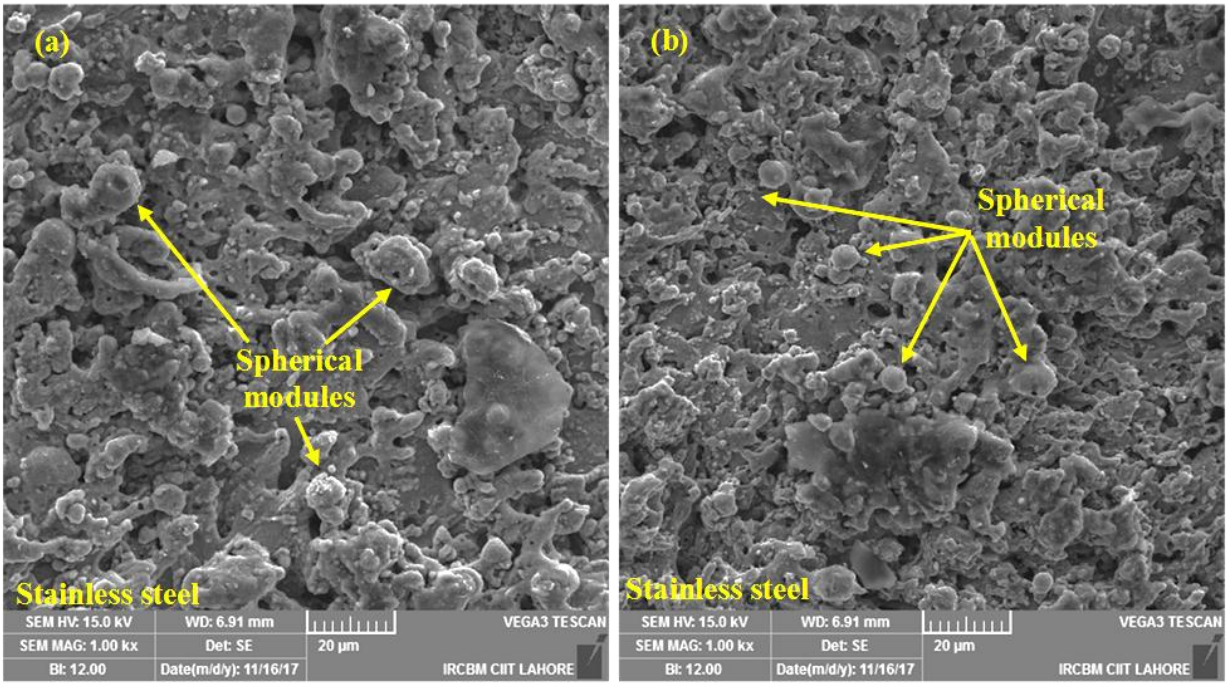

Figure 5.18; (a) SEM image of stainless steel layer at 1000x machined using 0.2 mm wire, (b) SEM image of stainless steel layer at 1000x machined using 0.3mm wire

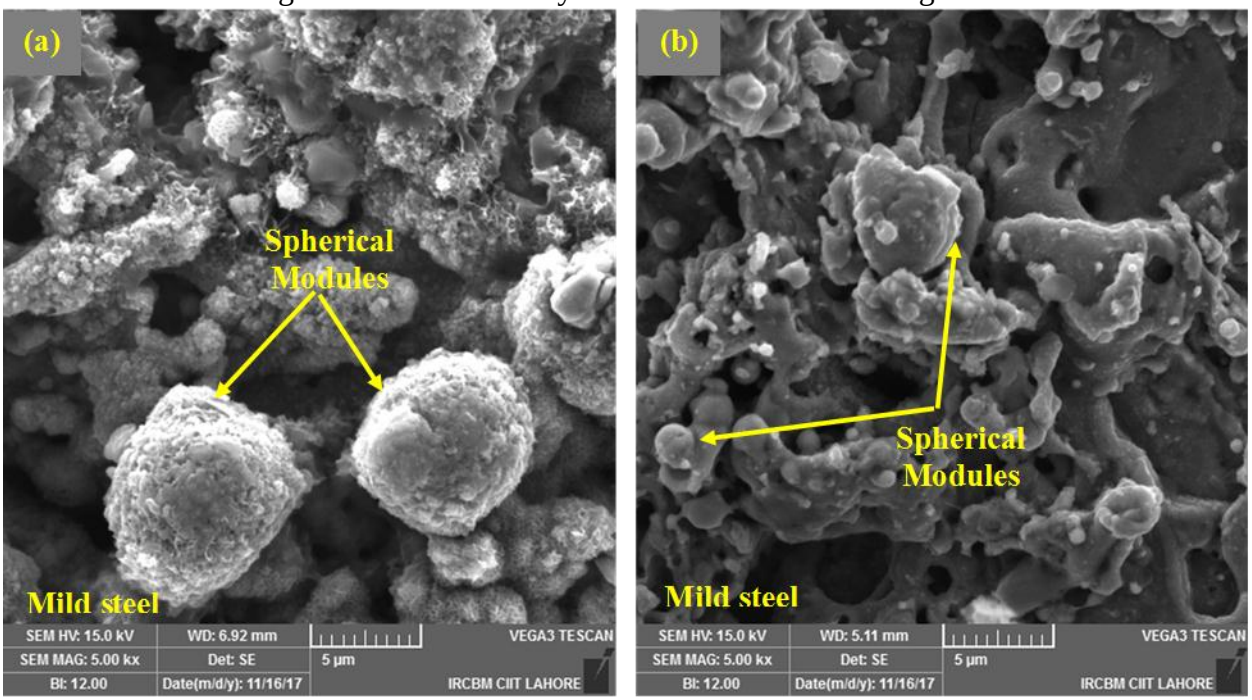

Figure 5.19: (a) SEM image of mild steel layer at 5000x machined using 0.2 mm, (b) SEM image of mild steel layer at 5000x machined at 0.3mm

5.4.3 Effect of pressure ratio (Pr) on surface roughness of cladded specimen

Pressure ratio is basically the ratio of flushing pressure of upper nozzle to the flushing pressure of lower nozzle. It is important to mention that although the effect of dielectric pressure on surface roughness has been investigated by other researchers but the effect of the pressure ratio is still to be evaluated which is discussed here.

The effect of pressure ratio has been found statistically significant for controlling the surface roughness of mild steel layer according to results of ANOVA shown in Table 5.8 but in case of stainless steel layer surface roughness, the said factor has failed to become a significant control parameter. This is attributed to the fact that more amount of material tends to be removed from mild steel surface as it has higher electrical conductivity (58.52×10^3 ohm^{-1} cm^{-1}), lower electrical resistivity (17×10^{-6} ohm.cm), lesser density (7.8g/cc) and lower hardness (39 HRA) in comparison to other layer as shown in Table 2.3. It has been found that Pressure ratio (Pr) is the second most contributing factor having percentage contribution of 19.3%.

Higher electrical conductivity and smaller resistivity of workpiece lead to increase the material removal rate [195]. Therefore, the more material is melted and vaporized from the mild steel surface thus, demands more appropriate level of flushing. Hence, the said input factor become more important with regard to the surface roughness of this layer. It has clearly been depicted from the SEM micrographs of the cut surface that the recast layer or white layer thickness observed on mild steel layer is more as compared to the thickness of white layer found on the stainless steel surface as shown in Figure 5.20 Figure 5.21. For instance, in 13th experimental run, about 6 μm thickness of re-cast layer has found to be deposited on the stainless steel surface whereas the magnitude of recast layer found on the mild steel surface is 19.5 μm (three folds the thickness of the white layer found on stainless steel surface). It is because of the fact that the spark produced in front of mild steel surface is more intense owing to have higher electrical conductivity. Consequently, more amount of material is being removed from the said layer of cladded specimen. Hence, it requires more appropriate level of flushing to flush away the melted debris.

Therefore, pressure ratio (Pr) is found to be the significant parameter in controlling the surface roughness of mild steel layer in WEDM of stainless-clad steel and necessitates a better flushing level as compared to stainless steel layer so the melted debris may not be re-solidify as recast layer. Moreover, mild steel surface also contains a deeper process affected region in comparison to depth

of process affected region observed on stainless steel surface as described in Figure 5.20 and Figure 5.21.

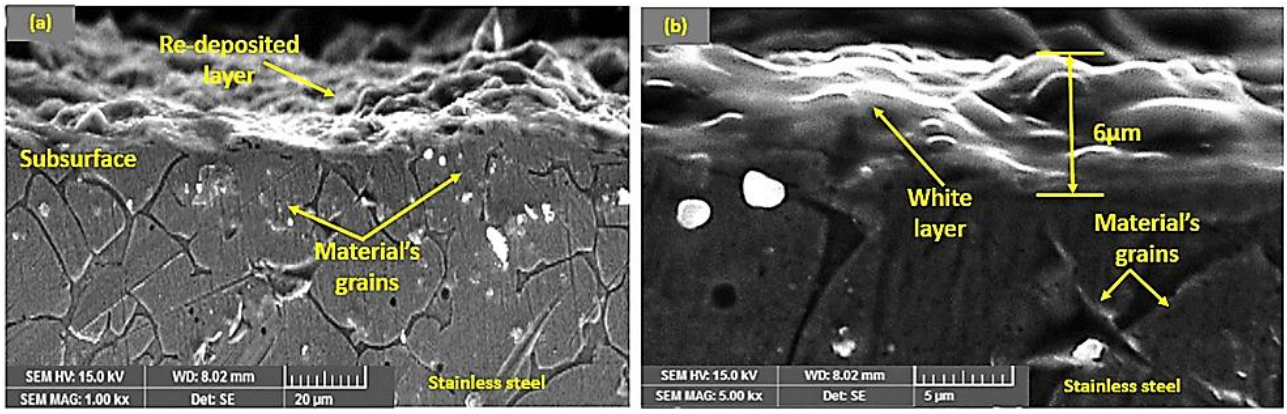

Figure 5.20; (a) SEM micrograph of stainless steel layer at 1000X, (b) SEM micrograph of stainless steel layer at 5000X

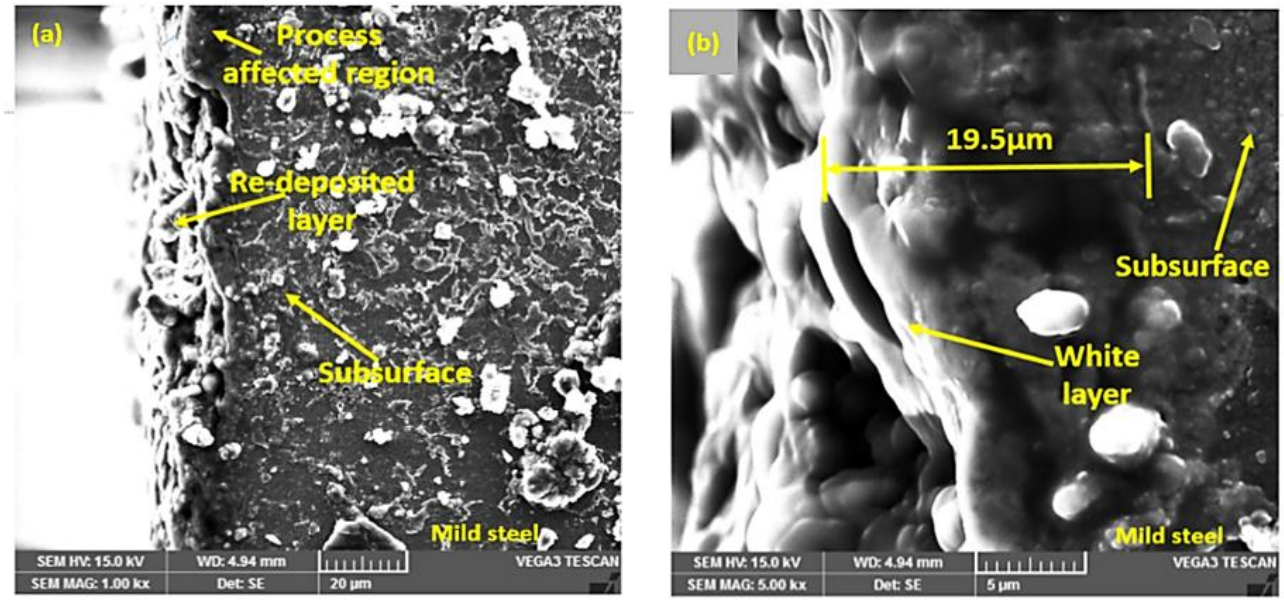

Figure 5.21; (a) SEM micrograph of mild steel layer at 1000X, (b) SEM micrograph of mild steel layer at 5000X

Furthermore, the value of pressure ratio (Pr) should be set at level 1 (upper nozzle flushing pressure is equal to the lower nozzle flushing pressure). Actually, the flushing dielectric exert a force on the moving brass wire electrode that causes wire vibrations.

These vibrations, not only yield rough surface but promote the chance of wire breakage [196]. Possibly the equal value of flushing pressure of both the nozzles reduces the magnitude of the force experienced by the wire electrode. Thus, the magnitude of wire vibrations also reduces and as a result better surface finish is obtained. The mentioned value of pressure ratio also results into better surface roughness of stainless steel layer as well as described in Figure 5.11. All the other parameters were found to be statistically insignificant for the roughness of both layers of stainless-clad steel in WEDM.

5.5 Mathematical modeling

Mathematical relationship of WEDM input parameters with the response variables has been established in this part of the study using multiple linear regression analysis. The description of this technique has already been provided. The regression models for the surface roughness of both layers are shown in Eqs. 5.3 and 5.4.

Surface roughness (stainless steel) = 3.09583 + 0.18 Or - 2.31667 D_W (5.3)
Surface roughness (mild steel) = 3.37167 + 0.135556 Or - 2.16667 D_W - 0.15 Pr (5.4)

The least square method was opted for calculating the constants and coefficients. Only those control factors have been considered for the development of regression model that are found to be significant for each selected response.

The developed regression models are then validated by ANOVA at 95% confidence interval. The results of the analysis are shown in Table 5.9 and Table 5.10. It is noticed that both the developed models have a p-value lesser than the predefined alpha value ($\alpha = 0.05$) showing that all the developed models are statistically significant.

Table 5.9 ANOVA of linear regression model of roughness of stainless steel layer

Source	DF	Seq SS	Adj SS	Adj MS	F	P
Regression	2	0.306808	0.306808	0.153404	7.18203	**0.006487**
Error	15	0.320392	0.320392	0.021359		
Total	17	0.627200				

Table 5.10 ANOVA of linear regression model of roughness of mild steel layer

Source	DF	Seq SS	Adj SS	Adj MS	F	P
Regression	3	0.247822	0.247822	0.082607	3.35629	**0.049502**
Error	14	0.344578	0.344578	0.024613		
Total	17	0.592400				

Additionally, the normal probability plot of residuals has also been drawn which is considered an effective tool to gauge the adequacy of the proposed regression model [190]. Normal probability plot of residuals for both the surfaces i.e. stainless steel and mild steel are described in Figure 5.22 and Figure 5.23.

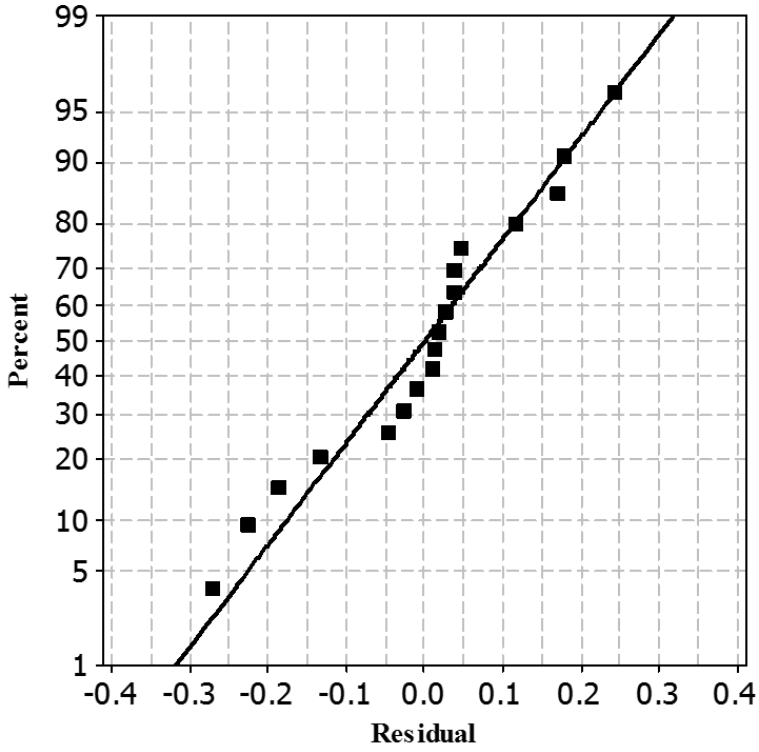

Figure 5.22 Normal probability plots of residuals for stainless steel

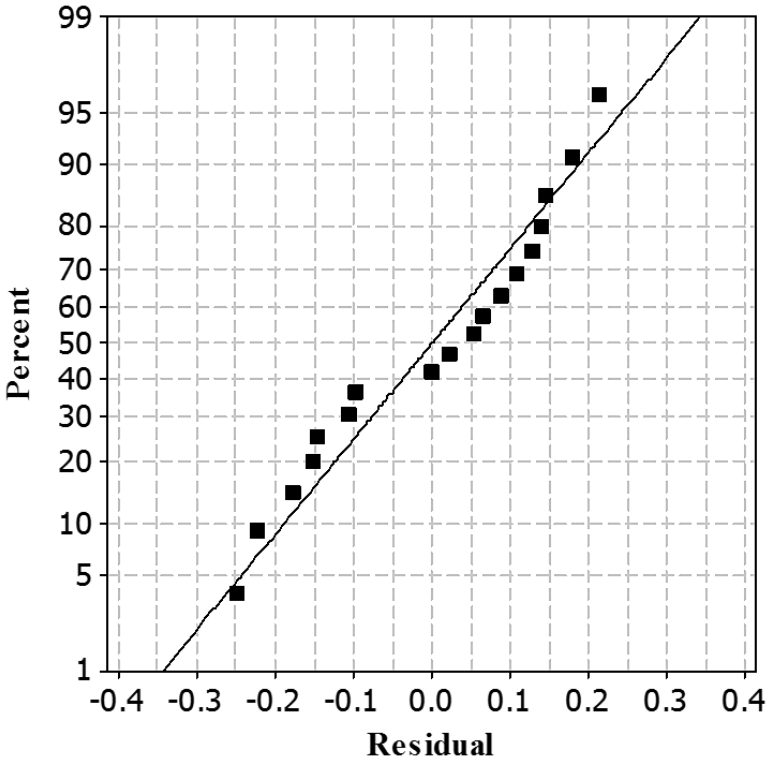

Figure 5.23 Normal probability plots of residuals for mild steel layer

Normal probability plot of residuals for the surface roughness of both the layers, have shown that that the residuals are normally distributed in both the cases. This means that the developed models are statistically validated. Moreover, the plot of residual versus observation order presented in Figure 5.24 and Figure 5.25 also highlight that residuals are randomly distributed around the mean line thus demonstrating that the developed models are fairly suited to the data.

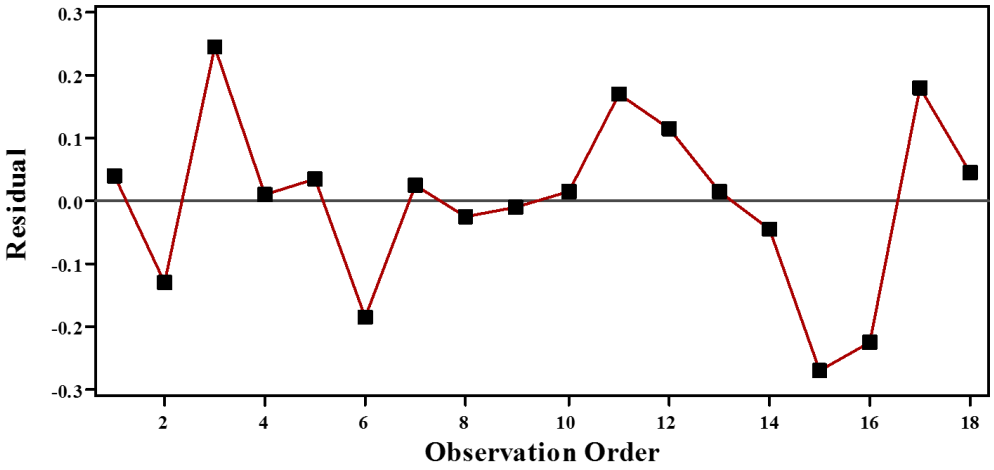

Figure 5.24 Plot of residual versus order (stainless steel layer)

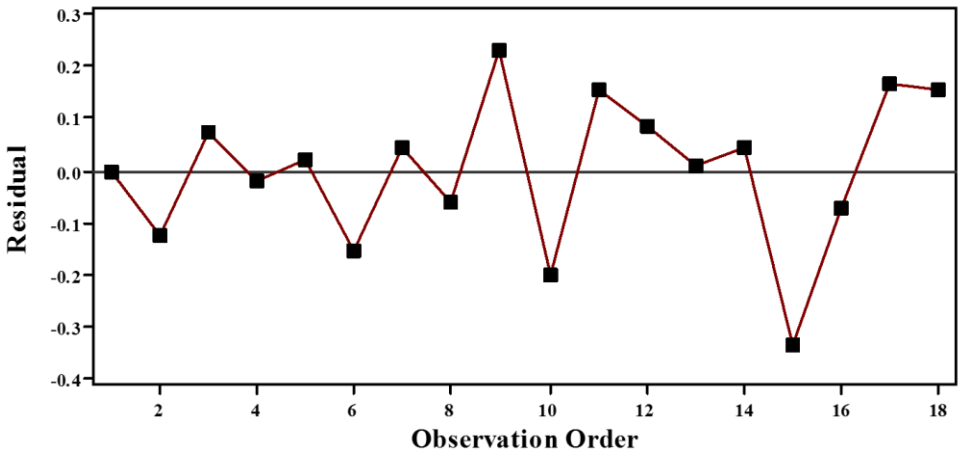

Figure 5.25 Plot of residual versus order (mild steel layer)

After statistically evaluating the authenticity of the developed models, the percentage error between experimental and model predicted values has been calculated. There exists an average error of about 3.6% between model predicted and experimental value of surface roughness of stainless steel layer and in case of mild steel layer surface roughness the average percentage error is about 3.7% as described in Table 5.11 and Table 5.12.

Table 5.11 Percentage error in exp. and pred. value of roughness of stainless steel layer

Exp. No.	Exp. value of surface roughness (µm)	Pred. value of surface roughness (µm)	% Error
1	2.62	2.58	1.55
2	2.68	2.81	4.63
3	2.94	2.70	8.89
4	2.59	2.58	0.39
5	2.85	2.81	1.42
6	2.51	2.70	7.04
7	2.84	2.81	1.07
8	2.67	2.70	1.11
9	2.57	2.58	0.39
10	2.89	2.88	0.35
11	2.93	2.76	6.16
12	3.11	2.99	4.01
13	3.01	2.99	0.67

14	2.83	2.88	1.74
15	2.49	2.76	9.78
16	2.65	2.88	7.99
17	2.94	2.76	6.52
18	3.04	2.99	1.67
	Average Percentage Error		3.63

Table 5.12 Percentage error in exp. and pred. value of roughness of mild steel layer

Exp. No.	**Exp. value of Surface roughness (µm)**	**Pred. value of Surface roughness (µm)**	**% Error**
1	2.75	2.75	0.08
2	2.8	2.92	4.24
3	2.84	2.77	2.51
4	2.64	2.66	0.83
5	2.99	2.97	0.71
6	2.66	2.82	5.53
7	2.97	2.92	1.58
8	2.71	2.77	2.19
9	2.98	2.75	8.28
10	2.75	2.95	6.81
11	2.95	2.80	5.44
12	3.19	3.10	2.76
13	3.02	3.01	0.18
14	3.04	3.00	1.46
15	2.51	2.84	11.71
16	2.92	3.00	2.54
17	3.01	2.84	5.88
18	3.17	3.01	5.16
	Average Percentage Error		3.77

According to the results shown in Table 5.11 and Table 5.12, it has been noticed that the difference betweenn model predicted and experiemtal values is quite minimal. The same has also been presented pictorially in the Figure 5.26and Figure 5.27 for sake of comparison at different experiemtal conditions. It has been revealed from the aforemetioned figures that the data points are closely spaced at all the experiemtal combinations for surfcae roughness of both the layers.

There are few data points where the difference is even smaller than the 1% such as in 4th, 9th, 10th and 13th experiemtal run in case of stainless steel layer and 1st, 4th, 5th and 13th experimetal run in case of mild steel layer surface roughness as represented by blue dotted circles in Figure 5.26 and Figure 5.27. The maximum difference between experiemental and predicted value of surface roughness has been observed during 15th experiemtal run with regard to the roughness of both layer of stainlss-clad steel in WEDM.

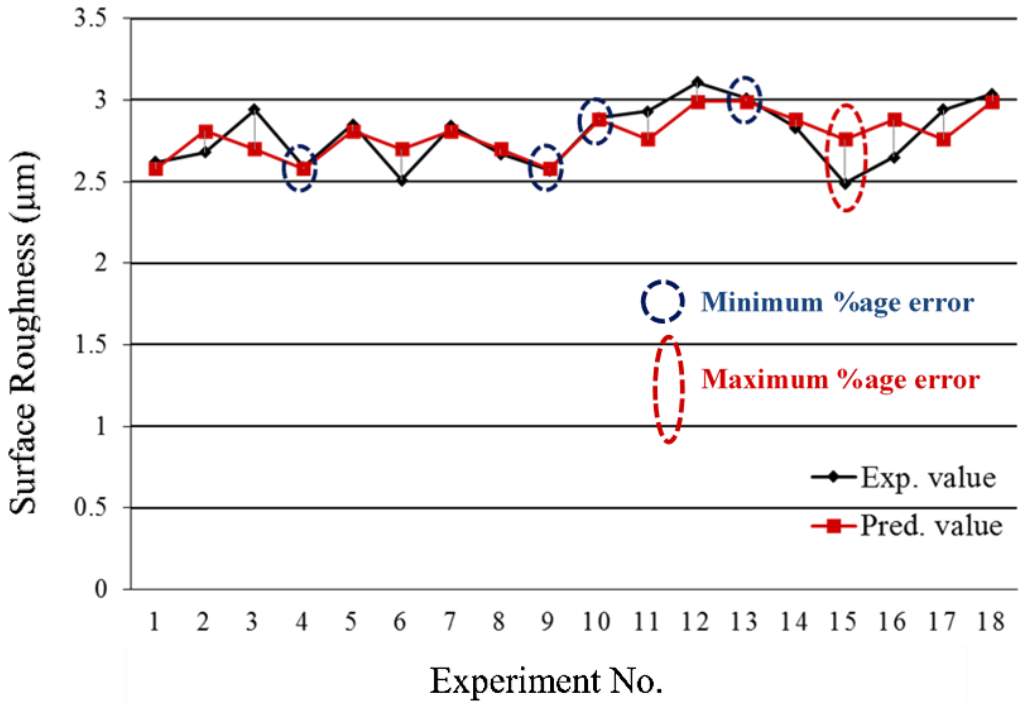

Figure 5.26 Comparison between pred. and exp. value of surface roughness of stainless steel layer

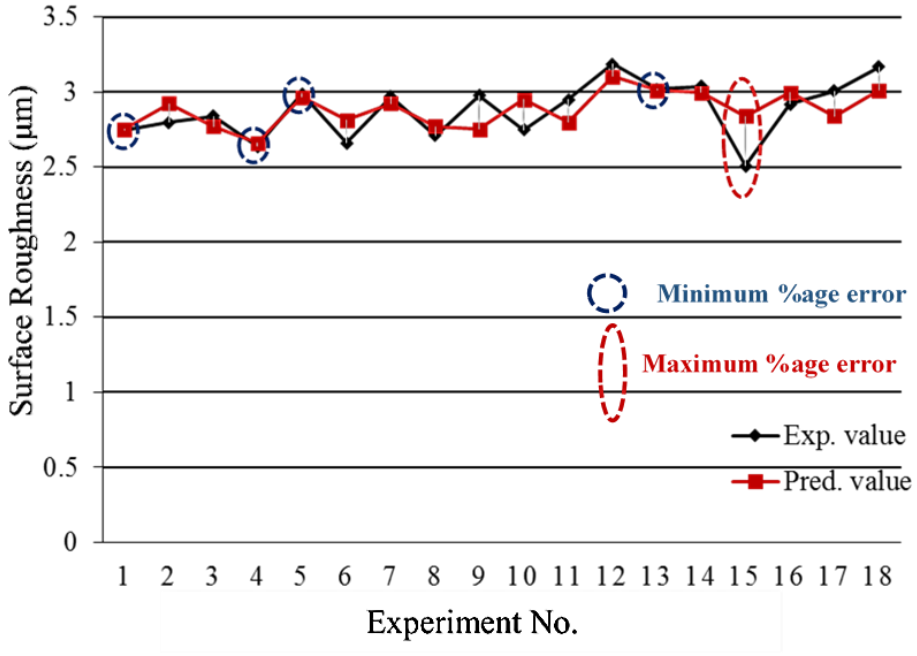

Figure 5.27 Comparison between pred. and exp. value of surface roughness of mild steel layer

It is also important to mention that stainless-clad steel is used in a composite form in the end use applications. Therefore, the reduction in the surface roughness of individual layer is not enough. Additionally, the difference between the values of roughness of the two layer is also found to be statistically significant. The significance is evaluated at a confidence interval of 95% (α =0.05) using paired t-test. The results of the test are tabulated in Table 5.13.

Table 5.13 Results of paired t-test for roughness of both layers

	No. of Observations	**Mean**	**Standard deviation**	**Standard error of mean**	**T value**	**P value**
Ra (stainless steel)	18	2.7867	0.1921	0.0453	-3.25	**0.005**
Ra (mild steel)	18	2.8833	0.1867	0.0440		
Difference	18	-0.0967	0.1260	0.0297		

It is evident from the results of paired t-test that p-value is 0.005 which is lesser than the defined alpha value (α = 0.05) which indicates that the difference between the surface roughness of both the layers are statistically significant. Hence, a multi-objective approach should be used in order to find the optimal combination of process parameters that results not only in the reduction of roughness of individual layer but also difference comes out to be minimum. The said technique is discussed in the next chapter.

5.6 Experimental results of spark gap

The results of measurement for the spark gap of stainless steel layer and mild steel layer are described in Table 5.14 and Table 5.15.

Table 5.14 Experimental results of spark gap (stainless steel surface)

Exp. No.	Or	LT_{SS} (mm)	LT_{MS} (mm)	D_W (mm)	Pr	SV (V)	P_{ON} (μs)	F_W (mm/s)	Spark gap (mm)
1	A	2	6	0.30	0.7	30	3	60	0.082
2	A	2	7	0.20	1.0	40	4	140	0.055
3	A	2	8	0.25	1.3	50	5	220	0.082
4	A	3	6	0.30	1.3	40	5	140	0.080
5	A	3	7	0.20	0.7	50	3	220	0.058
6	A	3	8	0.25	1.0	30	4	60	0.070
7	A	4	6	0.20	1.0	30	5	220	0.048
8	A	4	7	0.25	1.3	40	3	60	0.075
9	A	4	8	0.30	0.7	50	4	140	0.086
10	B	2	6	0.25	1.0	50	3	140	0.068
11	B	2	7	0.30	1.3	30	4	220	0.079
12	B	2	8	0.20	0.7	40	5	60	0.069
13	B	3	6	0.20	1.3	50	4	60	0.061
14	B	3	7	0.25	0.7	30	5	140	0.076
15	B	3	8	0.30	1.0	40	3	220	0.073
16	B	4	6	0.25	0.7	40	4	220	0.072
17	B	4	7	0.30	1.0	50	5	60	0.079
18	B	4	8	0.20	1.3	30	3	140	0.068

Table 5.15 Experimental results of spark gap (mild steel surface)

Exp. No.	Or	LT_{SS} (mm)	LT_{MS} (mm)	D_W (mm)	Pr	SV (V)	P_{ON} (µs)	F_W (mm/s)	Spark gap (mm)
1	A	2	6	0.30	0.7	30	3	60	0.070
2	A	2	7	0.20	1.0	40	4	140	0.066
3	A	2	8	0.25	1.3	50	5	220	0.095
4	A	3	6	0.30	1.3	40	5	140	0.059
5	A	3	7	0.20	0.7	50	3	220	0.125
6	A	3	8	0.25	1.0	30	4	60	0.079
7	A	4	6	0.20	1.0	30	5	220	0.063
8	A	4	7	0.25	1.3	40	3	60	0.083
9	A	4	8	0.30	0.7	50	4	140	0.073
10	B	2	6	0.25	1.0	50	3	140	0.052
11	B	2	7	0.30	1.3	30	4	220	0.073
12	B	2	8	0.20	0.7	40	5	60	0.079
13	B	3	6	0.20	1.3	50	4	60	0.083
14	B	3	7	0.25	0.7	30	5	140	0.069
15	B	3	8	0.30	1.0	40	3	220	0.059
16	B	4	6	0.25	0.7	40	4	220	0.076
17	B	4	7	0.30	1.0	50	5	60	0.071
18	B	4	8	0.20	1.3	30	3	140	0.055

5.6.1 ANOVA for spark gap

After finding the spark gap in both layers of cladded specimen, ANOVA has been performed in order to gauge the significant control factors with respect to the selected response attribute. The confidence interval of 95% has been chosen for evaluating the statistical significance of the input parameters for the spark gap in both the layers. The results of the analysis are presented in Table 5.16 and Table 5.17.

It has been noticed that two input factors namely; wire diameter of brass wire electrode, D_W (0.008) and pressure ratio, Pr (0.037) hold a p value lesser than the defined alpha value with regard to the spark gap produced in stainless steel layer. It means the described two input factors are significant for spark gap produced in stainless steel surface. However, in case of mild steel layer spark gap none of the factors is found to have a p value less than the defined alpha value. This shows that none of the factor found significant with respect to the spark gap of mild steel surface as per ANOVA results shown in Table 5.17.

Table 5.16 ANOVA of spark gap of stainless steel layer

Source	**DF**	**Seq SS**	**Adj SS**	**Adj MS**	**F**	**P**
Or	1	0.0000050	0.0000050	0.0000050	0.91	0.441
LT_{SS} (mm)	2	0.0000202	0.0000202	0.0000101	1.83	0.353
LT_{MS} (mm)	2	0.0001367	0.0001367	0.0000683	12.40	0.075
D_W (mm)	2	0.0012868	0.0012868	0.0006434	116.69	**0.008**
SV (V)	2	0.0000104	0.0000104	0.0000052	0.94	0.516
F_W (mm/s)	2	0.0000585	0.0000585	0.0000293	5.31	0.159
Pr	2	0.0002834	0.0002834	0.0001417	25.70	**0.037**
P_{ON} (µs)	2	0.0000087	0.0000087	0.0000043	0.79	0.559
Error	2	0.0000110	0.0000110	0.0000055		
Total	17	0.0018207				
	S = 0.00234817 R-Sq = 99.39% R-Sq(adj) = 94.85%					

Table 5.17 ANOVA of spark gap of mild steel layer

Source	**DF**	**Seq SS**	**Adj SS**	**Adj MS**	**F**	**P**
Or	1	0.0004909	0.0004909	0.0004909	8.86	0.097
LT_{SS} (mm)	2	0.0002477	0.0002477	0.0001239	2.23	0.309
LT_{MS} (mm)	2	0.0005861	0.0005861	0.0002930	5.29	0.159
D_W (mm)	2	0.0003636	0.0003636	0.0001818	3.28	0.234
SV (V)	2	0.0008003	0.0008003	0.0004002	7.22	0.122
F_W (mm/s)	2	0.0012556	0.0012556	0.0006278	11.33	0.081
Pr	2	0.0008523	0.0008523	0.0004262	7.69	0.115
P_{ON} (µs)	2	0.0000166	0.0000166	0.0000083	0.15	0.870
Error	2	0.0001109	0.0001109	0.0000554		
Total	17	0.0047240				
	S = 0.00744517 R-Sq = 97.65% R-Sq(adj) = 80.05%					

The percentage contribution of all the selected input parameters are then calculated to see the level of their influence on the selected response. As mentioned earlier that none of the control factor screened out as significant with respect to the spark gap of mild steel layer therefore percentage contribution of factors has only been calculated for the spark gap of stainless steel surface.

The percentage contribution of factors in controlling the amount of spark gap of stainless steel layer is presented in Figure 5.28. Wire diameter (D_W) of the brass wire electrode is found to be the most contributing factor with a percentage contribution of 71% in governing the spark gap produced in the stainless steel surface during WEDM of stainless-clad steel workpiece material. Pressure ratio (Pr) of the dielectric fluid is rated as the second most contributing factor having a percentage contribution of 16%. It is worth noting that accumulative percentage contribution of these two factors come out to be 87% which is a highly prominent contribution. Among the other parameter layer thickness of mild steel layer hold the maximum percentage contribution of 7%. The percentage contribution of error is about 1% (quite small magnitude of error). This highlights the accuracy of the developed model that it fits the data very well. The value of R-Sq.(adj.) has also been found more than 80% that is another proof of the adequacy of the model.

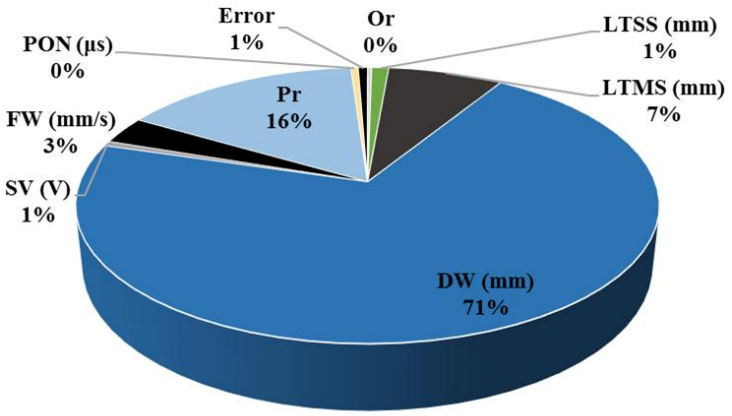

Figure 5.28 Percentage contribution of input parameters for spark gap of stainless steel layer

5.6.2 Parametric effects analysis for spark gap of stainless steel surface

Parametric effect analysis has been carried out after evaluating the statistical significance of control factors for selected response characteristic. The results of the analysis are described in the Figure 5.29.

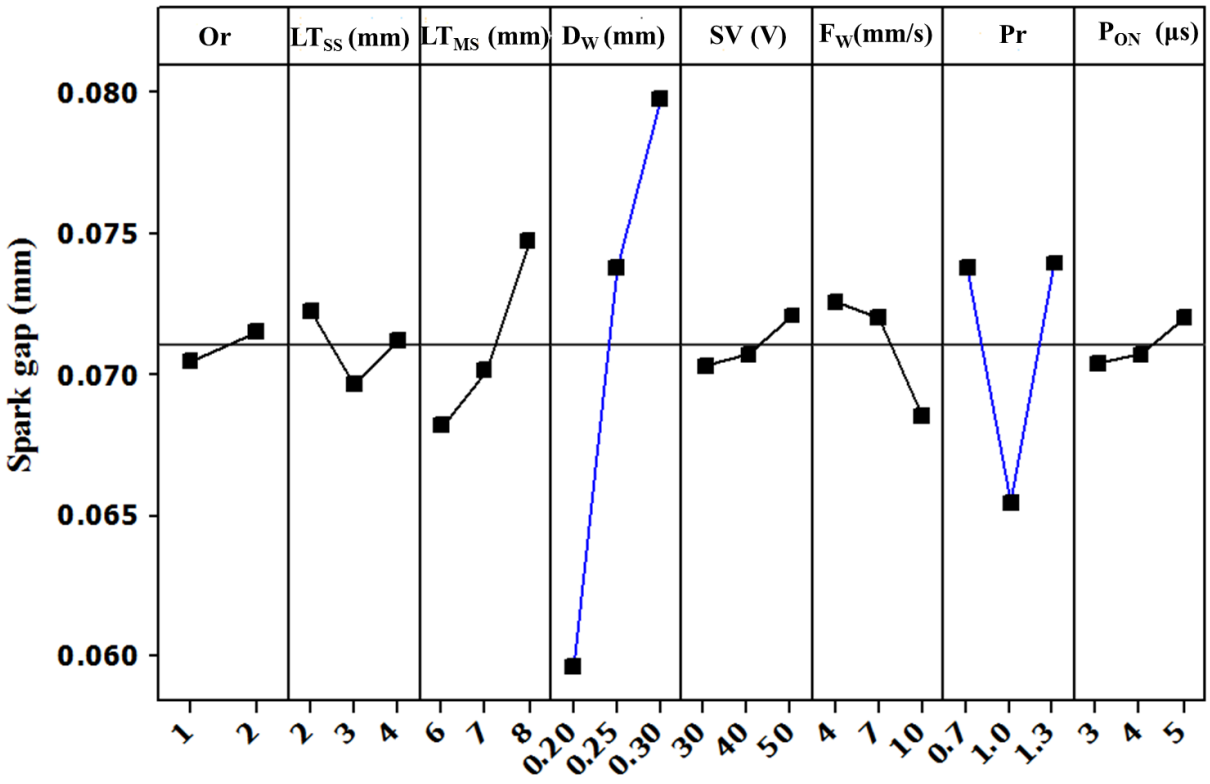

Figure 5.29 Effect of control factors on spark gap (stainless steel layer)

5.6.2.1 Effect of workpiece orientation on the spark gap of stainless steel layer

The results of main effects plot analysis have demonstrated that the workpiece orientation "A" (stainless steel layer lies at the top) is a preferred orientation with regard to the spark gap produced in the stainless steel layer in WEDM of cladded material. This might be due to the reason that the vibrations induced in the lateral direction in this orientation are of smaller magnitude due to which sideways sparking reduces.

Actually, in orientation “B” (mild steel surface faces the top), the stainless steel layer is subjected to cut by the deteriorated wire electrode because the wire has already subjected to the electric discharges during machining of upper layer of mild steel. The cutting efficiency of worn out wire reduces which in turn causes a delay in the machining of stainless steel surface. On the other end, dielectric fluid is exerting force on the wire electrode that causes wire vibrations. The formation of spark discharges also participate in increase the magnitude of these vibrations [196]. These induced vibration tend to move the wire in the lateral direction and as a result sideways sparking occurs. Consequently, spark gap increases while machining stainless-clad steel in the said orientation.

Therefore, it is better to place the workpiece in orientation “A” where unused wire electrode comes in contact with the stainless steel surface and after performing the cutting action enter s the second layer to perform the cutting action. In this orientation no delay in cutting has incurred as was observed in other orientation of workpiece (“B”). Hence, vibrations induced are of smaller magnitude that subsequently resulted into smaller spark gap in the stainless steel layer. It is also important to note that orientation “A” has also been found a preferred orientation for both the previously discussed responses i.e. cutting speed and surface roughness.

5.6.2.2 Effect of layer thickness on the spark gap

It has been found that layer thickness of the stainless steel layer (LT_{SS}) has no specific trend with regard to the spark gap of stainless steel surface. Initially, the value of spark gap reduces with the increase in the thickness of the said layer but later on it increases with the increase in the layer thickness of stainless steel (LT_{SS}). The effect of layer thickness of mild steel (LT_{MS}) is found to have a direct relationship with the selected response i.e. increase in the layer thickness of mild steel surface results into a corresponding increase in the spark gap. This is due to the reason that with the increase in the layer thickness of the said layer the overall machined length is increased that are likely to be deflected in the lateral direction owing the succession of electric discharge and force exerted by the dielectric fluid [197]. As, result cladded specimen is subjected to more sideways sparking that results into higher value of spark gap. A similar trend of workpiece thickness with regard to the spark gap has also been reported in WEDM of HC-HCR steel [163].

5.6.2.3 Effect of wire diameter on spark gap

The trend of the effect of wire diameter (D_W) is alike as that of layer thickness of mild steel layer (LT_{MS}) as shown in Figure 5.29. It is observed from the main effects plot shown in the Figure 5.29 that this parameter is of utmost importance for the spark gap of stainless steel layer. The results of ANOVA described in Table 5.16 also highlights that the selected control factor is significant with regard to the spark gap. Moreover, the percentage contribution of wire diameter (D_W) also found to be the maximum (71%) as shown in Figure 5.28. Similar findings regarding the effect of wire diameter (D_W) on the spark gap were also cited in another research work [198].

Basically with the increase in the diameter of wire (D_W) electrode the contact area between workpiece and the electrode increases. As wire is considered a cylindrical electrode that tends to perform machining action in the target material placed in front of this electrode. The increase in wire diameter not only increase the contact area between the front side and the workpiece material but sideways contact is also enhanced. Therefore, the zone of sideways sparking is seemed to be more disperse in contrast to the sideways spark zone of smaller diameter wire electrode (D_W). Thus, the spark gap produced by use of larger value of wire diameter in enlarged. The same has also been presented schematically in Figure 5.30.

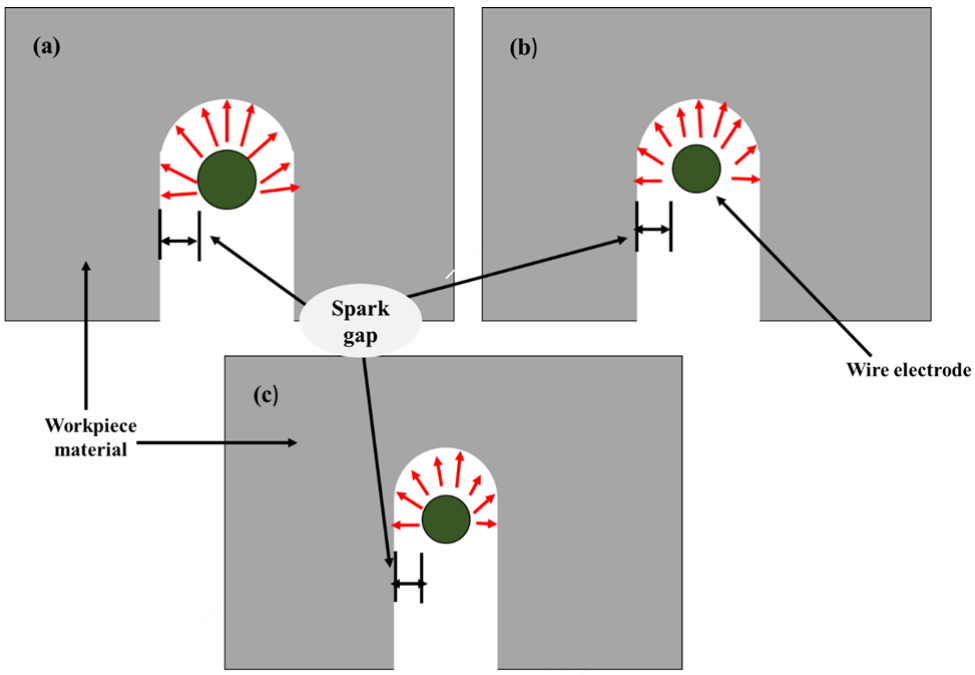

Figure 5.30 Schematic illustration of spark gap; (a) using D_W 0.3 mm, (b) using D_W 0.25 mm, (c) using D_W 0.2 mm

Kerf width produced in cladded material during WEDM using larger diameter wire is also seemed to be larger. Spark gap produced is observed to have a linear relationship with the kerf width. In case of larger diameter wire electrode the kerf width and subsequently the spark gap produced are of larger magnitude in comparison to the smaller diameter wire as shown in Figure 5.31.

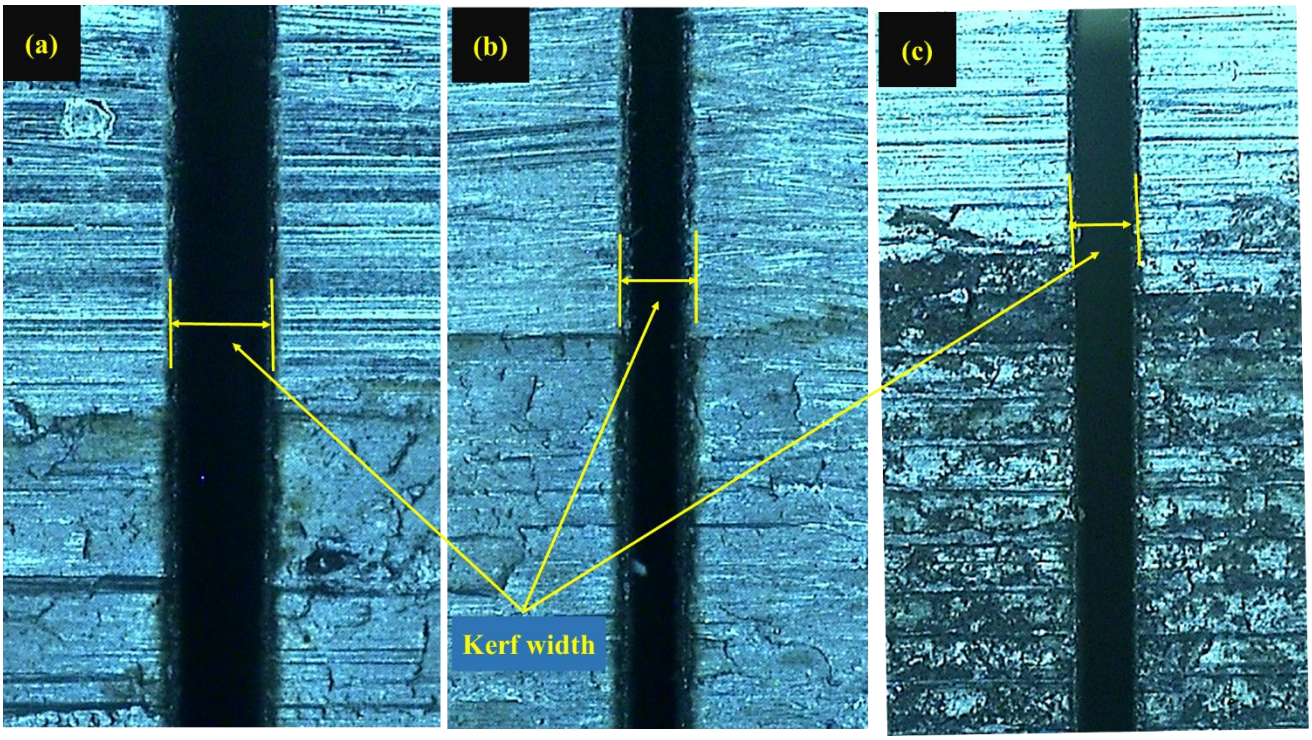

Figure 5.31 Kerf width produced; (a) using 0.3 mm wire electrode, (b) using 0.25 mm wire electrode, (c) using 0.2 mm wire electrode

5.6.2.4 Effect of servo voltage on spark gap

The results of parametric effects analysis have revealed that amount of spark gap produced has a direct relationship with the servo voltages. The increase in the value of the servo voltages results into a corresponding increase in the spark gap owing to the reason that servo voltages are responsible for maintaining a safe distance for sparking between the workpiece material and the wire electrode in both the dimensions (along the cut direction and in the lateral direction).

In WEDM servo voltages (SV) are accountable for maintaining a safe distance between electrode and the target material to avoid the chance of short circuiting. The increase in the value of this input parameter means that the wire electrode will stay a farther distance apart from the surface of the workpiece. That distance is kept maintained throughout the machined length. But as the wire fed into the workpiece after machining certain amount of material the magnitude of safe sparking distance has to be preserved in both directions (along the length of cut and in lateral direction). The value of that distance is fixed owing to have a set value of servo voltages (SV) in the direction along the length of cut but same distance has to be maintained in the lateral direction as well after removing certain amount of material from the specimen. With the increase in the value of said parameter the magnitude of offset distance increases not only along the length of cut but also in other direction. Therefore, a larger spark gap is generated in preserving the larger offset distance between wire electrode and the target material. Similar trend of the selected parameter with regard to the spark gap was also reported during WEDM of TiC/Fe metal matrix composite [14].

5.6.2.5 Effect of wire feed on spark gap

The effect of wire feed on the spark gap is seemed to be opposite to that of wire diameter as per the results of parametric effects analysis presented in Figure 5.29. The increase in the wire feed (F_W) results into the reduction of spark gap. This might be due to the reason that increasing the value of this input parameter tends to reduce the contact time between the wire electrode and the specimen. Also the amplitude of vibration is reduced with the increase in wire feed. Therefore, lesser impact has been transferred in lateral direction. Furthermore, it also facilitates the flushing of melted debris. Thus, spark gap produced is of smaller magnitude.

5.6.2.6 Effect of pressure ratio on spark gap

Pressure ratio (Pr) is revealed to be the one of contributing factor with regard to the spark gap as per ANOVA results described in Table 5.16. The value of spark gap reduces as the value of pressure ratio increases from 0.7 to 1.0 but from 1- 1.3 it increases once again. It has been noticed that minimum spark gap has been found by using the pressure ratio of 1 that means the flushing pressure of both nozzles were set equal.

The primary role of dielectric fluid is to flush away the melted debris along with providing the potential barrier between wire electrode and the workpiece material. An appropriate selection of flushing pressure of both the nozzles is essential to ensure the effective flushing of the debris which is mandatory for efficient and sustainable cutting. Inappropriate selection of flushing pressures not only results into poor evacuation of the debris but also creates significant vibrations in the wire electrode as well it may led to wire rupture. The surface of machined specimen also got effected by these induced vibrations [199]. The magnitude of these vibrations can be reduced by selecting the pressure ratio (Pr) of 1. Moreover, debris are removes efficiently from the cutting zone at the aforesaid value of pressure ratio. The reduction in wire vibrations led to reduce the sideways movement of the wire electrode and as a result sideways sparking reduces yielding smaller spark gap.

5.6.2.7 Effect of pulse on time on spark gap

Based on the main effects plot analysis, it has been revealed that pulse on time (P_{ON}) affects the spark gap in a similar way as the wire diameter (D_W) which is depicted in Figure 5.29. The magnitude of spark gap increases from 0.07 mm to 0.072 mm as the value of pules on time increases from 3 μs to 5 μs (approximately 3% increase). With the increase in the pulse on time sparking duration prolongs. The existence of spark discharges persist for longer period of time this in turns improve the material removal rate. As described earlier that material is not only removed from the front of the wire electrode but it is also machined by the sideways sparking as well. So, the amount of material removed from the front of the wire is not only increased but also more amount of material is evaporated due to the sideways sparking as well, as spark discharges are available for extended period of time. Subsequently, spark gap produced during WEDM is enlarged.

5.6.3 Mathematical relationship of input parameters with spark gap

A mathematical relationship has been developed in this part of work to correlate the effect of input parameters on the spark gap. The multiple linear regression technique has been selected for development of the regression model.

Only those control factors were chosen for the model development that were significant with respect to the selected response characteristic. The coefficients and the constant pertaining to the developed model have been calculated using least square method. The model is described in the below equation.

$$\boldsymbol{Spark\ gap = 0.020333 + 0.201667\ DW + 0.0002778\ Pr} \quad (\mathbf{5.5})$$

In the above mentioned equation, WD stands for wire diameter and Pr accounts for pressure ratio of the dielectric fluid. To ensure that the developed model is statistically significant ANOVA is carried out at a confidence interval of 95%. The results of the analysis are tabulated in Table 5.18.

Table 5.18 ANOVA for spark gap of stainless steel layer using multiple linear regression

Source	**DF**	**Seq SS**	**Adj SS**	**Adj MS**	**F**	**P**
Regression	2	0.0012202	0.0012202	0.0006101	15.2376	**0.000244**
Error	15	0.0006006	0.0006006	0.0000400		
Total	17	0.0018207				

The results of ANOVA shown in Table 5.18 clearly indicate that the developed model secured a p value of 0.00024 which is quite lower than the defined alpha value (0.005) and it also holds an f value of 15.237, thus projecting that the formulated mathematical model is statistically significant. Additionally, the adequacy of the spark gap regression model is also accessed through normal probability plot of residuals. The normal probability plot of residuals have been provided in Figure 5.32. The residuals are found distributed normally, thus validating the model's accuracy. Furthermore, the percentage error between experimental and model predicted values has been observed as well and is shown in Figure 5.33 and tabulated in Table 5.19. It has been noticed that there exists a small error between model predicted and experimental values of spark gap.

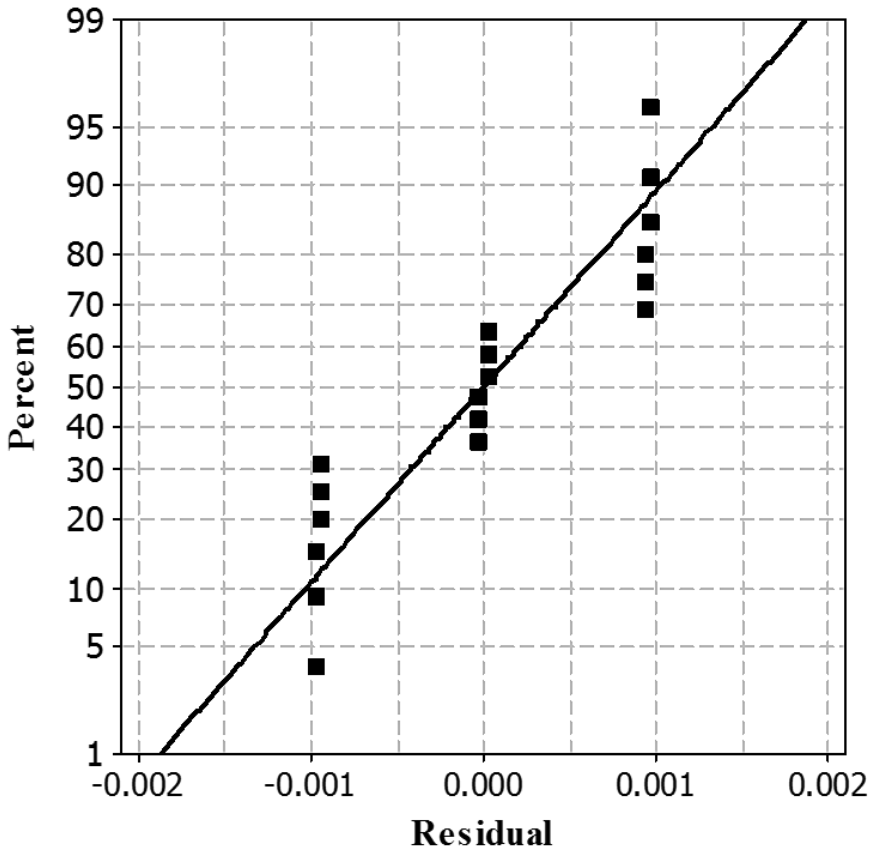

Figure 5.32 Normal probability plot of residuals for spark gap of stainless steel layer

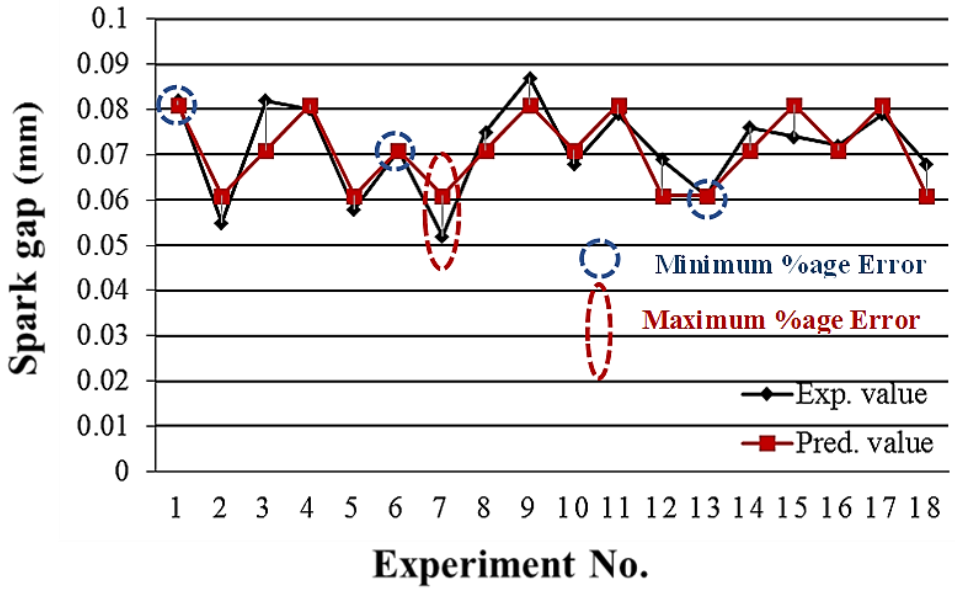

Figure 5.33 Percentage error between exp. and pred. values of spark gap

Table 5.19 Percentage error in exp. and pred. values of spark gap of stainless steel layer

Exp. No.	Exp. value of spark gap (mm)	Pred. value of spark gap (mm)	% Error
1	0.082	0.081	0.58
2	0.055	0.061	9.75
3	0.082	0.071	14.61
4	0.080	0.081	2.09
5	0.058	0.061	5.52
6	0.071	0.071	0.74
7	0.052	0.061	14.7
8	0.075	0.071	5.47
9	0.087	0.081	6.75
10	0.068	0.071	4.97
11	0.079	0.081	2.70
12	0.069	0.061	13.37
13	0.061	0.061	0.05
14	0.076	0.071	7.13
15	0.074	0.081	9.38
16	0.072	0.071	1.49
17	0.079	0.081	3.22
18	0.068	0.061	10.61
Average Percentage Error			6.6%

Based on the values of percentage error calculated for all the experimental runs it has been revealed that there exists an average error of about 6.6%. However at certain data points the average error is observed less than 1% highlighted by blue dotted circles in Figure 5.33. The maximum percentage error was recorded of about 14% that was in 7^{th} experimental run. This has also been mentioned in the Figure 5.33 by red dotted circle.

The trend of the effect of input parameters on the spark gap produced in mild steel surface is not discussed owing to the reason that none of the selected parameter is found significant for the selected response attribute as per the results presented in Table 5.17. Furthermore, paired t-test has also been carried out to assess the significance of the difference found between the values of spark gap of stainless steel layer and of mild steel layer at 95% confidence interval. The results of the paired t-test are shown in Table 5.20.

Table 5.20 Results of paired t-test for spark gap of both layers

	No. of Observations	**Mean**	**Standard deviation**	**Standard error of mean**	**T value**	**P value**
Spark gap (stainless steel)	18	0.07103	0.01035	0.00244		
Spark gap (mild steel)	18	0.07383	0.01667	0.00393	-0.58	**0.568**
Difference	18	-0.00281	0.02043	0.00482		

As depicted from the results of paired t-test, the p-value (0.568) has been found greater than the defined alpha value ($\alpha = 0.05$) which means that this difference is statistically insignificant. Therefore, the result of spark gap have only been discussed with stainless steel surface perspective. It is worth noting that the role of stainless steel layer is the only determined factor in controlling the overall value of spark gap produced in the cladded machined sample. Moreover, this surface has also found to have a noteworthy effect on the other selected response like cutting speed and surface roughness of the machined surface of cladded specimen.

Therefore, a due consideration should be given to this layer keeping in view its impact on the selected responses to optimize the process yield in terms of selected response characteristics.

Chapter 6
Parametric Optimization

After describing the results, analysis and a comprehensive discussion of selected responses in WEDM of stainless-clad steel, the optimal combinations of process parameters are developed with regard to the said responses in this part of the study.

6.1 Need for optimization

In every manufacturing process, the industry is always looking for that combination of process parameter which eventually maximizes the process yield. It is quite essential for their survival in this competitive environment. The requirement of optimization further intensifies if the process is expensive itself and also there is an involvement of number of process variables as in case of WEDM [200].

Although, WEDM is categorized as an accurate and precise machining process [10] but still the selection of appropriate value of input parameter to optimize the process output is considered a challenging task owing to the stochastic nature of the process [140]. A minute variation in the value of any parameter may cause a complicated change in the value of response in WEDM that eventually results into a productivity loss. The situation becomes more critical if dealing with more than one response. Therefore, it is necessary to find the optimal combination of parameter that not only justifies the process economics by providing higher productivity but also producing accurate part quality.

The optimal settings of input parameters with regard to the optimization of individual response characteristic have been found in this part of study using Signal-to-noise ratio analysis (S/N). The results of the aforementioned optimization technique are mention in forthcoming sections.

6.2 Signal-to-noise (S/N) ratio analysis

As a part of Taguchi's experimental design technique, Signal-to-noise ratio analysis is performed in order to find optimal settings of control factors for the selected responses namely; cutting speed, surface roughness and spark gap individually. There exists six S/N ratios as descried earlier. Out of which two types of S/N ratios; larger the better and smaller the better have been employed keeping in view of the desired outcome of the selected responses. The larger the better S/N ratio was used in case of cutting speed optimization as the larger value of this response is desired whereas for surface roughness and spark gap smaller the batter approach has been opted. The relationships 6.1 and 6.2 are used for finding larger the better and smaller the better S/N ratios.

$$\boldsymbol{\eta_{ij} = -10log(1/n \sum_{k=1}^{n} \frac{1}{Y_{ij}^2})} \qquad \textbf{(6.1)}$$

$$\boldsymbol{\eta_{ij} = -10log(1/n \sum_{k=1}^{n} Y_{ij}^2)} \qquad \textbf{(6.2)}$$

Here, η_{ij} is representing the S/N ratio of i^{th} response attribute in j^{th} experimental run, n is the total number of experiments and Y_{ij} accounts for the actual value of i^{th} response characteristic (cutting speed) in j^{th} experiment.

6.3 S/N ratio analysis for cutting speed optimization

The S/N ratio for the optimization of cutting speed are computed using the above mentioned relationship (larger the better). The results of S/N ratio analysis are tabulated in Table 6.1. According to S/N ratio analysis, the maximum value of S/N ratio is obtained during experiment number 12 and the minimum value of S/N ratio is observed during 9^{th} experimental run.

Larger value of S/N ratio demonstrates that the value of response attribute is higher for that particular setting of control factors and in case of counterpart reverse seemed to be true [201]. The ranks of all the input parameter with regard to the cutting speed during WEDM of cladded material have also been calculated and are provided in Table 6.2.

Table 6.1 S/N ratios for cutting speed

Experiment No.	S/N ratio	Experiment No.	S/N ratio
1	6.31941	**10**	5.43683
2	7.53154	**11**	6.07688
3	6.64877	**12**	8.26600
4	7.30976	**13**	6.92706
5	5.99886	**14**	8.13080
6	6.31941	**15**	3.04577
7	7.27224	**16**	6.19260
8	4.40216	**17**	5.43683
9	3.52183	**18**	4.50619

Table 6.2 Response Table for S/N ratios (Larger is better)

Level	Or	LT_{SS}	LT_{MS}	D_W	SV	F_W	Pr	P_{ON}
1	6.2	6.7	6.6	6.8	6.4	6.3	6.4	5.0
2	6.0	6.3	6.3	6.2	6.1	6.1	5.8	6.1
3		5.2	5.4	5.3	5.7	5.9	6.0	7.2
Delta	0.2	1.5	1.2	1.5	0.8	0.4	0.7	2.2
Rank	8	2	4	3	5	7	6	1

The ranking of factors is based on their delta value. The factor having a higher delta value holds a higher rank. The control factor having a higher rank will influence the response variable appreciably [202]. The results of the said analysis have revealed that pulse on time (P_{ON}) secured a rank of 1 (Delta = 2.2) which means this parameter is the most influential with respect to the cutting speed in WEDM of stainless-clad steel.

Moreover, this input parameter (P_{ON}) has also proved to be the most contributing factors having a percentage contribution of about 42% as per ANOVA results described in Figure 5.1. Thus, the results are in accordance with the previous analysis results.

Stainless steel layer thickness (LT_{SS}) is observed to have a rank of 2 (delta = 1.5) followed by diameter of wire electrode (D_W, rank 3), layer thickness of mild steel layer (LT_{MS}, rank 4), servo voltages (SV, rank 5), pressure ratio of dielectric fluid (Pr, rank 6), wire feed of brass wire (F_W, rank 7) and orientation of cladded material's workpiece (Or, rank 8). Optimal level values are determined for all the control factors based on the S/N ratio values shown in Table 6.2. The optimal level, level value and its unit are shown in Table 6.3.

Table 6.3 Optimal levels of input variables for selected response

Sr. No.	**Input WEDM parameters**	**Notation**	**Optimal settings for cutting speed**		
			Optimal Levels	**Level value**	**Units**
1	Orientation	"Or"	1	A	---
2	Stainless steel layer thickness	"LT_{SS}"	1	2	mm
3	Mild steel layer thickness	"LT_{MS}"	1	6	mm
4	Wire diameter	"D_W"	1	0.2	mm
5	Servo voltage	"SV"	1	30	V
6	Wire feed	"F_W"	1	60	mm/s
7	Pressure ratio	"Pr"	1	0.7	--
8	Pulse on-time	"P_{ON}"	3	5	µs

It has been noticed that level 1 of seven input parameters like orientation of workpiece (Or, A), layer thickness of stainless steel (LT_{SS}, 2 mm), mild steel layer thickness (LT_{MS}, 6 mm), diameter of wire electrode (D_W, 0.2 mm), servo voltages (SV, 30 V), wire feed (F_W, 60 mm/s) and pressure ratio (Pr, 0.7), is the optimal level for cutting speed optimization.

But in case of pulse on time (P_{ON}, 5 µs) level 3 is optimal level that results into higher cutting speed in WEDM of stainless-clad steel.

6.3.1 Confirmatory experiment

In order to validate the optimal settings of input parameters (tabulated in Table 6.3), a confirmatory experiment is performed. The results of confirmatory experiment are described in Table 6.4. The relationship described by A. Mohammadi et al. [203], was employed to compute the S/N ratio using optimal levels of control factors. The relationship pertaining to the current response S/N ratio calculation is shown in Eq. 6.3.

$$\eta_{cp} = \eta om + (\eta Or - \eta om) + (\eta LT_{SS} - \eta om) + (\eta LT_{MS} - \eta om) + (\eta D_W - \eta om) + (\eta SV - \eta om) + (\eta F_W - \eta om) + (\eta Pr - \eta om) + (\eta PON - \eta om) \quad (\mathbf{6.3})$$

Here η_{om} is representing overall mean of S/N ratios whereas ηOr, ηLTss, ηLT_{MS}, ηD_W, ηSV, ηF_W, ηPr and ηP_{ON} account for the S/N ratio of input parameters at their optimal levels.

Table 6.4 Confirmatory experiment results for cutting speed

Factors settings	Levels of parameters	Pred. value (mm/min)	Exp. value (mm/min)	Error (%)	Pred. S/N ratio(dB)	Exp. S/N ratio(dB)	Error (%)
Optimal Settings	Or1,LT_{SS}1, LT_{MS}1,D_W1, SV1,F_W1, Pr1, P_{ON}3	2.88	3.1	7.6%	9.82	9.5	3%
Non-Optimal Settings	Or2,LT_{SS}1, LT_{MS}3,D_W1, SV2,F_W1, Pr1, P_{ON}3	2.6	2.59	0.3%	8.31	8.3	0.5%
Percentage improvement in response value			**19.7%**		**Percentage improvement in S/N ratio**		**15.4%**

Based on the results of the confirmatory experiment, it is deduced that there exists about 20% improvement in the value of cutting speed by using the optimal settings of input parameters. The value of S/N ratio is also observed to be improved by 15% approximately. It is worth noting that these improvements are with respect to the maximum value of cutting speed and S/N ratio recorded during experimentation.

6.4 S/N ratio analysis for surface roughness optimization

The results of S/N ratio analysis for the optimization of surface roughness in WEDM of stainless-clad steel using smaller the better approach are tabulated in Table 6.5.

Table 6.5 S/N ratios of surface roughness

Experiment No.	S/N ratios of stainless steel layer surface roughness	S/N ratio of mild steel layer surface roughness
1.	-8.36603	-9.2480
2.	-8.56270	-8.9432
3.	-9.36695	-9.0664
4.	-8.26600	-8.8182
5.	-9.09690	-9.5134
6.	-7.99347	-8.4976
7.	-9.06637	-9.4551
8.	-8.53023	-8.6594
9.	-8.19866	-9.6860
10.	-9.21796	-8.7867
11.	-9.33735	-9.5424
12.	-9.85521	-10.0758
13.	-9.57133	-9.6001
14.	-9.03573	-9.6575
15.	-7.92399	-7.9935
16.	-8.46492	-9.3077
17.	-9.36695	-9.6575
18.	-9.65747	-10.0212

The rank of all the input variables with respect to surface roughness of both layers (stainless steel and mils steel) are calculated afterwards which are shown in Table 6.6 and Table 6.7.

Table 6.6 Response Table for S/N ratios of stainless steel layer surface roughness

Level	Or	LT_{SS}	LT_{MS}	D_W	SV	F_W	Pr	P_{ON}
1	-8.605	-9.118	-8.825	-9.302	-8.909	-8.947	-8.836	-8.799
2	-9.159	-8.648	-8.988	-8.768	-8.601	-8.823	-8.689	-8.688
3		-8.881	-8.833	-8.576	-9.136	-8.876	-9.122	-9.160
Delta	0.554	0.470	0.163	0.725	0.536	0.124	0.433	0.471
Rank	2	5	7	1	3	8	6	4

Table 6.7 Response Table for S/N ratios of mild steel layer surface roughness

Level	Or	LT_{SS}	LT_{MS}	D_W	SV	F_W	Pr	P_{ON}
1	-9.099	-9.277	-9.203	-9.581	-9.404	-9.290	-9.601	-9.037
2	-9.405	-9.013	-9.329	-8.889	-8.966	-9.319	-8.996	-9.263
3		-9.464	-9.223	-9.285	-9.385	-9.146	-9.158	-9.455
Delta	0.451	0.418	0.126	0.692	0.437	0.172	0.606	0.306
Rank	3	5	8	1	4	7	2	6

The parametric ranking for controlling the surface roughness of both the layers presented in Table 6.6 and Table 6.7 indicate that diameter of wire electrode (D_W) has secured a rank of 1 in governing the surface of stainless steel layer and mild steel layer owing to have the highest value of delta (0.725 for stainless steel surface and 0.692 for mild steel layer) among all the input factors during WEDM of the selected material. It is already discussed that the said control factor is the most contributing factor in determining the value of surface roughness of both layers (stainless steel and mild steel) in WEDM of cladded material as shown in

Table 5.6 and Table 5.8. Workpiece orientation (Or) holds a rank of 2 in case of stainless steel layer surface roughness and has a rank of 3 for mild steel layer surface roughness. This parameter is also rated as significant for surface roughness of both layer as per the results of ANOVA.

The ranks of the remaining parameters such as stainless steel layer thickness (LT_{SS}), mild steel layer thickness (LT_{MS}), servo voltages (SV), wire feed (F_w), pressure ratio (Pr) and pulse on time (P_{ON}) are 5, 7, 3, 8, 6 and 4 in case of stainless steel layer roughness and 5, 8, 4, 7, 2 and 6 with respect to the surface roughness of mild steel layer, respectively.

Afterwards, the optimal levels of the input parameters are identified based on the S/N ratio analysis. Optimal levels, their values along with units are tabulated in Table 6.8.

Table 6.8 Optimal levels of input variables for the selected response

Sr. No.	Input WEDM parameters	Notation	stainless steel surface roughness		mild steel surface roughness		Units
			Optimal Levels	Level value	Optimal Levels	Level value	
1	Orientation	"Or"	1	A	1	A	---
2	Stainless steel layer thickness	"LT_{SS}"	2	3	2	3	mm
3	Mild steel layer thickness	"LT_{MS}"	1	6	1	6	mm
4	Wire diameter	"D_W"	3	0.3	3	0.3	mm
5	Servo voltage	"SV"	2	40	2	40	V
6	Wire feed	"F_W"	2	140	3	220	mm/s
7	Pressure ratio	"Pr"	2	1	2	1	--
8	Pulse on-time	"P_{ON}"	2	4	1	3	µs

It is evident from the Table 6.8 that orientation "A" is preferred orientation for the selected response characteristics whereas in case of stainless steel layer thickness level 2 (3 mm) is the optimal level for surface roughness of both the layers. Level 1 (6 mm) of mild steel layer thickness and level 3 (0.3 mm) of wire diameter are found to be the optimal levels for both the responses. Servo voltage yields optimized surface roughness (smaller roughness) on the surfaces of both the layers if set at level 2 (40 V).

The level 2 of the remaining three parameters is observed to be optimal with regards to stainless steel layer surface finish whereas for mild steel layer surface roughness the optimal levels of the remaining three control factors are; level 3 (220 mm/s) of wire feed, level 2 (1) of pressure ratio and level 1 (3 µs) of pulse on time. It is interesting to note that significant control factors secured same optimal levels with respect to the surface roughness of both layers in WEDM of stainless-clad steel workpiece material. The optimal level of the significant factors is highlighted by dark brown dotted circles in the above Table.

6.4.1 Confirmatory tests

Confirmatory experiments is performed after evaluating the optimal settings of each response variable for the validation of the findings. The relationship mentioned above is to envisage the S/N ratios at optimum levels of input parameters. Results of confirmatory experiment performed at optimal levels of input parameters for stainless steel layer surface roughness improvement are described in Table 6.9.

Table 6.9 Confirmatory experiment results for surface roughness of stainless steel layer

Factors settings	**Levels of parameters**	**Pred. value (µm)**	**Exp. value (µm)**	**Error (%)**	**Pred. S/N ratio(dB)**	**Exp. S/N ratio(dB)**	**Error (%)**
Optimal Settings	Or1, $LT_{SS}2$, $LT_{MS}1$, D_W3, SV2, F_W2, Pr2, $P_{ON}2$	2.275	2.28	0.2%	-7.28047	-7.1587	2%
Non-Optimal Settings	Or2, $LT_{SS}2$, $LT_{MS}3$, D_W3, SV2, F_W3, Pr2, $P_{ON}1$	2.52	2.49	1.2%	-8.00507	-7.92399	1%
Percentage improvement in response value			**9.2%**		**Percentage improvement in S/N ratio**		**10.7%**

Results of confirmatory experiment revealed that surface finish of stainless steel is improved to 9.2% by using optimal settings of WEDM input parameters. The value of S/N ratio for surface roughness of stainless steel also improves by 10.7%. It important to mention that the value of

improvement in surface roughness of stainless steel layer (9.2%) is with respect to the minimum value of surface roughness recorded during the whole experimentation.

Another confirmatory test is conducted to validate the optimal combination of input parameters developed for the minimization of mild steel layer surface roughness.

Table 6.10 shows the confirmatory experiment results for improving the surface roughness of mild steel layer using optimal settings of control factors.

Table 6.10 Confirmatory experiment results for surface roughness of mild steel layer

Factors settings	**Levels of parameters**	**Pred. value (µm)**	**Exp. value (µm)**	**Error (%)**	**Pred. S/N ratio(dB)**	**Exp. S/N ratio(dB)**	**Error (%)**
Optimal Settings	Or1, $LT_{SS}2$, $LT_{MS}1$, D_W3, SV2, F_W3, Pr1, $P_{ON}1$	2.35	2.31	1.7%	-7.532	-7.272	3.6%
Non-Optimal Settings	Or2, $LT_{SS}2$, $LT_{MS}3$, D_W3, SV2, F_W3, Pr2, $P_{ON}1$	2.53	2.51	0.7%	-8.057	-7.993	0.8%
Percentage improvement in response value			**~ 9%**		**Percentage improvement in S/N ratio**		**~10 %**

It is depicted from the results of confirmatory experiment shown in

Table 6.10 that the surface roughness of mild steel layer has been improved by ~9% whereas an improvement of ~10% is seen in S/N ratio of surface roughness of mild steel layer.

The surface roughness profiles recorded for the two confirmatory experiments have also indicate that surface irregularities are minimized by using the optimal combination of input parameters in comparison to the surface irregularities found during cutting at non-optimal settings of control factors as presented in Figure 6.1.

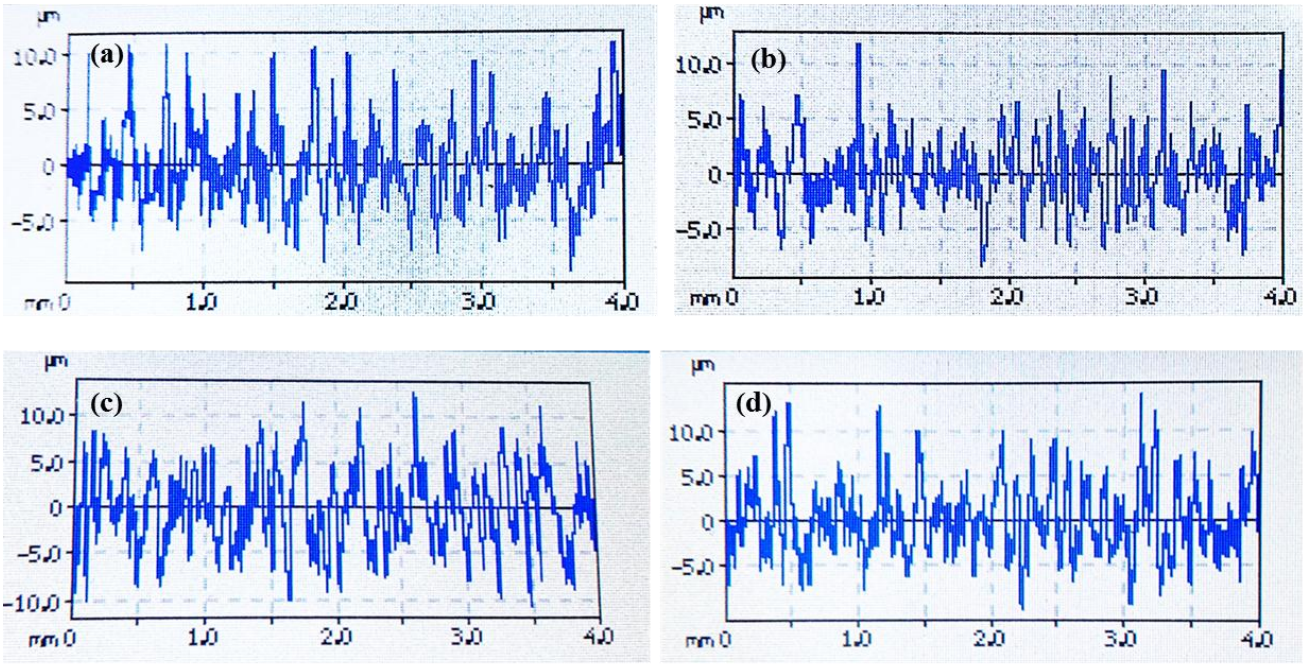

Figure 6.1 Roughness profiles; (a) stainless steel layer at non-optimal settings, (b) stainless steel layer at optimal settings, (c) mild steel layer at non-optimal settings, (d) mild steel layer at optimal settings

It has also been deduced from the roughness profiles presented above that surface texture found on the stainless steel layer is somewhat more smoother in contrast to that found on the surface of mild steel layer. This is mainly due to the fact that mild steel surface is subjected to more intense spark owing to its higher electrical conductivity and subsequently more material erosion take place from the said layer. As a result, surface finish of mild steel layer deteriorates.

Additionally, in both the confirmatory experiments it is noticed that the predicted result of each response characteristic is observed in good agreement with the experimental results. This validates the accuracy of the developed models showing model explains the variation fairly well.

Although optimal settings are developed for improving the surface roughness of both layers but still there is a need to find that combination of parameters that simultaneously optimize the roughness of both layers and also yields minimum difference between the roughnesses of two layers as this material has to be used in composite form. This has been done using grey relational analysis in the forthcoming section.

6.5 Grey relational analysis

The said technique has found to be interactive in dealing with incomplete, poor and uncertain statistics. This multi-objective optimization technique is a part of grey system theory, which has been proved quite feasible in solving problems involving complicated interrelationships between response attributes and multiple input parameters [204]. The grey rational analysis (GRA) method comprises of different steps are presented in Figure 6.2.

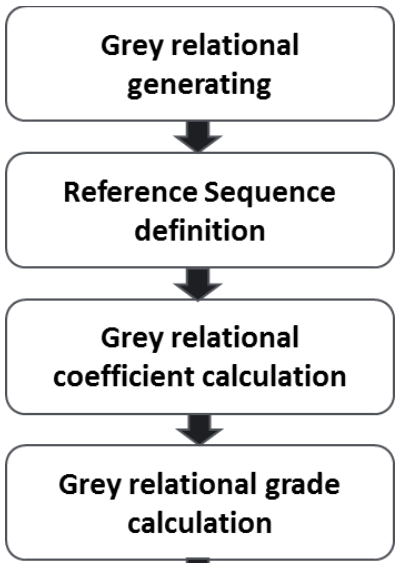

Figure 6.2 Steps in GRA method

As a first step in GRA method the performance of all alternatives is translated into a comparability sequence. This step is termed as grey relational generating. For the translation of performance of alternatives into comparability sequence three relationships are available that are smaller the better, larger the better and target the better.

The desired outcome of the selected response attribute is a deciding factor in selection of the mentioned relationships. For instance, in the present scenario the surface roughness of both layers (stainless steel and mild steel) and their difference are the selected response attributes and for all the narrated responses smaller value is required. Therefore,

smaller the better relationship has been opted that is described by the below equation 6.4.

$$X_{ij} = \frac{\mathrm{Max}\{Y_{ij}, i=1,2,\ldots,m\} - Y_{ij}}{\mathrm{Max}\{Y_{ij}, i=1,2,\ldots,m\} - \mathrm{Min}\{Y_{ij}, i=1,2,\ldots m\}} \qquad (6.4) \text{ for } i = 1, 2,\ldots m \ \& \ j= 1,2,\ldots..n$$

Where m denotes the alternatives and n accounts for attributes. The i^{th} alternative can be represented as $Y_i = (Y_{i1}, Y_{i2}, \ldots Y_{ij}, \ldots Y_{in})$, here Yij shows the performance of j^{th} attribute in i^{th} alternative. To convert the term Y_i into comparability sequence $X_i = (X_{i1}, X_{i2}, \ldots . X_{ij}, \ldots . X_{in})$ the above mentioned relationship has been opted. All the performance values have been scaled from 0 to 1 in grey relational generating procedure. In the next step the reference sequence has been defined. Any alternative foe which all of its performance values are nearer to or equal to 1 is considered to be the best therefore in the current study the reference sequence X_o ($X_{o1}, X_{o2, \ldots .}$ $X_{oj, \ldots ..}, X_{on}$) is defined as ($X_{o1}, X_{o2, \ldots .}$ $X_{oj, \ldots ..}, X_{on}$) = (1, 1,…1,……1). After that the comparability sequence which is nearer to the defined reference sequence is found.

The next step is to evaluate that how close X_{ij} is to X_{oj} which is done by calculating the grey relational coefficient. Following relationship has been used to find the grey relational coefficients.

$$\gamma(X_{oj}, X_{ij}) = \frac{\Delta_{min} + \zeta\Delta_{max}}{\Delta_{ij} + \zeta\Delta_{max}} \quad (6.5) \quad \text{for } i = 1, 2, \ldots, m \;\; j = 1, 2, \ldots, n$$

Here γ is representing grey relational coefficient and ζ account for distinguishing coefficient whereas Δ_{min} & Δ_{max} are the minimum and maximum values of difference between reference sequence and comparability sequence. Δij is calculated by using the relation described by equation 6.6.

$$\Delta_{ij} = | \; X_{oj} - X_{ij} \; | \quad (6.6)$$

Whereas Δ_{min} and Δ_{max} are found by the following equations 6.7 and 6.8.

$$\Delta_{min} = \text{Min}\{\Delta_{ij}, i = 1, 2, \ldots., m; j = 1, 2, \ldots., n\} \quad (6.7)$$

$$\Delta_{max} = \text{Max}\{\Delta_{ij}, i = 1, 2, \ldots., m; j = 1, 2, \ldots., n\} \quad (6.8)$$

The value of distinguishing coefficient (ζ) ranges from [0-1]. As a final step the grey relational grades for all the alternatives have been computed using the relationship presented by eq. 6.9.

$$\Gamma(X_o, X_i) = \sum_{j=1}^{n} w_j \, \gamma(x_{oj}, x_{ij}) \quad (6.9) \quad \text{for } i = 1,2,\ldots..,m$$

In equation 6.9 Γ represents the grey relational grade, w_j is the weight of attribute j and γ is the grey relational coefficient.

Grey relational grades (Γ) represents the degree of correlation between the comparability sequence and the defined reference sequence. The lager value of grey relational grade for a particular alternative indicates that the comparability sequence is closest to the reference sequence which means that the selected alternative is the best choice to optimize the all performance characteristics [205].

Using the above mentioned methodology, grey relational analysis is performed for simultaneous optimization of surface roughness of both layer with a due focus on minimizing the difference as well. The results pertaining to the selected optimization method are tabulated in Table 6.11.

Table 6.11 Results of grey relational analysis

	Grey relational generating			**Grey relational coefficients (GRC)**			**Grey relational grade (GRD) calculation**	**Rank of alternates**
Alternative No.	Ra (SS)	Ra (MS)	Difference (δ)	RA (SS)	RA (MS)	Difference (δ)	Grey relational Grades (GRD)	Ranking of Alternatives as per GRD
X_o	1	1	1					
1	0.79	0.65	0.72	0.70	0.59	0.64	0.643	5
2	0.69	0.57	0.74	0.62	0.54	0.66	0.607	8
3	0.27	0.51	0.79	0.41	0.51	0.71	0.541	10
4	0.84	0.81	0.92	0.76	0.72	0.87	0.782	2
5	0.42	0.29	0.69	0.46	0.41	0.62	0.499	15
6	0.97	0.78	0.67	0.94	0.69	0.60	0.744	3
7	0.44	0.32	0.72	0.47	0.43	0.64	0.511	14
8	0.71	0.71	0.95	0.63	0.63	0.91	0.723	4
9	0.87	0.31	0.00	0.79	0.42	0.33	0.516	13
10	0.35	0.65	0.69	0.44	0.59	0.62	0.547	9
11	0.29	0.35	1.00	0.41	0.44	1.00	0.616	6
12	0.00	0.00	0.85	0.33	0.33	0.76	0.477	16
13	0.16	0.25	1.03	0.37	0.40	1.05	0.609	7
14	0.45	0.22	0.51	0.48	0.39	0.51	0.458	17
15	1.00	1.00	1.00	1.00	1.00	1.00	1.000	1
16	0.74	0.40	0.36	0.66	0.45	0.44	0.517	12
17	0.27	0.26	0.87	0.41	0.40	0.80	0.536	11
18	0.11	0.03	0.72	0.36	0.34	0.64	0.447	18

Optimal settings of control factors are developed based on the results of grey relational analysis and are shown in Table 6.12. Optimal value of individual layer thickness is also suggested based on the said analysis. In practical applications layer thickness is specified by other design

considerations. However, the thickness of the clad is always in the form of a range so where ever choice is available during design stage the developed optimal settings can guide to provide better results in terms of surface quality.

Table 6.12 Optimal settings of input parameters

Sr. NO.	Control factor	Symbol	Optimal level	Units
1	Workpiece orientation	Or	2	--
2	Stainless steel layer thickness	LT_{SS}	2	mm
3	Mild steel layer thickness	LT_{MS}	3	mm
4	Wire diameter	D_W	3	mm
5	Servo voltage	SV	2	V
6	Wire feed	F_W	3	mm/s
7	Pressure ratio	Pr	2	--
8	Pulse on-time	P_{ON}	1	μs

6.5.1 Confirmatory experiment

A confirmatory experimental run is performed in order to validate the optimal settings of control factors that has been developed by using grey relational analysis. The results of the confirmatory test have been shown in Table 6.13. It is clear from the results of the experiment performed using optimal settings that there exists about 13.7% reduction in surface roughness of stainless steel layer and 20% reduction in the surface roughness of mild steel layer. Also the difference between the surface roughness values of both layers is observed to be quite small (0.02) as described in Table 6.13.

The roughness profiles of the cut surface machined as per the optimal settings are demonstrated in Figure 6.3. The roughness profiles recorded for the two surfaces; stainless steel surface and mild steel surface have shown that average surface roughness of machined specimen at optimal settings of input parameters seemed to be lower in comparison to the surface profiles generated by the using the non-optimal settings as depicted from the Figure 5.13 and Figure 6.3.

Table 6.13 Results of confirmatory test

Settings of control factors	Control factors levels	Surface roughness stainless steel layer	Surface roughness stainless steel layer	Difference (δ)
Optimal setting	Or 2, LT_{SS} 2, LT_{MS} 3, D_W 3, Pr 2, SV 2, F_W 3, P_{ON} 1	2.49µm	2.51µm	0.02
Other setting	Or 2, LT_{SS} 2, LT_{MS} 2, D_W 2, Pr 1, SV 1, F_W 2, P_{ON} 3	2.83µm	3.04µm	0.21

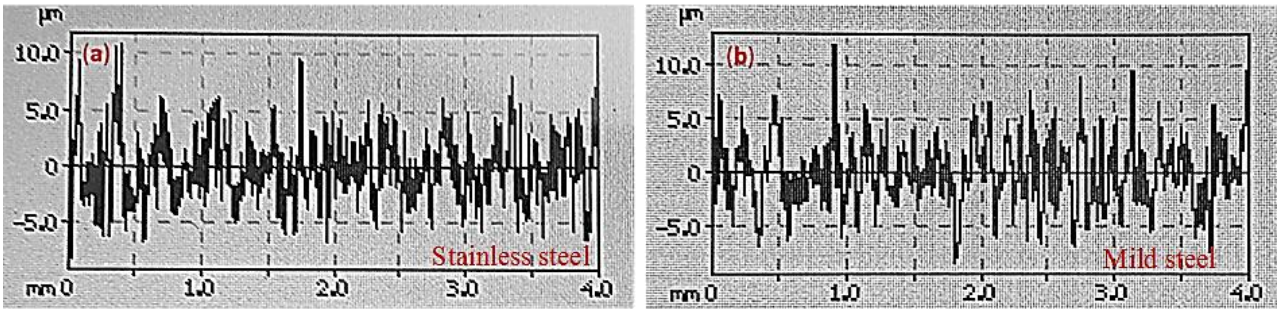

Figure 6.3 (a) Surface roughness profile of stainless steel at optimal settings (b) Surface roughness profile of mild steel at optimal settings

The SEM micrographs captured for the two layers of machined surface subjected to cut at optimal settings also revealed similar results which are provided in Figure 6.4. The surface irregularities imparted to the surface during WEDM at optimal combination of control factors are found to be smaller in contrast to those formed at cut surface subjected to non-optimal settings of WEDM input parameter in cutting stainless clad steel material. The diameters of spherical modules are observed to be smaller in both layers. Moreover, the melted re-deposits size has also been reduced and also both the surfaces contain shallow crates as compared to the situation portrayed inFigure 5.14, when machining is done with non-optimal settings of WEDM parameters.

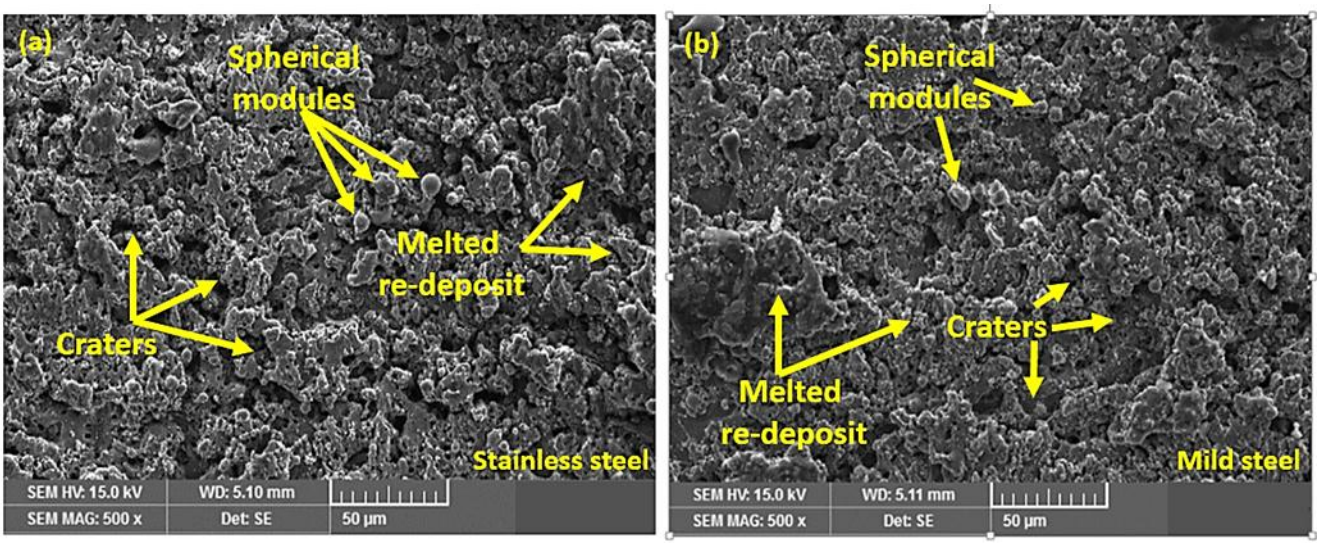

Figure 6.4 (a) SEM micrographs of stainless steel layer at optimal settings (b) SEM micrographs of mild steel layer at optimal settings

6.6 S/N ratio analysis for spark gap optimization

S/N ratio optimization technique has been employed in order to find the optimal combination of input parameters for the minimization of spark gap in WEDM of cladded material. The smaller the better approach is used for finding the optimal parametric combination as smaller value is the desired outcome. The results of the analysis are described in Table 6.14.

Table 6.14 S/N ratios of spark gap

Experiment No.	S/N ratio (dB)	Experiment No.	S/N ratio (dB)
1	21.7768	**10**	23.4139
2	25.1927	**11**	22.0475
3	21.7768	**12**	23.2230
4	21.9927	**13**	24.2934
5	24.8066	**14**	22.3837
6	23.0362	**15**	22.6743
7	26.4661	**16**	22.8534
8	22.4988	**17**	22.1026
9	21.2597	**18**	23.4139

The minimum value of S/N ratio of spark gap is seen during 9th experimental run (21.2597 dB) whereas in experiment number 7 the maximum value of S/N ratio has been recorded. Mean value of S/N ratio for each level of input parameter is calculated thereafter in order to find out the rank of each input parameter with regard to the selected response attribute. The ranking of factors is done on the basis of their delta value. The results regarding factor ranking are described in Table 6.15. The delta value of wire diameter, D_W (2.59) is found to be the maximum among all other parameters indicating that this factor holds the highest rank.

Table 6.15 Response Table for S/N ratios of spark gap

Level	**Or**	**LT_{SS}**	**LT_{MS}**	**D_W**	**SV**	**F_W**	**Pr**	**P_{ON}**
1	23.20	22.91	23.47	24.57	23.19	22.82	22.72	23.10
2	22.93	23.20	23.17	22.66	23.07	22.94	23.81	23.11
3		23.10	22.56	21.98	22.94	23.44	22.67	22.99
Delta	0.27	0.29	0.90	2.59	0.25	0.62	1.14	0.12
Rank	6	5	3	1	7	4	2	8

Pressure ratio (Pr) of the dielectric fluid has secured the rank 2 as its delta value is at second number (1.14). Among the other parameters layer thickness of mild steel (LT_{MS}) is ranked at number 3, followed by wire feed (F_W, rank 4), layer thickness of stainless steel layer (LT_{SS}, rank 5), orientation of workpiece (Or, rank 6), servo voltages (SV, rank 7) and pulse on time (P_{ON}, rank 8).

Optimal levels of control factors are found after ranking of factor based on the said analysis (S/N ratio). These levels along with their level values are mention in Table 6.16.

Table 6.16 Optimal settings of parameters for spark gap minimization

Sr. No.	Input WEDM parameters	Notation	Optimal settings for Spark Gap		
			Optimal Levels	Level value	Units
1	Orientation	"Or"	1	A	---
2	Stainless steel layer thickness	"LT_{SS}"	2	3	mm
3	Mild steel layer thickness	"LT_{MS}"	1	6	mm
4	Wire diameter	"D_W"	1	0.2	mm
5	Servo voltage	"SV"	1	30	V
6	Wire feed	"F_W"	3	220	mm/s
7	Pressure ratio	"Pr"	2	1	--
8	Pulse on-time	"P_{ON}"	2	4	µs

The same can also been inferred from the main effects plots of S/N ratios of spark gap presented in Figure 6.5.

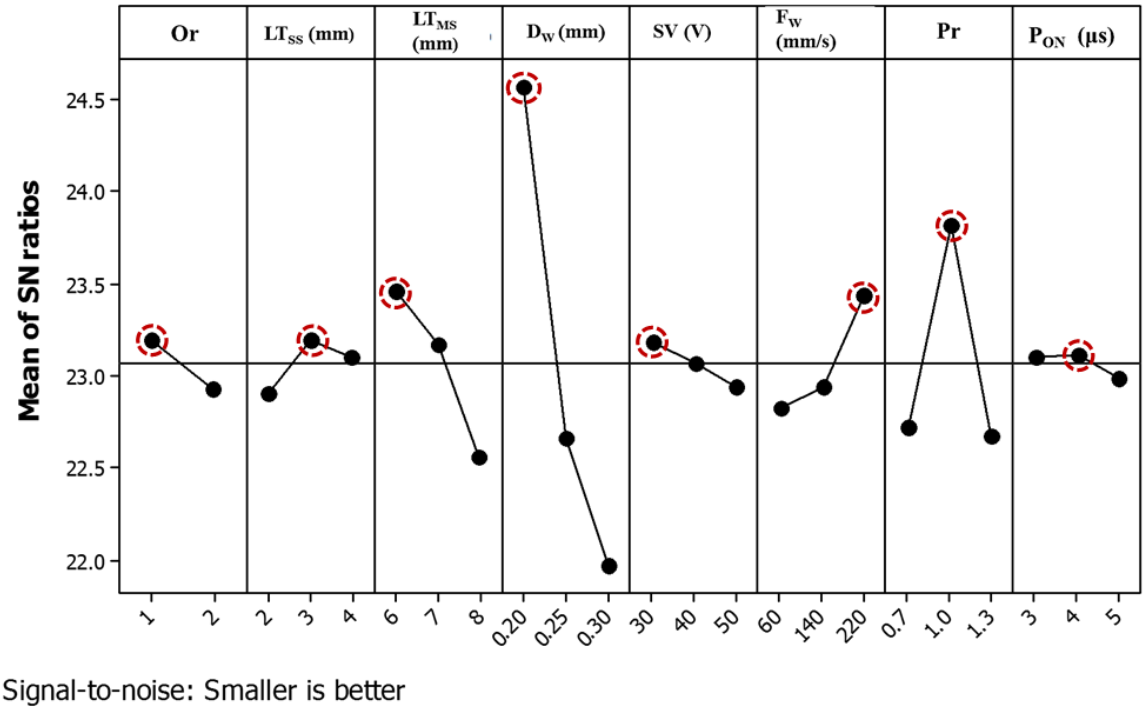

Figure 6.5 Main effects plot of S/N ratios of spark gap

The optimal levels are highlighted by dark brown dotted circles in the above figure. After finding the optimal levels of input parameters the next step is the validation of the developed optimal settings of factors. For this purpose, a confirmatory experiment has been performed the details of which are described in forth coming section.

6.6.1 Confirmatory test

Confirmatory experiment has been performed in order to authenticate the optimal settings of control factors for minimization of spark gap. The results of the confirmatory test are demonstrated in

Table 6.17.

Table 6.17 Confirmatory experiment results for spark gap optimization

Factors settings	**Levels of parameters**	**Pred. value (mm)**	**Exp. value (mm)**	**Error (%)**	**Pred. S/N ratio(dB)**	**Exp. S/N ratio(dB)**	**Error (%)**
Optimal Settings	Or1, LT_{SS}2, LT_{MS}1, D_W1, SV1, F_W3, Pr2, P_{ON}2	0.045	0.047	4.4%	26.74	26.19	2.1%
Non-Optimal Settings	Or1, LT_{SS}1, LT_{MS}3, D_W2, SV3, F_W3, Pr3, P_{ON}3	0.081	0.082	1.7%	21.89	21.77	0.5%
Percentage improvement in response value			**~ 42%**		**Percentage improvement in S/N ratio**		**~17 %**

There found about 42% improvement in the value of the spark gap produced during WEDM of cladded specimen by using optimal settings of control factors. The value of S/N ratio is also being improved by 17%.

Chapter 7

Conclusions and Recommendations for Future Work

The current chapter focuses on presenting the key findings drawn after a comprehensive analyses and a thorough discussion on the results recorded after experimentation as per L18 Taguchi's experimental design. It also highlights the scope for future work in the field of WEDM of cladded material.

7.1 Conclusions

In this research work the potential of WEDM is explored for machining of stainless-clad steel workpiece material. It has been noted that WEDM has proved to be an effective cutting technique for machining of cladded material. This in turn highlights the successful attainment of the first objective of the present research stated in section 1.3. Cutting speed, surface roughness and the spark gap are the selected performance attributes for accessing the performance of WEDM process. Experimentation has been performed as per L18 Taguchi's orthogonal array. Each experimental run is repeated three times in order to ensure the reliability of the results. After completion of experiments, effect of factors pertaining to the cladded workpiece and of WEDM process on the mentioned responses have thoroughly been investigated which was the second objective. The assessment and quantification of the effect of significant input parameters on response attributes have been done by comprehensive statistical analyses. Optimal parametric combinations are also developed for all the selected responses. Theses combinations are further validated through confirmatory tests which shows that responses are fairly improved by using purposed optimal parametric combinations. This is how the third objective is achieved. Finally, regression models have been developed and validated for each of the selected response variable. The magnitude of error for all the purposed models is also calculated and it is found that the developed models hold the high prediction accuracy which in turn shows the efficacious attainment of fourth objective.

The detailed elaboration of conclusions drawn from the present research work is presented below:

7.1.1 Cutting speed

- Cutting speed is observed to be increased with the increase in pulse on time (P_{ON}) however, increase in layer thickness of individual layer (LT_{SS} & LT_{MS}) and wire diameter (D_W) reduces the cutting rate.

- Pulse on time is proved to be the major contributing input parameter with regard to the cutting rate in WEDM of cladded material having a percentage contribution of 42.3%. Among rest of the control factors, layer thickness of stainless steel layer (LT_{SS}), diameter of wire electrode (D_W) and layer thickness of mild steel layer (LT_{MS}) are the factors contributing significantly towards controlling the cutting speed owing to have a percentage contribution of 19.4%, 17.5% and 9.6% respectively.

- The overall thickness of the workpiece material is also found to have a significant effect on the cutting rate. The increase in the overall thickness yields lower cutting rates whereas reverse observed to be true in case of smaller thickness.

- The contribution of layer thickness of stainless steel (LT_{SS}) is twofold in controlling the cutting rate in WEDM of stainless-clad steel in contrast to that of layer thickness of mild steel (LT_{MS}). This is mainly due to the difference in the thermo-electric properties (specifically electrical and thermal conductivity) of the two materials (stainless steel and mild steel).

- The role of workpiece orientation (Or) is observed to be statistically insignificant with respect to the cutting rate. However, cutting speed is improved if the workpiece is placed in the orientation "A" (stainless steel layer faces the top).

- Pulse on-time (P_{ON}) of 5 μsec, 2 mm layer thickness of stainless steel layer (LT_{SS}), 0.2 mm diameter of wire (D_W) electrode, 6 mm layer thickness of mild steel layer (LT_{MS}), servo voltages (SV) of 30V, wire feed (F_W) of 60 mm/sec and pressure ratio of 0.7 are found to be the optimal settings as per S/N ratio analysis that result into maximum cutting speed in WEDM of cladded material.

- The developed optimal combination of parameters provides an improvement of about 20% in the cutting speed (3.1 mm/min) with respect to the maximum cutting rate (2.59 mm/min) recorded during experimentation carried out as per selected DOE.

- Regression equation/model is also formulated for the prediction of cutting speed during WEDM of stainless-clad steel material. There found an average error of about 4.82% between model's predicted and experimental value of cutting speed thus shows high degree of congruity in predicted and experimental values of the said response attribute.

7.1.2 Surface roughness

- Workpiece orientation (Or) has proved to be the significant control factor affecting the surface roughness of both the layers in WEDM of stainless clad steel. The percentage contribution of O_r in controlling the surface roughness of stainless steel layer is found to be 23.3% whereas in case of mild steel layer it comes out to be 14%.

- Orientation (Or) "A" (stainless steel layer is at top) could be a preferred orientation as compared to the orientation (Or) "B" (mild steel layer is at top) in order to machine the stainless clad steel with minimum surface roughness.

- Wire diameter (D_W) has also been found to be a significant control factor influencing the roughness of both the surfaces. With respect to the percentage contribution the wire diameter (D_W) is the most contributing factor (~30% contribution). Larger diameter wire (0.3 mm) yields better surface finish on both the layers owing to a lower cutting speed which resulted into an appropriate flushing of melted debris.

- Pressure ratio (Pr) has also rated as a significant input parameter controlling the cut quality. Pressure ratio of 1 (dielectric pressure of upper and lower nozzles at equal setting) reduces the wire vibrations and consequently promises to yield relatively better surface finish.

- The surface roughness of both the layers (individually) as well as their relative difference is found to be minimal by using optimal combination of parameters obtained through grey relational analysis and validated by weighted S/N ratio analysis. Optimal combination of control factors are tabulated in table 8.

- SEM analysis of machined samples confirms that workpiece orientation and wire diameter played a pivotal role in determining the amount of discharge energy produced. The surface topographic features like melted re-deposits, craters depth and spherical modules diameter have been found to be of smaller magnitude if the cutting action is performed at lower discharge energy thus producing comparatively a better surface finish.

7.1.3 Spark gap

- Wire diameter (D_W) and pressure ratio (Pr) of dielectric fluid are found to be the significant control factors with regard to the spark gap produced in stainless steel layer (LT_{SS}). However, none of the selected input parameter is found to be significant for the spark gap produced in mild steel layer as per the results of ANOVA.

- The values of percentage contributions of factors revealed that wire diameter (D_W) is the most influential parameter in determining the spark gap in stainless steel layer during WEDM of cladded specimen having a percentage contribution of 71%. Pressure ratio (Pr) comes out to be the second most contributing factor with a percentage contribution of 16%.

- Spark gap is found insensitive with regard to the change in the thickness of the stainless-clad steel during WEDM.

- The impact of workpiece orientation (Or) is observed to be statistically insignificant for the spark gap produced in cladded material during WEDM. However, orientation "A" is proved to be the preferred orientation for the reduction in the spark gap.

- It has been noticed that smaller value of wire diameter (D_W), servo voltages (SV), pulse on time (P_{ON}), layer thickness of mild steel layer (LT_{MS}) and an equal value of flushing pressure of both the nozzles resulted into smaller spark gap. On the other end, higher value of wire feed (F_W) and an intermediate value of stainless steel layer (LTss) lower down the value of said response characteristic.

- Optimal settings of control factors with regard to the selected response variable have also been developed using S/N ratio analysis i.e. Or 1, LT_{SS} 2, LT_{MS} 1, D_W 1, SV 1, F_W 3, Pr 2 and P_{ON} 1. It has been found that there exists an improvement of about 42 % in the value of the response by using the optimal settings in contrast to the value of spark gap found at non-optimal settings.

- Regression model for the prediction of the spark gap in WEDM of cladded material is also developed and validated through confirmatory test. There exists an average error of about 6% between the model's predicted and experimental value of the spark gap produced in WEDM.

7.2 Recommendations for future work

Following areas are recommended for future work based on the findings of current research work;

- ❖ The machining performance of WEDM during tapered/profile cutting of cladded material can be investigated in future. As in some of its applications (shells, pipes etc.) tapered edge is required for the subsequent joining process which is difficult to machine through conventional means.
- ❖ The effect of sequential/multi-pass cutting strategy in WEDM of cladded material may be explored which may improve the quality of machined surface.
- ❖ The cutting performance of newly developed wire electrode materials such as diffused annealed wires and zinc coated brass wires may be investigated for WEDM of cladded material for better cutting rate and surface quality.

References

[1] Z. Dhib, N. Guermazi, M. Gaspérini, and N. Haddar, "Cladding of low-carbon steel to austenitic stainless steel by hot-roll bonding: Microstructure and mechanical properties before and after welding," Mater. Sci. Eng. A, vol. 656, pp. 130–141, 2016.

[2] J. R. Davis, "Stainless Steel Cladding and Weld Overlays," ASM Spec. Handb., vol. 06398G, pp. 107–119, 1994.

[3] P. K. Palani and N. Murugan, "Sensitivity analysis for process parameters in cladding of stainless steel by flux cored arc welding," J. Manuf. Process., vol. 8, no. 2, pp. 90–100, 2006.

[4] L. Smith, "Engineering with Clad Steel," Nickel Inst. Tech. Ser. Nº 10 064, pp. 1–24, 2012.

[5] P. Nieslony, P. Cichosz, G. M. Krolczyk, S. Legutko, D. Smyczek, and M. Kolodziej, "Experimental studies of the cutting force and surface morphology of explosively clad Ti-steel plates," Meas. J. Int. Meas. Confed., vol. 78, pp. 129–137, 2016.

[6] B. Azhiri, R. Teimouri, M. Ghasemi Baboly, and Z. Leseman, "Application of Taguchi, ANFIS and grey relational analysis for studying, modeling and optimization of wire EDM process while using gaseous media," Int. J. Adv. Manuf. Technol., 2014.

[7] A. Varun and N. Venkaiah, "Simultaneous optimization of WEDM responses using grey relational analysis coupled with genetic algorithm while machining EN 353," Int. J. Adv. Manuf. Technol., 2014.

[8] I. Maher, A. A. D. Sarhan, and M. Hamdi, "Review of improvements in wire electrode properties for longer working time and utilization in wire EDM machining," Int. J. Adv. Manuf. Technol., 2014.

[9] N. Pragadish and M. Pradeep Kumar, "Optimization of Dry EDM Process Parameters Using Grey Relational Analysis," Arab. J. Sci. Eng., vol. 41, no. 11, pp. 4383–4390, 2016.

[10] M. Altug, M. Erdem, and C. Ozay, "Experimental investigation of kerf of Ti6Al4V exposed to different heat treatment processes in WEDM and optimization of parameters using genetic algorithm," Int. J. Adv. Manuf. Technol., 2015.

[11] K. Kanlayasiri and S. Boonmung, "Effects of wire-EDM machining variables on surface roughness of newly developed DC 53 die steel: Design of experiments and regression model," J. Mater. Process. Technol., 2007.

[12] N. G. Patil and P. K. Brahmankar, “Determination of material removal rate in wire electro-discharge machining of metal matrix composites using dimensional analysis,” Int. J. Adv. Manuf. Technol., 2010.

[13] Y. Huang et al., “Optimization of cutting conditions of YG15 on rough and finish cutting in WEDM based on statistical analyses,” Int. J. Adv. Manuf. Technol., 2013.

[14] P. Saha, D. Tarafdar, S. K. Pal, P. Saha, A. K. Srivastava, and K. Das, “Modeling of wire electro-discharge machining of TiC/Fe in situ metal matrix composite using normalized RBFN with enhanced k-means clustering technique,” Int. J. Adv. Manuf. Technol., 2009.

[15] A. Muttamara, Y. Fukuzawa, N. Mohri, and T. Tani, “Probability of precision micro-machining of insulating Si3N 4 ceramics by EDM,” in Journal of Materials Processing Technology, 2003, vol. 140, no. 1–3 SPEC., pp. 243–247.

[16] V. T. Bhanu Kiran, “Numerical Simulation of Multilayer Hardfacing on Low Carbon Steel,” IACSIT Int. J. Eng. Technol., vol. 3, no. 1, 2011.

[17] “Metal Cladding.” [Online]. Available: ps://corrosion-doctors.org/MetalCoatings/Cladding.htm. [Accessed: 15-May-2017].

[18] P. K. Palani and N. Murugan, “Development of mathematical models for prediction of weld bead geometry in cladding by flux cored arc welding,” Int. J. Adv. Manuf. Technol., vol. 30, no. 7–8, pp. 669–676, 2006.

[19] J. H. F. Gomes, S. C. Costa, A. P. Paiva, and P. P. Balestrassi, “Mathematical modeling of weld bead geometry, quality, and productivity for stainless steel claddings deposited by FCAW,” J. Mater. Eng. Perform., vol. 21, no. 9, pp. 1862–1872, 2012.

[20] T. Kannan and J. Yoganandh, “Effect of process parameters on clad bead geometry and its shape relationships of stainless steel claddings deposited by GMAW,” Int. J. Adv. Manuf. Technol., vol. 47, no. 9–12, pp. 1083–1095, 2010.

[21] B. Chakrabarti, H. Das, S. Das, and T. K. Pal, “Effect of process parameters on clad quality of duplex stainless steel using GMAW process,” Trans. Indian Inst. Met., vol. 66, no. 3, pp. 221–230, 2013.

[22] M. K. Saha and S. Das, “A Review on Different Cladding Techniques Employed to Resist Corrosion,” J. Assoc. Eng. India, vol. 86, no. 1–2, p. 51, 2016.

[23] B. Khara, N. D. Mandal, A. Sarkar, M. Sarkar, B. Chakrabarti, and S. Das, “Weld Cladding with Austenitic Stainless Steel for Imparting Corrosion Resistance,” Indian Weld. J., vol. 49, no. 1, p. 74, 2016.

[24] “The World Market for Special Steel Clad Plate - SMI - Steel Market Intelligence.” [Online]. Available: https://www.steel-intelligence.com/product-reports/articles/the-market-for-clad-plate.html. [Accessed: 20-Aug-2017].

[25] “What is clad plate and why heavy industry loves it _ ShapeCUT.” [Online]. Available: https://www.shapecut.com.au/blog/what-is-clad-plate-and-why-heavy-industry-love-it/. [Accessed: 28-Oct-2017].

[26] A. S. Shahi and S. Pandey, “Modelling of the effects of welding conditions on dilution of stainless steel claddings produced by gas metal arc welding procedures,” J. Mater. Process. Technol., vol. 196, no. 1–3, pp. 339–344, 2008.

[27] T. Kannan and N. Murugan, “Effect of flux cored arc welding process parameters on duplex stainless steel clad quality,” J. Mater. Process. Technol., vol. 176, no. 1–3, pp. 230–239, 2006.

[28] N. Venkateswara Rao, G. Madhusudhan Reddy, and S. Nagarjuna, “Weld overlay cladding of high strength low alloy steel with austenitic stainless steel - Structure and properties,” Mater. Des., vol. 32, no. 4, pp. 2496–2506, 2011.

[29] A. K. Singh, G. M. Reddy, and K. S. Rao, “Pitting corrosion resistance and bond strength of stainless steel overlay by friction surfacing on high strength low alloy steel,” Def. Technol., vol. 11, no. 3, pp. 299–307, 2015.

[30] T. Takeuchi et al., “Microstructural changes of a thermally aged stainless steel submerged arc weld overlay cladding of nuclear reactor pressure vessels,” in Journal of Nuclear Materials, 2012, vol. 425, no. 1–3, pp. 60–64.

[31] R. Kacar and M. Acarer, “An investigation on the explosive cladding of 316L stainless steel-din-P355GH steel,” J. Mater. Process. Technol., vol. 152, no. 1, pp. 91–96, 2004.

[32] Y. Lyu, Y. Sun, and F. Jing, “On the microstructure and wear resistance of Fe-based composite coatings processed by plasma cladding with B4C injection,” Ceram. Int., vol. 41, 2015.

[33] B. Carcel, J. Sampedro, A. Ruescas, and X. Toneu, “Corrosion and wear resistance improvement of magnesium alloys by laser cladding with Al-Si,” in Physics Procedia, 2011, vol. 12, no. PART 1, pp. 353–363.

[34] “CLAD MANUFACTURING PROCESS.” [Online]. Available: http://teknacorp.com/wp-content/uploads/pdf/CLAD_MANUFACTURING_PROCESS.pdf. [Accessed: 28-Sep-2017].

[35] “Solid-State Welding Processes.” [Online]. Available: http://slideplayer.com/slide/7102505/. [Accessed: 28-Jan-2018].

[36] Y. Jing, Y. Qin, X. Zang, and Y. Li, “The bonding properties and interfacial morphologies of clad plate prepared by multiple passes hot rolling in a protective atmosphere,” J. Mater. Process. Technol., vol. 214, no. 8, pp. 1686–1695, 2014.

[37] “New Alloys Group-Bimetals, Clad Metals, Permalloys.” [Online]. Available: http://newalloysgroup.com/process.html. [Accessed: 22-Feb-2018].

[38] J. Banker and B. Craig, “Titanium: A solution for highly corrosive hydrometallurgical applications- alloy selection, cladding and fabrication,” Proc. ALTA 2009 Nickel-Cobalt Conf., no. January, 2009.

[39] X. Shi, K. Yu, L. Jiang, C. Li, Z. Li, and X. Zhou, “Microstructural characterization of Ni-201 weld cladding onto 304 stainless steel,” Surf. Coatings Technol., vol. 334, pp. 19–28, 2018.

[40] X. Y. Cao, P. Zhu, X. F. Ding, Y. H. Lu, and T. Shoji, “An investigation on microstructure and mechanical property of thermally aged stainless steel weld overlay cladding,” J. Nucl. Mater., vol. 486, pp. 172–182, 2017.

[41] K. H. Ling, Y. K. Fuh, T. C. Kuo, and S. Xun-Tu, “Effect of welding sequence of a multi-pass temper bead in gas-shielded flux-cored arc welding process: hardness, microstructure, and impact toughness analysis,” Int. J. Adv. Manuf. Technol., vol. 81, no. 5–8, pp. 1033–1046, 2015.

[42] C. S. Wu, L. Wang, W. J. Ren, and X. Y. Zhang, “Plasma arc welding: Process, sensing, control and modeling,” J. Manuf. Process., vol. 16, no. 1, pp. 74–85, 2014.

[43] P. Kah, R. Suoranta, and J. Martikainen, “Advanced gas metal arc welding processes,” Int. J. Adv. Manuf. Technol., vol. 67, no. 1–4, pp. 655–674, 2013.

[44] “WELDING PROCESSES Arc Welding Resistance Welding Oxyfuel Gas Welding.” [Online]. Available: http://slideplayer.com/slide/4235658/. [Accessed: 02-Mar-2018].

[45] “CLADDING SAW & ESW (WIRE & FLUX).” [Online]. Available: http://phoenixweld.com/product/cladding-nozzle-sk60/. [Accessed: 29-Mar-2018].

[46] “Plasma welding.” [Online]. Available: http://www.ionix.fi/en/technologies/plasma-processing/plasma-welding/. [Accessed: 29-Mar-2018].

[47] Z. M. Liu, S. L. Cui, Z. Luo, C. Z. Zhang, Z. M. Wang, and Y. C. Zhang, “Plasma arc welding: Process variants and its recent developments of sensing, controlling and modeling,” Journal of Manufacturing Processes, vol. 23. pp. 315–327, 2016.

[48] “Advantages and Disadvantages of plasma arc cladding.” [Online]. Available: http://www.rfwireless-world.com/Terminology/Advantages-and-Disadvantages-of-Plasma-Arc-Welding-and-Cutting.html. [Accessed: 29-Mar-2018].

[49] “Plasma: The fourth state of matter.” [Online]. Available: http://www.fabricatingandmetalworking.com/2016/02/plasma-the-fourth-state-of-matter/. [Accessed: 02-Apr-2018].

[50] P. Asadi, K. Kazemi-choobi, and A. Elhami, “World’s largest Science , Technology & Medicine Open Access book publisher Welding of Magnesium Alloys.”

[51] M. Dhahri, J. E. Masse, J. F. Mathieu, G. Barreau, and M. Autric, “CO2 Laser Welding of Magnesium alloys,” in Proceedings of SPIE - The International Society for Optical Engineering, 2000, pp. 725–732.

[52] X. Cao, M. Jahazi, J. P. Immarigeon, and W. Wallace, “A review of laser welding techniques for magnesium alloys,” J. Mater. Process. Technol., vol. 171, no. 2, pp. 188–204, 2006.

[53] M. Marya and G. R. Edwards, “Factors controlling the magnesium weld morphology in deep penetration welding by a CO2laser,” J. Mater. Eng. Perform., vol. 10, no. 4, pp. 435–443, 2001.

[54] “Laser welding with a high-quality laser.” [Online]. Available: http://www.kurios.de/en/services/laser-welding.php. [Accessed: 02-Apr-2018].

[55] “Applications _ Laser Cladding Singapore – Laser-Powder-Cladding.” [Online]. Available: http://www.laser-clad.com/applications/. [Accessed: 02-Apr-2018].

[56] “Home Page _ AkmeLogi.” [Online]. Available: http://www.akmelogi.com/?page=home. [Accessed: 02-Apr-2018].

[57] M. Analysis, “Laser Cladding - Oil & Gas Industry.” [Online]. Available: http://www.alspi.com/lasercladding-oilandgas.htm. [Accessed: 02-Apr-2018].

[58] “Laser cladding services _ Oil Industry Products & Services by Castolin Eutectic.” [Online]. Available: http://www.castolin-eutectic-oiltec.com/node/57460/. [Accessed: 02-Apr-2018].

[59] “Laser Cladding.” [Online]. Available: https://www.kondex.com/lasercladding.html. [Accessed: 02-Apr-2018].

[60] M. K. Singh, Unconventional Manufacturing Process. New Age International Pvt Ltd Publishers, 2008.

[61] P. Chatterjee and S. Chakraborty, “Nontraditional machining processes selection using evaluation of mixed data method,” Int. J. Adv. Manuf. Technol., vol. 68, no. 5–8, pp. 1613–1626, 2013.

[62] N. K. Jain, V. K. Jain, and K. Deb, “Optimization of process parameters of mechanical type advanced machining processes using genetic algorithms,” Int. J. Mach. Tools Manuf., vol. 47, no. 6, pp. 900–919, 2007.

[63] S. Samanta and S. Chakraborty, “Parametric optimization of some non-traditional machining processes using artificial bee colony algorithm,” Eng. Appl. Artif. Intell., vol. 24, no. 6, pp. 946–957, 2011.

[64] Y. Nukman, A. Farooqi, O. Al-Sultan, A. R. A. Alnasser, and M. S. H. Bhuiyan, “A Strategic Development of Green Manufacturing Index (GMI) Topology Concerning the Environmental Impacts,” in Procedia Engineering, 2017, vol. 184, pp. 370–380.

[65] “Introduction to Non-Traditional Machining Non-Traditional Machining.” [Online]. Available: https://www.slideshare.net/VTKanth/introduction-to-nontraditional-machining-63835552%0A. [Accessed: 06-Apr-2018].

[66] S. Kalpakjian and S. R. Schmid, “Manufacturing engineering and technology,” Manuf. Eng. Technol., 2014.

[67] A. Akkurt, “The cutting front side geometry in the applications of D3 cold work tool steel material via abrasive water jet,” Gazi Univ. J. Sci., vol. 26, no. 2, pp. 225–239, 2013.

[68] A. Akkurt, “The effect of material type and plate thickness on drilling time of abrasive water jet drilling process,” Mater. Des., vol. 30, no. 3, pp. 810–815, 2009.

[69] H. A. G. El-Hofy, “Fundamentals of machining processes: conventional and nonconventional processes, second ed. Taylor & Francis.,” Taylor Fr., vol. second ed, p. 2013, 2013.

[70] X. Chu, K. Zhu, C. Wang, Z. Hu, and Y. Zhang, “A Study on Plasma Channel Expansion in Micro-EDM,” Mater. Manuf. Process., vol. 31, no. 4, pp. 381–390, 2016.

[71] H. Marashi, A. A. D. Sarhan, I. Maher, and M. Sayuti, “Techniques to Improve EDM Capabilities: A Review,” in Comprehensive Materials Finishing, vol. 1–3, 2016, pp. 171–202.

[72] Z. Hui, Z. Liu, Z. Cao, and M. Qiu, “Effect of Cryogenic Cooling of Tool Electrode on Machining Titanium Alloy (Ti-6Al-4V) during EDM,” Mater. Manuf. Process., vol. 31, no. 4, pp. 475–482, 2016.

[73] K. Dhakar and A. Dvivedi, “Dry and Near-Dry Electric Discharge Machining Processes,” in Advanced Manufacturing Technologies, 2017, pp. 249–266.

[74] N. Mohd Abbas, D. G. Solomon, and M. Fuad Bahari, “A review on current research trends in electrical discharge machining (EDM),” Int. J. Mach. Tools Manuf., vol. 47, no. 7–8, pp. 1214–1228, 2007.

[75] Y.Wong, L.Lim, I. Rahuman, and W.Tee, “Near-mirror-finish phenomenon in EDM using powder-mixed dielectric,” J. Mater. Process. Technol., vol. 79, no. 1–3, pp. 30–40, 1998.

[76] P. Peças and E. Henriques, “Influence of silicon powder-mixed dielectric on conventional electrical discharge machining,” Int. J. Mach. Tools Manuf., vol. 43, no. 14, pp. 1465–1471, 2003.

[77] R. Toshimitsu, A. Okada, R. Kitada, and Y. Okamoto, “Improvement in Surface Characteristics by EDM with Chromium Powder Mixed Fluid,” in Procedia CIRP, 2016, vol. 42, pp. 231–235.

[78] A. Gholipoor, H. Baseri, and M. R. Shabgard, “Investigation of near dry EDM compared with wet and dry EDM processes,” J. Mech. Sci. Technol., vol. 29, no. 5, pp. 2213–2218, 2015.

[79] Y. Shen et al., “High-speed dry electrical discharge machining,” Int. J. Mach. Tools Manuf., vol. 93, pp. 19–25, 2015.

[80] Y.-C. Lin, “Optimal Machining Parameters of EDM in Gas Based on Response Surface Methodology,” Int. J. Mater. Sci. Appl., vol. 5, no. 6, p. 241, 2016.

[81] Z. Yu, T. Jun, and K. Masanori, “Dry electrical discharge machining of cemented carbide,” J. Mater. Process. Technol., vol. 149, no. 1–3, pp. 353–357, 2004.

[82] M. Kunieda, S. Furuoya, and N. Taniguchi, “Improvement of EDM Efficiency by Supplying Oxygen Gas into Gap,” CIRP Ann. - Manuf. Technol., vol. 40, no. 1, pp. 215–218, 1991.

[83] P. Govindan and S. S. Joshi, “Experimental characterization of material removal in dry electrical discharge drilling,” Int. J. Mach. Tools Manuf., vol. 50, no. 5, pp. 431–443, 2010.

[84] I. Beşliu, H. P. Schulze, M. Coteaţă, and D. Amarandei, “Study on the dry electrical discharge machining,” Int. J. Mater. Form., vol. 3, no. SUPPL. 1, pp. 1107–1110, 2010.

[85] S. S. Rahman, M. Z. I. Ashraf, M. S. Bashar, M. Kamruzzaman, A. K. M. Nurul Amin, and M. M. Hossain, “Crystallinity, surface morphology, and chemical composition of the recast layer and rutile-TiO2formation on Ti-6Al-4V ELI by wire-EDM to enhance biocompatibility,” Int. J. Adv. Manuf. Technol., vol. 93, no. 9–12, pp. 3285–3296, 2017.

[86] S. Singh Sidhu and P. Singh Bains, “Study of the Recast Layer of Particulate Reinforced Metal Matrix Composites machined by EDM,” in Materials Today: Proceedings, 2017, vol. 4, no. 2, pp. 3243–3251.

[87] M. P. Jahan, Y. S. Wong, and M. Rahman, “Evaluation of the effectiveness of low frequency workpiece vibration in deep-hole micro-EDM drilling of tungsten carbide,” J. Manuf. Process., vol. 14, no. 3, pp. 343–359, 2012.

[88] G. S. Prihandana, T. Sriani, and M. Mahardika, “Improvement of machining time in micro-EDM with workpiece vibration and graphite powder mixed in dielectric fluid,” Indian J. Eng. Mater. Sci., vol. 19, no. 6, pp. 375–378, 2012.

[89] J. W. Mwangi, G. N. Nyakoe, B. W. Ikua, H. Zeidler, and K. S. Karanja, “Effect of Low Frequency Vibration in Electrical Discharge Machining of AlSiC Metal Matrix Composite,” J. Sustain. Res. Eng., vol. 1, no. 2, pp. 45–50, 2014.

[90] M. T. Shervani-Tabar, K. Maghsoudi, and M. R. Shabgard, “Effects of simultaneous ultrasonic vibration of the tool and the workpiece in ultrasonic assisted EDM,” Int. J. Comput. Methods Eng. Sci. Mech., vol. 14, no. 1, pp. 1–9, 2013.

[91] M. Ghoreishi and J. Atkinson, “A comparative experimental study of machining characteristics in vibratory, rotary and vibro-rotary electro-discharge machining,” J. Mater. Process. Technol., vol. 120, no. 1–3, pp. 374–384, 2002.

[92] J. Qian, F. Yang, J. Wang, B. Lauwers, and D. Reynaerts, “Material removal mechanism in low-energy micro-EDM process,” CIRP Ann. - Manuf. Technol., vol. 64, no. 1, pp. 225–228, 2015.

[93] K. Egashira, A. Matsugasako, H. Tsuchiya, and M. Miyazaki, “Electrical discharge machining with ultralow discharge energy,” Precis. Eng., vol. 30, no. 4, pp. 414–420, 2006.

[94] C. C. Kao and A. J. Shih, “Sub-nanosecond monitoring of micro-hole electrical discharge machining pulses and modeling of discharge ringing,” Int. J. Mach. Tools Manuf., vol. 46, no. 15, pp. 1996–2008, 2006.

[95] M. S. Rasheed and M. H. Abidi, “Analysis of Influence of micro-EDM Parameters on MRR, TWR and Ra in Machining Ni-Ti Shape Memory Alloy,” Int. J. Recent Technol. Eng., vol. 1, no. 4, pp. 32–37, 2012.

[96] H. Huang, H. Zhang, L. Zhou, and H. Y. Zheng, “Ultrasonic vibration assisted electro-discharge machining of microholes in Nitinol,” J. Micromechanics Microengineering, vol. 13, no. 5, pp. 693–700, 2003.

[97] Z. Wansheng, W. Zhenlong, D. Shichun, C. Guanxin, and W. Hongyu, “Ultrasonic and electric discharge machining to deep and small hole on titanium alloy,” J. Mater. Process. Technol., vol. 120, no. 1–3, pp. 101–106, 2002.

[98] A. Viswanath, T. Li, and Y. Gianchandani, “Batch mode microultrasonic machining (μ USM) using workpiece vibration,” J. Microelectromechanical Syst., vol. 24, no. 1, pp. 1–3, 2015.

[99] G. Mandaloi, S. Singh, P. Kumar, and K. Pal, “Effect on crystalline structure of AISI M2 steel using tungsten-thorium electrode through MRR, EWR, and surface finish,” Meas. J. Int. Meas. Confed., vol. 90, pp. 74–84, 2016.

[100] M. Sreenivasa Rao and N. Venkaiah, “A modified cuckoo search algorithm to optimize Wire-EDM process while machining Inconel-690,” J. Brazilian Soc. Mech. Sci. Eng., vol. 39, no. 5, pp. 1647–1661, 2017.

[101] Y. Qin et al., “Micro-manufacturing: Research, technology outcomes and development issues,” Int. J. Adv. Manuf. Technol., vol. 47, no. 9–12, pp. 821–837, 2010.

[102] R. K. Garg, K. K. Singh, A. Sachdeva, V. S. Sharma, K. Ojha, and S. Singh, “Review of research work in sinking EDM and WEDM on metal matrix composite materials,” Int. J. Adv. Manuf. Technol., vol. 50, no. 5–8, pp. 611–624, 2010.

[103] S. Abulais, “Current Research trends in Electric Discharge Machining(EDM):Review,” Int. J. Sci. Eng. Res., vol. 5, no. 6, pp. 100–118, 2014.

[104] S. Kumar, R. Singh, T. P. Singh, and B. L. Sethi, “Surface modification by electrical discharge machining: A review,” J. Mater. Process. Technol., vol. 209, no. 8, pp. 3675–3687, 2009.

[105] Y. S. Wong, M. Rahman, H. S. Lim, H. Han, and N. Ravi, “Investigation of micro-EDM material removal characteristics using single RC-pulse discharges,” in Journal of Materials Processing Technology, 2003, vol. 140, no. 1–3 SPEC., pp. 303–307.

[106] S. Singh and A. Bhardwaj, “Review to EDM by Using Water and Powder-Mixed Dielectric Fluid,” J. Miner. Mater. Charact. Eng., vol. 10, no. 2, pp. 199–230, 2011.

[107] S. K. Choudhary and R. S. Jadoun, “Current Advanced Research Development of Electric Discharge Machining (EDM): A Review,” Int. J. Res. Advent Technol., vol. 2, no. 3, pp. 2321–9637, 2014.

[108] A. Jamwal, A. Aggarwal, N. Gautam, A. Devarapalli, and M. Engineering, “Electro-Discharge Machining: Recent Developments and Trends Research Studies Conducted in EDM,” 2018.

[109] P. Dewan, “Latest Trends in Electro Discharge Machining,” Eur. J. Adv. Eng. Technol., vol. 2, no. 5, pp. 66–71, 2015.

[110] “Applications of Die-sinking EDM.” [Online]. Available: http://www.edm-machines.com/total-machine-tools/34743624.html. [Accessed: 11-Apr-2018].

[111] R. Kumar and S. Singh, “Current Research Trends in Wire Electrical Discharge Machining: An Overview,” Int. J. Emerg. Technol., vol. 3, no. 1, pp. 33–40, 2012.

[112] K. H. Ho, S. T. Newman, S. Rahimifard, and R. D. Allen, “State of the art in wire electrical discharge machining (WEDM),” Int. J. Mach. Tools Manuf., vol. 44, no. 12–13, pp. 1247–1259, 2004.

[113] Y. S. Liao, T. J. Chuang, and Y. P. Yu, “On-line workpiece height estimation and its application in servo feed control of WEDM process,” in Procedia CIRP, 2013, vol. 6, pp. 226–231.

[114] G. Feng, “A survey on analysis and design of model-based fuzzy control systems,” IEEE Trans. Fuzzy Syst., vol. 14, no. 5, pp. 676–697, 2006.

[115] Z. Wansheng et al., “A New Model of WEDM-CNC System with Digitizer/Player Architecture,” in Procedia CIRP, 2016, vol. 42, pp. 210–214.

[116] J. Yuan, C. L. Liu, X. Liu, K. Wang, and T. Yu, “Incorporating prior model into Gaussian processes regression for WEDM process modeling,” Expert Syst. Appl., vol. 36, no. 4, pp. 8084–8092, 2009.

[117] M. T. Yan and C. C. Fang, “Application of genetic algorithm-based fuzzy logic control in wire transport system of wire-EDM machine,” J. Mater. Process. Technol., vol. 205, no. 1–3, pp. 128–137, 2008.

[118] Y. S. Liao, M. P. Cheng, and K. W. Liao, “An on-line pulse trains analysis system of the wire-EDM process,” J. Mater. Process. Technol., vol. 209, no. 9, pp. 4417–4422, 2009.

[119] A. W. J. Hsue, “Improvement of Wire-EDM Finishing Processes through Adaptive Fuzzy Logic Control Algorithm,” Mater. Sci. Forum, vol. 594, pp. 407–414, 2008.

[120] M. T. Yan and H. T. Chien, “Monitoring and control of the micro wire-EDM process,” Int. J. Mach. Tools Manuf., vol. 47, no. 1, pp. 148–157, 2007.

[121] M. E. I. E. Boccadoro and ir F. Dauw, “About the Application of Fuzzy Controllers in High-Performance Die-Sinking EDM Machines,” CIRP Ann. - Manuf. Technol., vol. 44, no. 1, pp. 147–150, 1995.

[122] C. T. Lin, I. F. Chung, and S. Y. Huang, “Improvement of machining accuracy by fuzzy logic at corner parts for wire-EDM,” Fuzzy Sets Syst., vol. 122, no. 3, pp. 499–511, 2001.

[123] O. Yilmaz, O. Eyercioglu, and N. N. Z. Gindy, “A user-friendly fuzzy-based system for the selection of electro discharge machining process parameters,” J. Mater. Process. Technol., vol. 172, no. 3, pp. 363–371, 2006.

[124] M. R. Shabgard, M. A. Badamchizadeh, G. Ranjbary, and K. Amini, “Fuzzy approach to select machining parameters in electrical discharge machining (EDM) and ultrasonic-assisted EDM processes,” J. Manuf. Syst., vol. 32, no. 1, 2013.

[125] W. M. Lee and Y. S. Liao, “Adaptive control of the WEDM process using a self-tuning fuzzy logic algorithm with grey prediction,” Int. J. Adv. Manuf. Technol., vol. 34, no. 5–6, pp. 527–537, 2007.

[126] Z. Zhang, W. Ming, G. Zhang, Y. Huang, X. Wen, and H. Huang, “A new method for on-line monitoring discharge pulse in WEDM-MS process,” Int. J. Adv. Manuf. Technol., vol. 81, no. 5–8, pp. 1403–1418, 2015.

[127] S. Kwon, S. Lee, and M. Yang, “Experimental investigation of the real-time micro-control of the WEDM process,” Int. J. Adv. Manuf. Technol., vol. 79, no. 9–12, pp. 1483–1492, 2015.

[128] I. Cabanes, E. Portillo, M. Marcos, and J. A. Sánchez, “An industrial application for on-line detection of instability and wire breakage in wire EDM,” J. Mater. Process. Technol., vol. 195, no. 1–3, pp. 101–109, 2008.

[129] A. Okada, Y. Uno, M. Nakazawa, and T. Yamauchi, “Evaluations of spark distribution and wire vibration in wire EDM by high-speed observation,” CIRP Ann. - Manuf. Technol., vol. 59, no. 1, pp. 231–234, 2010.

[130] K. T. Hoang and S.-H. Yang, “A new approach for Micro-WEDM control based on Real-Time estimation of material removal rate,” Int. J. Precis. Eng. Manuf., vol. 16, no. 2, pp. 241–246, 2015.

[131] A. Caggiano, R. Teti, R. Perez, and P. Xirouchakis, “Wire EDM monitoring for zero-defect manufacturing based on advanced sensor signal processing,” in Procedia CIRP, 2015, vol. 33, pp. 315–320.

[132] A. Caggiano, R. Perez, T. Segreto, R. Teti, and P. Xirouchakis, “Advanced Sensor Signal Feature Extraction and Pattern Recognition for Wire EDM Process Monitoring,” in Procedia CIRP, 2016, vol. 42, pp. 34–39.

[133] R. Bobbili, V. Madhu, and A. K. Gogia, “Effect of wire-EDM machining parameters on surface roughness and material removal rate of high strength armor steel,” Mater. Manuf. Process., vol. 28, no. 4, pp. 364–368, 2013.

[134] A. Mandal, A. R. Dixit, A. K. Das, and N. Mandal, “Modeling and Optimization of Machining Nimonic C-263 Superalloy using Multicut Strategy in WEDM,” Mater. Manuf. Process., vol. 31, no. 7, pp. 860–868, 2016.

[135] R. T. Yang, C. J. Tzeng, Y. K. Yang, and M. H. Hsieh, “Optimization of wire electrical discharge machining process parameters for cutting tungsten,” Int. J. Adv. Manuf. Technol., vol. 60, no. 1–4, pp. 135–147, 2012.

[136] P. M. Gopal, K. S. Prakash, and S. Jayaraj, “WEDM of Mg/CRT/BN composites: Effect of materials and machining parameters,” Materials and Manufacturing Processes, pp. 1–8, 2017.

[137] R. Chalisgaonkar and J. Kumar, “Optimization of WEDM process of pure titanium with multiple performance characteristics using Taguchi’s DOE approach and utility concept,” Front. Mech. Eng., vol. 8, no. 2, pp. 201–214, 2013.

[138] G. Selvakumar, K. B. Jiju, and R. Veerajothi, “Experimental Study on Wire Electrical Discharge Machining of Tapered Parts,” Arab. J. Sci. Eng., vol. 41, no. 11, pp. 4431–4439, 2016.

[139] V. Singh, R. Bhandari, and V. K. Yadav, “An experimental investigation on machining parameters of AISI D2 steel using WEDM,” International Journal of Advanced Manufacturing Technology, pp. 1–12, 2016.

[140] M. P. G. Ajai and J. Gian, “Multi-objective Optimization of Process Parameters in Wire Electric Discharge Machining of Ti-6-2-4-2 Alloy,” pp. 1465–1476, 2014.

[141] K. Kumar and S. Agarwal, “Multi-objective parametric optimization on machining with wire electric discharge machining,” Int. J. Adv. Manuf. Technol., vol. 62, no. 5–8, pp. 617–633, 2012.

[142] M. R. Shabgard, A. Gholipoor, and M. Hatami, “Wire electrical discharge machining of ASP30 tool steel,” J. Mech. Sci. Technol., vol. 30, no. 8, pp. 3799–3804, 2016.

[143] A. Alias, B. Abdullah, and N. M. Abbas, “WEDM: Influence of machine feed rate in machining Titanium Ti-6Al-4V using brass wire and constant current (4A),” in Procedia Engineering, 2012, vol. 41, pp. 1812–1817.

[144] M. Azam, M. Jahanzaib, J. A. Abbasi, and A. Wasim, “Modeling of cutting speed (CS) for HSLA steel in wire electrical discharge machining (WEDM) using moly wire,” J. Chinese Inst. Eng. Trans. Chinese Inst. Eng. A/Chung-kuo K. Ch’eng Hsuch K’an, vol. 39, no. 7, pp. 802–808, 2016.

[145] P. Sharma, D. Chakradhar, and S. Narendranath, “Effect of wire diameter on surface integrity of wire electrical discharge machined Inconel 706 for gas turbine application,” J. Manuf. Process., vol. 24, pp. 170–178, 2016.

[146] N. Tosun, C. Cogun, and A. Inan, “The Effect of Cutting Parameters on Workpiece Surface Roughness in Wire EDM,” Mach. Sci. Technol., vol. 7, no. 2, pp. 209–219, 2003.

[147] J. G. LÓPEZ, P. VERLEYSEN, and J. DEGRIECK, “Effect of fatigue damage on static and dynamic tensile behaviour of electro-discharge machined Ti-6Al-4V,” Fatigue Fract. Eng. Mater. Struct., vol. 35, no. 12, pp. 1120–1132, 2012.

[148] N. Z. Khan, Z. A. Khan, A. N. Siddiquee, A. K. Chanda, and K. Arindam, “Investigations on the effect of wire EDM process parameters on surface integrity of HSLA : a multi-performance characteristics optimization,” Prod. Manuf. Res., vol. 2, no. 1, pp. 501–518, 2014.

[149] P. Raju, M. M. M. Sarcar, and B. Satyanarayana, “Optimization of Wire Electric Discharge Machining Parameters for Surface Roughness on 316 L Stainless Steel Using Full Factorial Experimental Design,” Procedia Mater. Sci., vol. 5, pp. 1670–1676, 2014.

[150] M. Saini, R. Sharma, G. Singh, P. Mangla, R. sharma, and Amit Sethi, “Optimizations of machining parameter in wire edm for 316l stainless steel by using Taguchi method, ANOVA, and grey analysis,” Int. J. Mech. Eng. Technol., vol. 7, no. 2, pp. 307–320, 2016.

[151] A. Ikram, N. A. Mufti, M. Q. Saleem, and A. R. Khan, “Parametric optimization for surface roughness, kerf and MRR in wire electrical discharge machining (WEDM) using Taguchi design of experiment,” J. Mech. Sci. Technol., vol. 27, no. 7, pp. 2133–2141, 2013.

[152] M. Durairaj, D. Sudharsun, and N. Swamynathan, “Analysis of process parameters in wire EDM with stainless steel using single objective Taguchi method and multi objective grey relational grade,” in Procedia Engineering, 2013, vol. 64, pp. 868–877.

[153] K. Rajmohan and A. S. Kumar, “Experimental investigation and prediction of optimum process parameters of micro-wire-cut EDM of 2205 DSS,” International Journal of Advanced Manufacturing Technology, pp. 1–15, 2016.

[154] V. Parashar, A. Rehman, J. L. Bhagoria, and Y. M. Puri, “Kerfs width analysis for wire cut electro discharge machining of SS 304L using design of experiments,” Indian J. Sci. Technol., vol. 3, no. 4, pp. 369–373, 2010.

[155] D. Ghodsiyeh, A. Golshan, and J. A. Shirvanehdeh, “Review on current research trends in wire electrical discharge machining (WEDM),” Indian J. Sci. Technol., vol. 6, no. 2, pp. 154–166, 2013.

[156] Y. S. Liao, J. T. Huang, and H. C. Su, “A study on the machining-parameters optimization of wire electrical discharge machining,” J. Mater. Process. Technol., vol. 71, no. 3, pp. 487–493, 1997.

[157] K. T. Hoang and S. H. Yang, “Kerf analysis and control in dry micro-wire electrical discharge machining,” Int. J. Adv. Manuf. Technol., vol. 78, no. 9–12, pp. 1803–1812, 2015.

[158] D. V. S. S. S. V Prasad and A. G. Krishna, “Empirical modeling and optimization of kerf and wire wear ratio in wire electrical discharge machining,” Int. J. Adv. Manuf. Technol., vol. 77, no. 1–4, pp. 427–441, 2015.

[159] A. Pramanik, A. K. Basak, and M. N. Islam, “Effect of reinforced particle size on wire EDM of MMCs,” Int. J. Mach. Mach. Mater., vol. 17, no. 2, p. 139, 2015.

[160] S. Habib and A. Okada, “Study on the movement of wire electrode during fine wire electrical discharge machining process,” J. Mater. Process. Technol., vol. 227, pp. 147–152, 2016.

[161] T. Kamei, A. Okada, and Y. Okamoto, “High-speed Observation of Thin Wire Movement in Fine Wire EDM,” in Procedia CIRP, 2016, vol. 42, pp. 596–600.

[162] M. Nishikawa and M. Kunieda, “Prediction of wire-EDMed surface shape by in-process measurement of wire electrode behavior,” Seimitsu Kogaku Kaishi/Journal Japan Soc. Precis. Eng., vol. 75, no. 9, pp. 1078–1082, 2009.

[163] S. M. Singu et al., “Experimental investigations on wire vibration , spark gap , MRR and surface roughness in wedm for HC-HCR steel,” vol. 8, no. 8, pp. 127–139, 2017.

[164] S. K. Garg, A. Manna, and A. Jain, “Experimental investigation of spark gap and material removal rate of Al/ZrO2(P)-MMC machined with wire EDM,” J. Brazilian Soc. Mech. Sci. Eng., vol. 38, no. 2, pp. 481–491, 2016.

[165] A. Kumar, V. Kumar, and J. Kumar, “Semi-empirical model on MRR and overcut in WEDM process of pure titanium using multi-objective desirability approach,” J. Brazilian Soc. Mech. Sci. Eng., vol. 37, no. 2, pp. 689–721, 2015.

[166] A. Manna and B. Bhattacharyya, “Taguchi and Gauss elimination method: A dual response approach for parametric optimization of CNC wire cut EDM of PRAlSiCMMC,” Int. J. Adv. Manuf. Technol., vol. 28, no. 1–2, pp. 67–75, 2006.

[167] M. Cavazzuti, Optimization methods: From theory to design scientific and technological aspects in mechanics. 2013.

[168] K. S. H. Prasad, C. S. Rao, and D. N. Rao, “Application of Design of Experiments to Plasma Arc Welding Process : A Review,” J. Brazilian Soc. Mech. Sci. Eng., vol. 34, no. 1, pp. 75–81, 2012.

[169] R. H. Myers, C. M. Anderson-Cook, and D. C. Montgomery, Response Surface Methodology: Process and Product Optimization Using Designed Experiments. 2016.

[170] J. Kechagias, “An experimental investigation of the surface roughness of parts produced by LOM process,” Rapid Prototype. J., vol. 13, no. 1, pp. 17–22, 2007.

[171] G. Chauhan, K. K. Pant, and K. D. P. Nigam, “Development of green technology for extraction of nickel from spent catalyst and its optimization using response surface methodology,” Green Process. Synth., vol. 2, no. 3, pp. 259–271, 2013.

[172] J. Antony, “Taguchi or classical design of experiments: a perspective from a practitioner,” Sens. Rev., vol. 26, no. 3, pp. 227–230, 2006.

[173] G. Barman, A. Kumar, and P. Khare, “Removal of congo red by carbonized low-cost adsorbents: Process parameter optimization using a Taguchi experimental design,” J. Chem. Eng. Data, vol. 56, no. 11, pp. 4102–4108, 2011.

[174] S. K. Gauri and S. Chakraborty, “Multi-response optimization of WEDM process using principal component analysis,” Int. J. Adv. Manuf. Technol., vol. 41, no. 7–8, pp. 741–748, 2009.

[175] A. Muniappan, C. Thiagarajan, and S. Somasundaram, “Optimization of kerf width obtained in WEDM of Aluminum hybrid composite using Taguchi method,” ARPN J. Eng. Appl. Sci., vol. 12, no. 2, pp. 382–388, 2017.

[176] A. Goswami and J. Kumar, “Investigation of surface integrity, material removal rate and wire wear ratio for WEDM of Nimonic 80A alloy using GRA and Taguchi method,” Eng. Sci. Technol. an Int. J., vol. 17, no. 4, pp. 173–184, 2014.

[177] B. K. Lodhi and S. Agarwal, “Optimization of machining parameters in WEDM of AISI D3 steel using taguchi technique,” in Procedia CIRP, 2014, vol. 14, pp. 194–199.

[178] M. N. Islam and A. Pramanik, “Comparison of Design of Experiments via Traditional and Taguchi Method,” J. Adv. Manuf. Syst., vol. 15, no. 3, 2016.

[179] J. Sun, Y. Yang, and D. Wang, “Parametric optimization of selective laser melting for forming Ti6Al4V samples by Taguchi method,” Opt. Laser Technol., vol. 49, pp. 118–124, 2013.

[180] J. Ribeiro, H. Lopes, L. Queijo, and D. Figueiredo, “Optimization of cutting parameters to minimize the surface roughness in the end milling process using the Taguchi method,” Period. Polytech. Mech. Eng., vol. 61, no. 1, pp. 30–35, 2017.

[181] J. Z. Zhang, J. C. Chen, and E. D. Kirby, “Surface roughness optimization in an end-milling operation using the Taguchi design method,” J. Mater. Process. Technol., vol. 184, no. 1–3, pp. 233–239, 2007.

[182] J. M. López-Cacho, P. L. González-R, B. Talero, A. M. Rabasco, and M. L. González-Rodríguez, “Robust Optimization of Alginate-Carbopol 940 Bead Formulations,” Sci. World J., vol. 2012, pp. 1–15, 2012.

[183] “Design of Experiments,” 2017. [Online]. Available: https://www.slideshare.net/RonaldShewchuk/design-of-experiments-72572089. [Accessed: 21-Mar-2018].

[184] G. Zhang, Z. Zhang, J. Guo, W. Ming, M. Li, and Y. Huang, “Modeling and optimization of medium-speed WEDM process parameters for machining SKD11,” Mater. Manuf. Process., vol. 28, no. 10, pp. 1124–1132, 2013.

[185] W. Ming, Z. Zhang, G. Zhang, Y. Huang, J. Guo, and Y. Chen, “Multi-objective optimization of 3D-surface topography of machining YG15 in WEDM,” Mater. Manuf. Process., vol. 29, no. 5, pp. 514–525, 2014.

[186] A. Asghar, A. A. Abdul Raman, and W. M. A. W. Daud, “A comparison of central composite design and Taguchi method for optimizing Fenton process.,” Scientific World Journal., vol. 2014, p. 869120, 2014.

[187] N. TOSUN, C. Çoğun, and G. Tosun, “A study on kerf and material removal rate in wire electrical discharge machining based on Taguchi method,” J. Mater. Process. Technol., vol. 152, no. 3, pp. 316–322, 2004.

[188] V. Gaikwad and V. S. Jatti, “Optimization of material removal rate during electrical discharge machining of cryo-treated NiTi alloys using Taguchi’s method,” J. King Saud Univ. - Eng. Sci., 2016.

[189] H. Kumar, A. Manna, R. Kumar, and M. Engg, “Analysis of parametric effects on response characteristics and faults diagnosis during WEDM of Al / SiCp-MMCs,” no. Aimtdr, pp. 1–7, 2014.

[190] S. Darwish, N. Ahmed, A. M. Alahmari, and N. A. Mufti, “A study of micro-channel size and spatter dispersion for laser beam micro-milling,” Mater. Manuf. Process., vol. 32, no. 2, pp. 171–184, 2017.

[191] A. Pramanik and G. Littlefair, “Wire EDM Mechanism of MMCs with the Variation of Reinforced Particle Size,” Mater. Manuf. Process., vol. 31, no. 13, pp. 1700–1708, 2016.

[192] K. Kanlayasiri and S. Boonmung, “An investigation on effects of wire-EDM machining parameters on surface roughness of newly developed DC53 die steel,” J. Mater. Process. Technol., vol. 187–188, pp. 26–29, 2007.

[193] S. Rajendran, M. Sakthivel, and S. Dharamalingam, “Investigation on Effect of Surface Integrity and Layer Thickness Using T90Mn2W50Cr45 Tool Steel,” Mater. Manuf. Process., vol. 6914, no. August 2014, p. 140808143743007, 2014.

[194] A. A. Khan, M. H. F. A. Hazza, M. R. H. C. Daud, and N. S. B. M. Kamal, “Optimization of Surface Quality of Mild Steel Machined by Wire EDM Using Simulated Annealing Algorithm,” in Proceedings - 2015 4th International Conference on Advanced Computer Science Applications and Technologies, ACSAT 2015, 2016.

[195] S. F. Miller, A. J. Shih, and J. Qu, “Investigation of the spark cycle on material removal rate in wire electrical discharge machining of advanced materials,” Int. J. Mach. Tools Manuf., vol. 44, no. 4, pp. 391–400, 2004.

[196] S. Habib, “Optimization of machining parameters and wire vibration in wire electrical discharge machining process,” Mech. Adv. Mater. Mod. Process., vol. 3, no. 1, p. 3, 2017.

[197] G. Zhang, H. Li, Z. Zhang, W. Ming, N. Wang, and Y. Huang, “Vibration modeling and analysis of wire during the WEDM process,” Mach. Sci. Technol., vol. 20, no. 2, pp. 173–186, 2016.

[198] N. B. V Prasad and C. V. S. Parameswararao, “Studies on Wire Selection for Machining with W E D M,” vol. 3, no. 3, pp. 300–303, 2015.

[199] P. Sun, “Effect of the Vibration on Machining Gap of WEDM,” Appl. Mech. Mater., vol. 395–396, pp. 1053–1056, 2013.

[200] D. Ghodsiyeh, A. Golshan, and S. Izman, “Multi-objective process optimization of wire electrical discharge machining based on response surface methodology,” J. Brazilian Soc. Mech. Sci. Eng., vol. 36, no. 2, pp. 301–313, 2014.

[201] A. Shah, N. A. Mufti, D. Rakwal, and E. Bamberg, “Material removal rate, kerf, and surface roughness of tungsten carbide machined with wire electrical discharge machining,” J. Mater. Eng. Perform., vol. 20, no. 1, pp. 71–76, 2011.

[202] K. Ishfaq, R. Naveed, S. A. Khan, A. Hussain, and F. Noor, “Taguchi based optimization of machining parameters to control surface roughness using TiAlN-coated tungsten carbide milling cutter,” vol. 23, no. 2, pp. 19–28, 2016.

[203] A. Mohammadi, A. Fadaei Tehrani, E. Emanian, and D. Karimi, “A new approach to surface roughness and roundness improvement in wire electrical discharge turning based on statistical analyses,” Int. J. Adv. Manuf. Technol., vol. 39, no. 1–2, pp. 64–73, 2008.

[204] J. Morán, E. Granada, J. L. Míguez, and J. Porteiro, “Use of grey relational analysis to assess and optimize small biomass boilers,” in Fuel Processing Technology, 2006, vol. 87, no. 2, pp. 123–127.

[205] Y. Kuo, T. Yang, and G. W. Huang, “The use of grey relational analysis in solving multiple attribute decision-making problems,” Comput. Ind. Eng., vol. 55, no. 1, pp. 80–93, 2008.